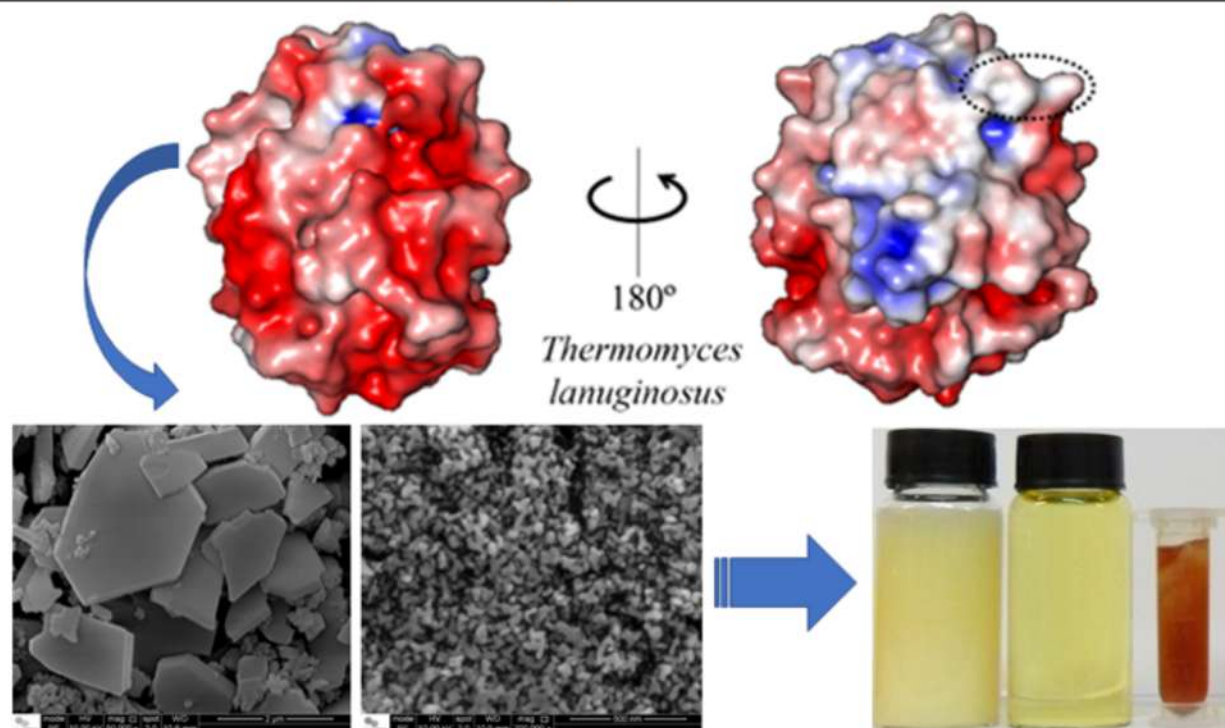


# Eclética Química Journal

Volume 46 • special issue 1 • 2021



## Metallo-stannosilicates as inorganic supports for enzymes immobilization Synergistic effect = $82\pm 6\%$ of enzymes and $63.3\pm 0.7\%$ of FAEES yield

Recent advances in the use of Langmuir monolayers as cell membrane models

Dengue fusion peptides in interaction with model membranes – a fluorescence study

Purification and characterization of embryo-specific soy urease (*Glycine max*) and its antifungal potential against *Paracoccidioides brasiliensis*

Production and biochemical characterization of xylanases synthesized by the thermophilic fungus *Rasamsonia emersonii* S10 by solid-state cultivation

Antioxidative activity of gold and platinum nanoparticles assessed through electron spin resonance

Metallo-stannosilicates as inorganic supports to immobilization of lipase from *Thermomyces lanuginosus* for biodiesel production



**UNIVERSIDADE ESTADUAL PAULISTA**

**Reitor**

Pasqual Barretti

**Vice-Reitora**

Maysa Furlan

**Pró-Reitora de Graduação**

Celia Maria Giacheti

**Pró-Reitora de Pós-Graduação**

Maria Valnice Boldrin

**Pró-Reitor de Pesquisa**

Edson Cocchieri Botelho

**Pró-Reitor de Extensão Universitária e Cultura**

Raul Borges Guimarães

**Pró-Reitor de Planejamento Estratégico e Gestão**

Estevão Tomomitsu Kimpara



**INSTITUTO DE QUÍMICA**

**Diretor**

Sidney José Lima Ribeiro

**Vice-Diretora**

Denise Bevilaqua

## Editorial Team

### Editor-in-Chief

**Prof. Assis Vicente Benedetti**, São Paulo State University, Institute of Chemistry, Araraquara, Brazil

### Editors Section

**Prof. Elso Drigo Filho**, São Paulo State University, Institute of Biosciences, Languages and Exact Sciences, São José do Rio Preto, Brazil

**Prof. Fernando Luis Fertonani**, São Paulo State University, Institute of Biosciences, Languages and Exact Sciences, São José do Rio Preto, Brazil

### Editors

**Prof. Antonio Eduardo Mauro**, São Paulo State University, Institute of Chemistry, Araraquara, Brazil

**Prof. Horacio Heinzen**, University of the Republic, Faculty of Chemistry, Montevideo, Uruguay

**Prof. Marcos Carlos de Mattos**, Federal University of Ceará, Center of Sciences, Fortaleza, Brazil

**Prof. Maria Célia Bertolini**, São Paulo State University, Institute of Chemistry, Araraquara, Brazil

**Prof. Patrícia Hatsue Suegama**, Federal University of Grande Dourados, Faculty of Exact and Technological Sciences, Dourados, Brazil

**Prof. Paulo Clairmont Feitosa Lima Gomes**, São Paulo State University, Institute of Chemistry, Araraquara, Brazil

### Editorial Board

**Prof. Bayardo Baptista Torres**, University of São Paulo, Institute of Chemistry, São Paulo, Brazil

**Prof. Enric Brillas**, University of Barcelona, Faculty of Chemistry, Barcelona, Spain

**Prof. Francisco de Assis Leone**, University of São Paulo, Faculty of Philosophy, Sciences and Literature, Ribeirão Preto, Brazil

**Prof. Ivano Gerardt Rolf Gutz**, University of São Paulo, Institute of Chemistry, São Paulo, Brazil

**Prof. Jairton Dupont**, Federal University of Rio Grande do Sul, Institute of Chemistry, Porto Alegre, Brazil

**Prof. José Antônio Maia Rodrigues**, University of Porto, Faculty of Sciences, Porto, Portugal

**Prof. Lauro Kubota**, University of Campinas, Institute of Chemistry, São Paulo, Brazil

**Prof. Massuo Jorge Kato**, University of São Paulo, Institute of Chemistry, São Paulo, Brazil

**Prof. Roberto Santana da Silva**, University of São Paulo, Faculty of Pharmaceutical Sciences, Ribeirão Preto, Brazil

**Prof. Verónica Cortés de Zea Bermudez**, University of Trás-os-Montes and Alto Douro, School of Life and Environmental Sciences, Vila Real, Portugal

### EDITORIAL PRODUCTION

**Ctrl K Produção Editorial** – Araraquara, Brazil

digite@ctrlk.com.br

## Editorial

This volume honors Prof. João Ruggiero Neto and Prof. Márcio Francisco Colombo, two experimental physicists who made relevant contributions to Biophysics' development in the worldwide scientific community. They were also founding of the Physics Department of the Institute of Biosciences, Humanities and Exact Sciences, Universidade Estadual Paulista (UNESP), campus of São José do Rio Preto, SP, Brazil. Both are Full Professors from this institution.

The scientific contributions of the honorees in the field of Molecular Biophysics are remarkable. Prof. Colombo centered his work on the role of hydration on the mechanism of allosteric regulation, having published a seminal paper on the role of water in the structure of hemoglobin<sup>1</sup>. On his part, Prof. Ruggiero Neto had worked along with drug intercalation and condensation of DNA molecules, with phase transition on lipidic mono and bilayers and on the membrane lytic activity of peptides. An important paper is on the anticancer properties of a peptide extracted from the venom of a São Paulo wasp, *Polybia paulista*<sup>2</sup>.

Beyond their scientific production, including some mutual collaborations, another essential feature of the two honorees for academic life is their kindness, friendship, collaboration, and disposition to work for the greater good. Regarding this, it is better to mention a colleague who has known and nurtured their friendship for decades, Prof. Oswaldo Baffa Filho (Full Professor-University of São Paulo, USP). He reports, "João and I did our doctorate in the same period and defended our theses on the same day. We had an intense and fruitful interaction; I learned a lot from him. His academic rigor, supported on deep basic knowledge, critical vision, and camaraderie, resulted in a strong friendship that remains despite time and distance. With Márcio I also had an intense relationship. I met him while he was still an undergraduate, we participated in the student movement, and I think our friendship brought him to the laboratory where he developed his master and doctoral programs. We lived in a student community in São Carlos with many research activities and healthy social life. Márcio's restless and questioning spirit was always noticeable".

This volume focuses on Biochemistry and Molecular Biophysics. The first article written by Pereira and Oliveira Jr shows the recent advances in cell membrane models. Olivier, Cespedes, Pazin, Cilli and Ito present results involving membrane models and their interaction with dengue peptides. The authors Ângelo, Cruz, Pattaro Jr, Zanzarin, Rodrigues, Pilau, Kioshima, Fernandez and Seixas show results on *Glycine max* and its possible application as an antifungal agent. Zanoni, Oliveira, Perrone, Ortega, Boscolo, Gomes and Rodriguez sign a paper on the characterization of xylanases produced by a thermophilic fungus. Kinoshita, Lima, Guidelli and Baffa Filho show results on the study of gold and platinum nanoparticles using electron spin resonance (ESR). The text of da Silva, Vasconcellos and Nery rationalize aspects of biodiesel production.

Prof. Colombo recently retired, while Prof. Ruggiero Neto is yet active on academic tasks. This special edition is to honor these two academics, recognizing and thanking their trajectory of more than three decades dedicated to higher education and scientific research in Brazil.

**Prof. Dr. Elso Drigo Filho (Guest Editor)**

**Prof. Dr. Fernando Luis Fertonani (Guest Editor)**

## References

1. Colombo, M. F., Rau, D. C., Parsegian, V. A., Protein solvation in allosteric regulation: a water effect on hemoglobin, *Science* 256 (5057) (1992) 655-659. <https://doi.org/10.1126/science.1585178>
2. Leite, N. B., Aufderhorst-Roberts, A., Palma, M. S., Connell, S. D., Ruggiero Neto, J., Beales, P. A. PE and PS Lipids Synergistically Enhance Membrane Poration by a Peptide with Anticancer Properties, *Biophysical Journal* 109 (5) (2015) 936-947. <https://doi.org/10.1016/j.bpj.2015.07.033>

## **Editor's note**

The articles published in this special issue followed all the standard procedures used by the Eclética Química Journal and fulfilled all the qualitative requirements of selection, peer review and editing. Readers can find papers covering the Biochemistry and Molecular Biophysics areas, in line with the editorial profile of Eclética Quím. J., with the following subjects: recent advances in using Langmuir monolayers as cell membrane models; dengue fusion peptides interacting with model membranes; production and biochemical characterization of xylanases; antioxidative activity of gold and platinum nanoparticles; purification and characterization of *Glycine max*, a potential antifungal; metallo-stannosilicates as support to immobilize lipase for biodiesel production.

**Prof. Dr. Assis Vicente Benedetti**  
**Editor-in-Chief**

## Citation databases: Eclética Quim. J. is indexed



\*Click on the images to follow the links.

EBSCO has no link available. The address is for subscribers only.

## INSTRUCTIONS FOR AUTHORS

### BEFORE YOU SUBMIT

#### 1. Check *Eclét. Quim. J.*'s focus and scope

**Eclética Química Journal** is a peer-reviewed quarterly publication of the Institute of Chemistry of São Paulo State University (UNESP). It publishes original researches as articles, reviews and short reviews in **all areas of Chemistry**.

#### 2. Types of papers

- a. Original articles
- b. Reviews
- c. Short reviews
- d. Communications
- e. Technical notes
- f. Articles in education in chemistry and chemistry-related areas

Manuscripts submitted for publication as full articles and communications must contain original and unpublished results and should not have been submitted elsewhere either partially or whole.

##### a. Original articles

The manuscript must be organized in sections as follows:

1. Introduction
  2. Experimental
  3. Results and Discussion
  4. Conclusions
- References

Sections titles must be written in bold and sequentially numbered; only the first letter should be in uppercase letter. Subsections, numbered as exemplified, should be written in normal and italic letters; only the first letter should be in uppercase letter.

Example:

##### **1. Introduction**

###### ***1.1 History***

##### **2. Experimental**

###### ***2.1 Surface characterization***

###### ***2.1.1 Morphological analysis***

##### b. Reviews

Review articles should be original and present state-of-the-art overviews in a coherent and concise form covering the most relevant aspects of the topic that is being revised and indicate the likely future directions of the field. Therefore,

before beginning the preparation of a Review manuscript, send a letter (one page maximum) to the Editor with the subject of interest and the main topics that would be covered in the Review manuscript. The Editor will communicate his decision in two weeks. Receiving this type of manuscript does not imply acceptance to be published in **Elet. Quím. J.** It will be peer-reviewed.

### c. Short reviews

Short reviews should present an overview of the state-of-the-art in a specific topic within the scope of the Journal and limited to 5,000 words. Consider a table or image as corresponding to 100 words. Before beginning the preparation of a Short Review manuscript, send a letter (one page maximum) to the Editor with the subject of interest and the main topics that would be covered in the Short Review manuscript.

### d. Communications

Communications should cover relevant scientific results and are limited to 1,500 words or three pages of the Journal, not including the title, authors' names, figures, tables and references. However, Communications suggesting fragmentation of complete contributions are strongly discouraged by Editors.

### e. Technical notes

Descriptions of methods, techniques, equipment or accessories developed in the authors' laboratory, as long as they present chemical content of interest. They should follow the usual form of presentation, according to the peculiarities of each work. They should have a maximum of 25 pages, including figures, tables, diagrams, etc.

### f. Articles in education in chemistry and chemistry-correlated areas

Research manuscript related to undergraduate teaching in Chemistry and innovative experiences in undergraduate and graduate education. They should have a maximum of 25 pages, including figures, tables, diagrams, and other elements.

## 3. Special issues

Special issues with complete articles dedicated to Symposia and Congresses and to special themes or in honor of scientists with relevant contributions in Chemistry and correlate areas can be published by **Elet. Quím. J.** under the condition that a previous agreement with Editors is established. All the guides of the journal must be followed by the authors.

## 4. Approval

Ensure all authors have seen and approved the final version of the article prior to submission. All authors must also approve the journal you are submitting to.

## ETHICAL GUIDELINES

Before starting the submission process, please be sure that **all ethical aspects mentioned below were followed**. Violation of these ethical aspects may preclude authors from submitting or publishing articles in **Elet. Quím. J.**

**a. Coauthorship:** The corresponding author is responsible for listing as coauthors only researchers who have really taken part in the work, for informing them about the entire manuscript content and for obtaining their permission to submit and publish it.



**b. Nonauthors:** Explicit permission of a nonauthor who has collaborated with personal communication or discussion to the manuscript being submitted to **Eclet. Quím. J.** must be obtained before being cited.

**c. Unbiased research:** Authors are responsible for carefully searching for all the scientific work relevant to their reasoning irrespective of whether they agree or not with the presented information.

**d. Citation:** Authors are responsible for correctly citing and crediting all data taken from other sources. This requirement is not necessary only when the information is a result of the research presented in the manuscript being submitted to **Eclet. Chem. J.**

**e. Direct quotations:** The word-for-word reproduction of data or sentences as long as placed between quotation marks and correctly cited is not considered ethical deviation when indispensable for the discussion of a specific set of data or a hypothesis.

**f. Do not cite:** Master's Degree dissertations and PhD theses are not accepted; instead, you must cite the publications resulted from them.

**g. Plagiarism:** Plagiarism, self-plagiarism, and the suggestion of novelty when the material was already published are unaccepted by **Eclet. Quím. J.** Before reviewing a manuscript, the **Turnitin antiplagiarism software** will be used to detect any ethical deviation.

**h. Simultaneous submissions** of the same manuscript to more than one journal is considered an ethical deviation and is conflicted to the declaration has been done below by the authors.

**i. Studies with humans or other animals:** Before submitting manuscripts involving human beings, materials from human or animals, the authors need to confirm that the procedures established, respectively, by the institutional committee on human experimentation and Helsinki's declaration, and the recommendations of the animal care institutional committee were followed. Editors may request complementary information on ethical aspects.

## COPYRIGHT NOTICE

The corresponding author transfers the copyright of the submitted manuscript and all its versions to **Eclet. Quím. J.**, after having the consent of all authors, which ceases if the manuscript is rejected or withdrawn during the review process.

When a published manuscript in *Eclet. Quím. J.* is also published in other Journal, it will be immediately withdrawn from *Eclet. Quím. J.* and the authors informed of the Editor decision.

Self-archive to institutional, thematic repositories or personal webpage is permitted just after publication. The articles published by **Eclet. Quím. J.** are licensed under the [Creative Commons Attribution 4.0 International License](#).

## PUBLICATION CHARGES

**Eclética Química Journal** is supported by the Institute of Chemistry/UNESP and publication is free of charge for authors.

# MANUSCRIPT PREPARATION

## COVER LETTER

We provide a template to help you prepare your cover letter. To download it, click [here](#).

The cover letter **MUST** include:

### 1. Identification of authors

- a. The authors' full names (they must be written in full and complete, separated by comma)

|                 |           |
|-----------------|-----------|
| João M. José    | Incorrect |
| J. M. José      | Incorrect |
| João Maria José | Correct!  |

- b. E-mail addresses and affiliations (**neither more nor less than two instances**) of all authors;
- c. ORCID ID links;
- d. A plus sign (+) indicating the corresponding author.

**Example:**

Author Full Name<sup>1+</sup>, Author Full Name<sup>2</sup>

1. University, Faculty or Institute, City, Country.
2. Company, Division or Sector or Laboratory, City, Country.

+ Author 1: address@mail.com, ORCID: <https://orcid.org/xxxx-xxxx-xxxx-xxxx>

Author 2: address@mail.com, ORCID: <https://orcid.org/xxxx-xxxx-xxxx-xxxx>

### 2. Authors' contribution

We request authors to include author contributions according to CRediT taxonomy standardized contribution descriptions. **CRediT (Contributor Roles Taxonomy)** is a high-level taxonomy, including 14 roles, that can be used to represent the roles typically played by contributors to scientific scholarly output. The roles describe each contributor's specific contribution to the scholarly output.

- a. Please, visit this link (<https://casrai.org/credit/>) to find out which role(s) the authors fit into;
- b. Do not modify the role names; do not write "all authors" in any role. Do not combine two or more roles in one line.**
- c. If there are any roles that no author has engaged in (such as funding in papers that were not funded), write "Not applicable" in front of the name of the role;
- d. Write the authors' names according to the **American Chemistry Society (ACS) citation style**.

**Example:**

**Conceptualization:** Foster, J. C.; O'Reilly, R. K.

**Data curation:** Varlas, S.; Couturaud, B.; Coe, J.; O'Reilly, R. K.

**Formal Analysis:** Foster, J. C.; Varlas, S.

**Funding acquisition:** Not applicable.

**Investigation:** Foster, J. C.; O'Reilly, R. K.

**Methodology:** Coe, J.; O'Reilly, R. K.

**Project administration:** O'Reilly, R. K.

**Resources:** Coe, J.

**Software:** Not applicable.

**Supervision:** O'Reilly, R. K.

**Validation:** Varlas, S.; Couturaud, B.

**Visualization:** Foster, J. C.

**Writing – original draft:** Foster, J. C.; Varlas, S.; Couturaud, B.; Coe, J.; O'Reilly, R. K.

**Writing – review & editing:** Foster, J. C.; Varlas, S.; Couturaud, B.; Coe, J.; O'Reilly, R. K.

#### 4. Indication of reviewers

We kindly ask the authors to suggest **five** suitable reviewers, providing full name, affiliation, and email.

#### 5. Other information

- a. The authors must write one paragraph remarking the novelty and relevance of the work;
- b. The corresponding author must declare, on behalf of the other authors, that the manuscript being submitted is original and its content has not been published previously and is not under consideration for publication elsewhere;
- c. The authors must inform if there is any conflict of interest.

#### 6. Acknowledgements and funding

Acknowledgements and funding information will be requested after the article is accepted for publication.

#### 7. Data availability statement

A data availability statement informs the reader where the data associated with your published work is available, and under what conditions they can be accessed. Therefore, authors must inform if:

Data will be available upon request;

All dataset were generated or analyzed in the current study; or

Data sharing is not applicable.

### MANUSCRIPT

We provide a template to help you prepare your manuscript. To download it, click [here](#).

#### 1. General rules

Only manuscripts written in English will be accepted. British or American usage is acceptable, but they should not be mixed. Non-native English speakers are encouraged to have their manuscripts professionally revised before submission.

Manuscripts must be sent in editable files as \*.doc, \*.docx or \*.odt. The text must be typed using font style Times New Roman and size 12. Space between lines should be 1.5 mm and paper size A4, top and bottom margins 2.5 cm, left and right margins 2.0 cm.

All contributions must include an **abstract** (170 words maximum), **three to five keywords** and a **graphical abstract** (8 cm wide × 8 cm high).

**Supplementary information:** all type of articles accepts supplementary information (SI) that aims at complementing the main text with material that, for any reason, cannot be included in the article.

## TITLE

The title should be concise, explanatory and represent the content of the work. The title must have only the first letter of the sentence in uppercase. The following are not allowed: acronyms, abbreviations, geographical location of the research, en or em dashes (which must be replaced by a colon). Titles do not have full point.

## ABSTRACT

Abstract is the summary of the article. The abstract must be written as a running text not as structured topics, but its content should present background, objectives, methods, results, and conclusion. It cannot contain citations. The text should be written in a single paragraph with a **maximum of 170 words**.

## KEYWORDS

Keywords are intended to make it easier for readers to find the content of your text. As fundamental tools for database indexing, they act as a gateway to the text. The correct selection of keywords significantly increases the chances that a document will be found by researchers on the topic, and consequently helps to promote the visibility of an article within a myriad of publications.

## FIGURES, TABLES AND EQUATIONS

Figures, tables and equations must be written with initial capital letter followed by their respective number and period, in bold, without adding zero “**Table 1**”, preceding an explanatory title. Tables, Figures and Equations should appear after the first citation and should be numbered according to the ascending order of appearance in the text (1, 2, 3...).

Figures, tables, schemes and photographs already published by the same or different authors in other publications may be reproduced in manuscripts of **Elet. Quim. J.** only with permission from the editor house that holds the copyright.

Nomenclature, abbreviations, and symbols should follow IUPAC recommendations.

## DATA AVAILABILITY STATEMENT

The data availability statement informs the reader where the data associated with your work is available, and under what conditions they can be accessed. They also include links (where applicable) to the data set.

- a. The data are available in a data repository (cite repository and the DOI of the deposited data);
- b. The data will be available upon request;
- c. All data sets were generated or analyzed in the current study;
- d. Data sharing is not applicable (in cases where no data sets have been generated or analyzed during the current study, it should be declared).

## GRAPHICAL ABSTRACT

The graphical abstract must summarize the manuscript in an interesting way to catch the attention of the readers. As already stated, it must be designed with 8 cm wide × 8 cm high, and a 900-dpi resolution is mandatory for this journal. It must be submitted as \*.jpg, \*.jpeg, \*.tif or \*.ppt files as supplementary file.

We provide a template to help you prepare your GA. To download it, click [here](#).

## SUPPLEMENTARY INFORMATION

When appropriate, important data to complement and a better comprehension of the article can be submitted as Supplementary File, which will be published online and will be made available as links in the original article. This might include additional figures, tables, text, equations, videos or other materials that are necessary to fully document the research contained in the paper or to facilitate the readers' ability to understand the work.

Supplementary material should be presented in appropriate .docx file for text, tables, figures and graphics. All supplementary figures, tables and videos should be referred in the manuscript body as "Table S1, S2...", "Fig. S1, S2..." and "Video S1, S2 ...".

**At the end of the main text the authors must inform:** This article has supplementary information.

Supplementary information will be located following the article with a different DOI number from that of the article, but easily related to it.

## CITATION STYLE GUIDE

From 2021 on, the **Eclet. Quim. J.** will follow the [ACS citation style](#).

Indication of the sources is made by authorship and date. So, the reference list is organized alphabetically by author.

Each citation consists of two parts: the in-text citation, which provides brief identifying information within the text, and the reference list, a list of sources that provides full bibliographic information.

We encourage the citation of primary research over review articles, where appropriate, in order to give credit to those who first reported a finding. Find out more about our commitments to the principles of [San Francisco Declaration on Research Assessment \(DORA\)](#).

### What information you must cite?

- a. Exact wording taken from any source, including freely available websites;
- b. Paraphrases of passages;
- c. Summaries of another person's work;
- d. Indebtedness to another person for an idea;
- e. Use of another researchers' work;
- f. Use of your own previous work.

You do not need to cite **common knowledge**.

Example:

Water is a tasteless and odorless liquid at room temperature (common knowledge, no citation needed)

### In-text citations

You can choose to cite your references within or at the end of the phrase, as showed below.

### Within the cited information:

One author: Finnegan states that the primary structure of this enzyme has also been determined (2004).  
Two authors: Finnegan and Roman state that the structure of this enzyme has also been determined (2004).  
Three or more authors: Finnegan et al. state that the structure of this enzyme has also been determined (2004).

#### **At the end of the cited information:**

One author: The primary structure of this enzyme has also been determined (Finnegan, 2004).  
Two authors: The primary structure of this enzyme has also been determined (Finnegan and Roman, 2004).  
Three or more authors: The primary structure of this enzyme has also been determined (Finnegan et al., 2004).

If you need to cite more than one reference in the same brackets, separate them with semicolon and write them in alphabetic order:

The primary structure of this enzyme was determined (Abel et al., 2011; Borges, 2004; Castro et al., 2021).

### **Bibliographic references**

#### **Article from scientific journals**

Foster, J. C.; Varlas, S.; Couturaud, B.; Coe, J.; O'Reilly, R. K. Getting into Shape: Reflections on a New Generation of Cylindrical Nanostructures' Self-Assembly Using Polymer Building Block. *J. Am. Chem. Soc.* **2019**, *141* (7), 2742–2753. <https://doi/10.1021/jacs.8b08648>

#### **Book**

Hammond, C. *The Basics of Crystallography and Diffraction*, 4th ed.; International Union of Crystallography Texts on Crystallography, Vol. 21; Oxford University Press, 2015.

#### **Book chapter**

Hammond, C. Crystal Symmetry. In *The Basics of Crystallography and Diffraction*, 4th ed.; International Union of Crystallography Texts on Crystallography, Vol. 21; Oxford University Press, 2015; pp 99–134.

#### **Book with editors**

*Mom the Chemistry Professor: Personal Accounts and Advice from Chemistry Professors Who Are Mothers*, 2nd ed.; Wozniak, K., Charlebois, A., Cole, R. S., Marzabadi, C. H., Webster, G., Eds.; Springer, 2018.

#### **Website**

ACS Publications Home Page. <https://pubs.acs.org/> (accessed 2019-02-21).

#### **Document from a website**

American Chemical Society, Committee on Chemical Safety, Task Force for Safety Education Guidelines. *Guidelines for Chemical Laboratory Safety in Academic Institutions*. American Chemical Society, 2016. <https://www.acs.org/content/dam/acsorg/about/governance/committees/chemicalsafety/publications/acs-safety-guidelines-academic.pdf> (accessed 2019-02-21).

#### **Conference proceedings**

Nilsson, A.; Petersson, F.; Persson, H. W.; Jönsson, H. Manipulation of Suspended Particles in a Laminar Flow. In *Micro Total Analysis Systems 2002, Proceedings of the  $\mu$ TAS 2002 Symposium*, Nara, Japan, November 3–7, 2002; The Netherlands, 2002; pp 751–753. [https://doi.org/10.1007/978-94-010-0504-3\\_50](https://doi.org/10.1007/978-94-010-0504-3_50)

#### **Governmental and legislation information**

Department of Commerce, United States Patent and Trademark Office. Section 706.02 Rejection of Prior Art [R-07.2015]. *Manual of Patent Examining Procedure (MPEP)*, 9th ed., rev. 08.2017, last revised January 2018. <https://www.uspto.gov/web/offices/pac/mpep/s706.html#d0e58220> (accessed 2019-03-20).

### Patent

Lois-Caballe, C.; Baltimore, D.; Qin, X.-F. Method for Expression of Small RNA Molecules within a Cell. US 7 732 193 B2, 2010.

### Streaming data

American Chemical Society. Game of Thrones Science: Sword Making and Valyrian Steel. *Reactions*. YouTube, April 15, 2015. <https://www.youtube.com/watch?v=cHRcGoje4j4> (accessed 2019-02-28).

For more information, you can access the [ACS Style Quick Guide](#) and the [Williams College LibGuides](#).

## SUBMITTING YOUR MANUSCRIPT

The corresponding author should submit the manuscript online by clicking [here](#). If you are a user, register by clicking [here](#).

At the **User home** page, click in **New submission**.

In Step 1, select a section for your manuscript, verify one more time if you followed all these rules in **Submission checklist**, add Comments for the Editor if you want to, and click Save and continue.

In Step 2, you will **upload your manuscript**. Remember it will pass through a double-blind review process. So, do not provide any information on the authorship.

In Step 3, enter **submission's metadata**: authors' full names, valid e-mail addresses and ORCID ID links (with "http" not "https"). Add title, abstract, contributors and supporting agencies, and the list of references.

In Step 4, upload the **cover letter**, the **graphical abstract** and other **supplementary material** you want to include in your manuscript.

In Step 5, you will be able to check all submitted documents in the **File summary**. If you are certain that you have followed all the rules until here, click in **Finish submission**.

## REVIEW PROCESS

The time elapsed between the submission and the first response of the reviewers is around three months. The average time elapsed between submission and publication is around seven months.

Resubmission (manuscripts "rejected in the present form" or subjected to "revision") must contain a letter with the responses to the comments/criticism and suggestions of reviewers/editors should accompany the revised manuscript. All modifications made to the original manuscript must be highlighted.

If you want to check our Editorial process, click [here](#).

## EDITOR'S REQUIREMENTS

Authors who have a manuscript accepted in **Eclét. Quím. J.** may be invited to act as reviewers.

Only the authors are responsible for the correctness of all information, data and content of the manuscript submitted to **Eclet. Quim. J.** Thus, the Editors and the Editorial Board cannot accept responsibility for the correctness of the material published in **Eclet. Quim. J.**

### **Proofs**

After accepting the manuscript, **Eclet. Quim. J.** technical assistants will contact you regarding your manuscript page proofs to correct printing errors only, i.e., other corrections or content improvement are not permitted. The proofs shall be returned in three working days (72 h) via email.

### **Appeal**

Authors may only appeal once about the decision regarding a manuscript. To appeal against the Editorial decision on your manuscript, the corresponding author can send a rebuttal letter to the editor, including a detailed response to any comments made by the reviewers/editor. The editor will consider the rebuttal letter, and if deemed appropriate, the manuscript will be sent to a new reviewer. The Editor decision is final.

## **Contact**

If you have any question, please contact our team:

Prof. Assis Vicente Benedetti  
Editor-in-Chief  
[ecletica@journal.iq.unesp.br](mailto:ecletica@journal.iq.unesp.br)

Letícia Amanda Miguel and Jéssica Odoni  
Technical support  
[ecletica@ctrlk.com.br](mailto:ecletica@ctrlk.com.br)



## SUMMARY

|                                |   |
|--------------------------------|---|
| EDITORIAL BOARD .....          | 3 |
| EDITORIAL .....                | 4 |
| EDITOR'S NOTE .....            | 5 |
| DATABASE .....                 | 6 |
| INSTRUCTIONS FOR AUTHORS ..... | 7 |

## ORIGINAL ARTICLES

|  |    |
|--|----|
| Recent advances in the use of Langmuir monolayers as cell membrane models .....  | 18 |
| <i>Andressa Ribeiro Pereira, Osvaldo Novais de Oliveira Junior</i>   |    |
| Dengue fusion peptides in interaction with model membranes – a fluorescence study .....  | 30 |
| <i>Danilo da Silva Olivier, Graziely Ferreira Cespedes, Wallance Moreira Pazin, Eduardo Maffud Cilli, Amando Siuiti Ito</i>  |    |
| Purification and characterization of embryo-specific soy urease ( <i>Glycine max</i> ) and its antifungal potential against <i>Paracoccidioides brasiliensis</i> .....   | 41 |
| <i>Elisângela Andrade Ângelo, Tainá Michelle da Cruz, José Renato Pattaro Júnior, Daniele Maria Zanzarin, Franciele Abigail Vilugron Rodrigues, Eduardo Jorge Pilau, Érika Seki Kioshima, Maria Aparecida Fernandez, Flavio Augusto Vicente Seixas</i> |    |
| Production and biochemical characterization of xylanases synthesized by the thermophilic fungus <i>Rasamsonia emersonii</i> S10 by solid-state cultivation .....   | 53 |
| <i>Jéssica de Araujo Zanoni, Isabela Brunozi de Oliveira, Olavo Micali Perrone, Julieth Orduña Ortega, Maurício Boscolo, Eleni Gomes, Gustavo Orlando Bonilla-Rodriguez</i>  |    |
| Antioxidative activity of gold and platinum nanoparticles assessed through electron spin resonance .....   | 68 |
| <i>Angela Kinoshita, Iara Lima, Éder José Guidelli, Oswaldo Baffa Filho</i>  |    |
| Metallo-stannosilicates as inorganic supports to immobilization of lipase from <i>Thermomyces lanuginosus</i> for biodiesel production .....   | 75 |
| <i>Danilo Antonio da Silva, Adriano de Vasconcellos, José Geraldo Nery</i>   |    |

## Recent advances in the use of Langmuir monolayers as cell membrane models

Andressa Ribeiro Pereira<sup>1+</sup>, Osvaldo Novais de Oliveira Junior<sup>1</sup>

1. University of São Paulo, São Carlos Institute of Physics, São Carlos, Brazil.

**+Corresponding author:** Andressa Ribeiro Pereira, **Phone:** +55 11 98229-0202, **Email address:** [andressa.arp@gmail.com](mailto:andressa.arp@gmail.com)

### ARTICLE INFO

*Article history:*

**Received:** July 10, 2020

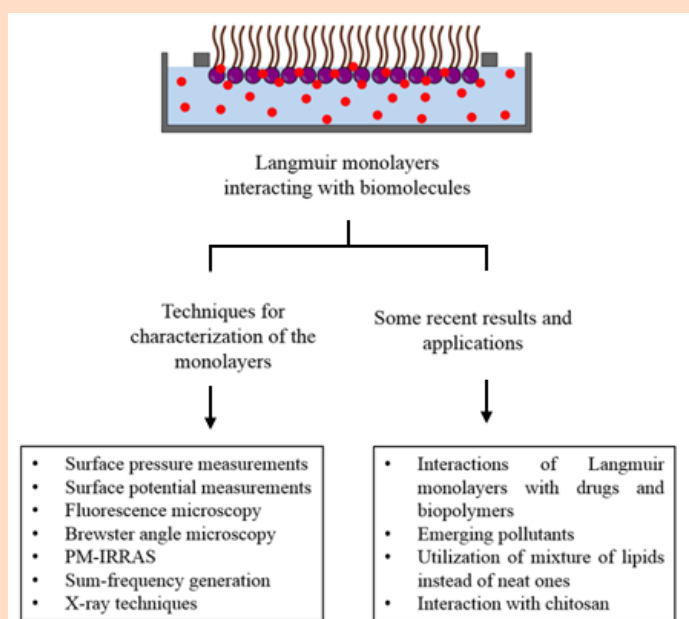
**Accepted:** September 07, 2020

**Published:** April xx, 2021

### Keywords

1. Langmuir monolayers
2. cell membrane models
3. chitosans
4. pharmaceutical drugs

**ABSTRACT:** Understanding the role of biomolecules in cells at the molecular level has been the trade of Prof. Marcio Francisco Colombo and Prof. João Ruggiero Neto in their carriers, which is why it was found appropriate to address the use of Langmuir monolayers as cell membrane models in this special issue. In the review paper, we elaborate upon the reasons why Langmuir monolayers are good models with the possible control of membrane composition and molecular packing. After describing several experimental methods to characterize the Langmuir monolayers, we discuss selected results from the last five years where monolayers were made to interact with pharmaceutical drugs, emerging pollutants and other biologically-relevant molecules. The challenges to take the field forward are also commented upon.



## 1. Introduction

Langmuir monolayers<sup>1-3</sup> have long been used as simplified membrane models as they mimic half of the cell membranes that are formed by a fluid lipid bilayer containing proteins and polysaccharides<sup>4,5</sup>. The reason why membrane models are employed is the difficulty to characterize the cells directly, particularly if molecular-level information is required. Since the seminal works by RAYLEIGH<sup>6</sup>, Langmuir<sup>7</sup> and Nandi and Vollhardt<sup>8</sup>, monolayers have been utilized for *in situ* characterization of surfactant molecules at the air-liquid interface and in the formation of Langmuir-Blodgett (LB) films<sup>9,10</sup>. Because lateral organization is important and there are specific lipid functions in biomembranes, the Langmuir monolayer model is advantageous, as the area per molecule and lipid composition are controlled precisely. Furthermore, with monolayers, one may investigate biomolecule-membrane interactions by modifying and controlling the lipid charge and structure, and subphase conditions, such as pH and concentration of the biologically-relevant molecules<sup>11,12</sup>.

Since the 1990s, novel *in situ* methods have been made available to study liquid interfaces with microscopic and molecular resolution, as described in recent reviews<sup>1-3,13</sup>. In Section 2 in this review paper, we describe several methods to characterize Langmuir monolayers, while selected results from the last five years with monolayers used as membrane models are discussed in Section 3. These results refer to a few topics that have gained prominence, *viz.* interaction with pharmaceutical drugs and emerging pollutants, enzyme activity, use of lipid mixtures to better mimic a real membrane and interaction with chitosans.

## 2. Methodology

Langmuir monolayers are obtained with instruments referred to as Langmuir troughs, with which a solution of an amphiphilic material is spread at the air-water interface. These Langmuir troughs are made of inert materials, usually Teflon, and contain movable barriers, one pressure sensor and one dipper. For monolayer formation, a small volume of a diluted solution of the selected compound in a volatile organic solvent (usually chloroform) is spread over the water surface. The barriers allow the area occupied to be varied and the dipper permits immersion of substrates for LB film deposition. The pressure sensor measures the surface pressure ( $\pi$ ), normally with the Wilhelmy method<sup>14</sup>. After solvent evaporation, the barriers

compress the molecules at a constant rate, which makes them oriented in relation to the water surface, with the hydrophobic portions facing air and hydrophilic portions in contact with the water. When the film is closely packed and continues to be compressed, collapse occurs with disordered layers being formed<sup>15</sup>. There are several methods to study the properties of a Langmuir monolayer. For various spectroscopic and microscopy methods and other *in situ* characterization techniques, the Langmuir trough is installed to give access to the measuring systems. In this review paper, we shall introduce methods which have been employed in Brazil or by Brazilian researchers in collaboration with international partners.

### 2.1 Surface pressure measurements

The most popular way to characterize Langmuir monolayers is to obtain the surface pressure-area ( $\pi$ -A) isotherm<sup>3</sup>. From the isotherms, one may determine the molecular area, monolayer phases, collapse behavior, compressibility and interaction with species in the subphase. The measurement is usually done in a pseudo-equilibrium condition, with a continuous compression of the monolayer while the surface pressure is monitored. Surface pressure is measured by either of two main methods: the Langmuir balance, which is a differential measurement, and the Wilhelmy plate, an absolute method that involves the forces acting on the plate (made of platinum or filter paper) partially immersed in the subphase<sup>3</sup>. The surface pressure ( $\pi$ ) is defined as the difference between the surface tension of one subphase in absence of the compound ( $\gamma_0$ ) and in the monolayer presence ( $\gamma$ ), as in Eq. 1:

$$\pi = \gamma_0 - \gamma \quad (1)$$

The minimum pressure is zero and the maximum is around 73 mN m<sup>-1</sup> (at 25 °C), which corresponds to the surface tension of pure water if the monolayer is stable<sup>14</sup>. The factors that affect the shape of surface-pressure isotherms include experimental conditions and chemical modification of the molecule's structures, such as their polarity, size and shape<sup>16</sup>. The analysis of surface pressure isotherms yields information on the collapse pressure and the compressibility modulus ( $C_S^{-1}$ )<sup>17</sup>. The latter allows one to characterize the state of the monolayers and the phase transitions, and may be calculated using Eq. 2:

$$C_S^{-1} = -A \frac{d\pi}{dA} \quad (2)$$

where  $A$  corresponds to the mean molecular area and  $\pi$  is the surface pressure.

## 2.2 Surface potential measurements

The surface potential ( $\Delta V$ ) technique has been utilized over decades with Langmuir monolayers. It is defined as the potential difference between an aqueous surface in the presence of a Langmuir monolayer and a surface without the monolayer. This measurement provides information about the dipole moments of the film-forming materials, in addition to changes in orientation of water molecules in the subphase and of the double-layer formed in ionized monolayers between the electrolytic subphase and the headgroups<sup>3</sup>. The measurement of surface potential is usually made with a Kelvin probe in a vibrating capacitor scheme. The surface potential changes when the film is compressed, owing to reorientation of the head or tail groups. Theoretical models have been used to relate the measured potentials with the dipole moments of the molecules. In one of these models<sup>18</sup>, the monolayer was considered as a three-layer capacitor, each layer with its “effective” dipole moment and local dielectric constant. As the interactions between the molecules are weak for large areas per molecule, the surface potential of the monolayer is zero. During monolayer compression, there is a critical area in which the potential is no longer null and increases rapidly with the decrease in area per molecule. It is worth mentioning that the surface potential is more sensitive to the organization of the Langmuir monolayers than the surface pressure<sup>14</sup>.

## 2.3 Fluorescence microscopy

Fluorescence microscopy is used to obtain structural information and study the dynamics of possible chemical and structural changes in Langmuir monolayers. The technique requires that molecules in the monolayer contain dyes or chromophores<sup>14</sup>, with an incident light (from the air or from the water) exciting the monolayer material or incorporated dyes. As the solubility of the fluorescent probe depends on the monolayer state, a contrast is originated upon changing these states<sup>3</sup>. Therefore, with fluorescence microscopy one may inspect the molecular aggregates and domains at different film compression stages. The analysis of fluorescence microscopy data may be difficult due to the possible segregation of probe molecules, which can form separate monolayer phases<sup>19</sup>. This occurs because a fluorescent amphiphilic molecule can be added to the

monolayer. Since this probe could act as an impurity in the monolayer, its solubility can vary in the coexisting phases. Also, significant are the possible photochemical transformations in the fluorescent probes, which should be accounted for<sup>20,21</sup>.

## 2.4 Brewster angle microscopy

Brewster angle microscopy (BAM) was reported in 1991, independently, by two groups: Hénon and Meunier from France and Hönig and Möbius from Germany<sup>21,22</sup>. Similarly to fluorescence microscopy, BAM allows the observation of the mesoscopic morphology and ordering of condensed phase domains<sup>23</sup>. One of the main advantages of BAM compared to fluorescence microscopy is that it does not require external probes, which means that the monolayers may be visualized on a mesoscopic scale without external interference<sup>24</sup>. Brewster angle microscopy also provides information about monolayer phases, packing of the molecules, phase transitions and chemical modifications<sup>25</sup>. The principle of BAM is based on reflection spectroscopy. The plane interface reflectivity between two media of refractive index ( $n_1$  and  $n_2$ ) depends on the polarization ( $\alpha$ ) of the incident light and on the angle of this incidence ( $\theta$ ). For  $p$  polarization (electric field in the plane of incidence) and considering a Fresnel interface, the reflectivity vanishes at the Brewster angle ( $\theta_B$ ), as indicated in Eq. 3:

$$\tan[\theta_B] = n_2/n_1 \quad (3)$$

Condensed monolayer phases affect the refractive index with measurable changes in reflectivity<sup>24</sup>. Three origins may be identified for the reflectivity: the thickness and roughness of the interface and the anisotropy of the monolayer<sup>21</sup>. For the air-water interface, the Brewster angle is  $53^\circ$  for  $p$  polarization light. When a monolayer is introduced, a new interface is formed and  $\alpha$  is changed. Thus, the light is reflected and can be observed with a microscope, which allows for monolayer visualization<sup>26,27</sup>.

## 2.5 Polarization modulation infrared reflection absorption spectroscopy (PM-IRRAS)

Spectroscopy in the infrared region allows one to investigate vibration modes of the chemical bonds. For Langmuir monolayers, it has become frequent to employ polarization-modulated infrared reflection absorption spectroscopy (PM-IRRAS). This method is

sensitive to the component of the perpendicular dipole moment in relation to the substrate<sup>14</sup>, thus yielding information on the orientation of film-forming molecules<sup>28,29</sup>. The importance of polarization modulation is related to the minimization of the absorption of the water vapor and making PM-IRRAS surface specific<sup>30</sup>. Polarization modulated infrared reflection absorption spectroscopy was developed around 1990 and has been utilized with metallic substrates as well as in Langmuir monolayers. It combines Fourier transform and mid-infrared reflection spectroscopy with polarization modulation of the incident beam with two-channel electronic and mathematical processing of the detected signal<sup>31</sup>. By alternating *s*- and *p*-polarizations in the impinging light at a high frequency using a photoelastic modulator, the reflectivity of both polarizations are detected. The difference between them yields surface specific information while their sum serves as reference. The ratio between the difference and sum is the PM-IRRAS signal, in which the gas phase absorbance is compensated<sup>32</sup>. With PM-IRRAS one may distinguish between in-plane and out-of-plane vibrations. For instance, positive bands correspond to the vibrations parallel to the water surface, while negative bands are due to vibration modes normal to the water surface<sup>3</sup>.

## 2.6 Sum-frequency generation

Sum-frequency generation spectroscopy (SFG) has been developed as a surface-specific technique for interfaces and surfaces<sup>33,34</sup>. As a second-order nonlinear optical process, SFG is forbidden under the electric-dipole approximation in media with centrosymmetry, and a signal is only measured when the inversion symmetry is broken<sup>35,36</sup>. Sum-frequency generation spectroscopy utilizes different input/output polarization combinations, which provide a great deal of structural information<sup>37</sup>, including for different Langmuir monolayer phases. A unique feature of SFG is the possibility to investigate the interfacial water layers, which can be affected by changes in ion concentration and pH<sup>38,39</sup>. In SFG, two input laser beams overlap to generate an output at a frequency which is the sum of the incoming frequencies. One frequency is visible while the infrared beam is tunable. When this infrared frequency approaches a surface resonance, the SFG output is enhanced and a spectrum of the surface or the interface is obtained<sup>40</sup>, in some cases identifying the chemical groups<sup>41</sup>. The vibrational spectrum is thus obtained with the detection of the light with summed frequencies<sup>42</sup>.

In general, infrared spectroscopy has enough sensitivity to detect a surface monolayer. However, the spectrum is usually complicated and the information about the conformation of the monolayer chain is indirect. In SFG, on the other hand, the spectra of the hydrocarbon chains are simplified by the intrinsic selection rules and they are sensitive to chain conformation, which means that they can be used to provide qualitative information about chain conformation<sup>40</sup>. The selection rules for sum frequency involve the asymmetric environment, and the asymmetry must be satisfied in molecular and macroscopic levels. On a macroscopic scale, the sum frequency is inactive, because isotropic distribution of molecules in the bulk phase is centrosymmetric. For interfacial molecules to be active, a net polar orientation is necessary, since no SFG signal is observed when the surface structure is completely disordered<sup>42,43</sup>.

## 2.7 X-ray techniques

The structure of Langmuir monolayers started to be investigated in detail in the 1980s when synchrotron light sources became available. With grazing incidence X-ray diffraction (GIXD) measurements, it was possible to determine the in-plane structures for the first time, including tilt directions and tilt angles with Angstrom resolution<sup>44</sup>. This technique is based on the total reflection phenomenon, in which the electromagnetic wave propagates at a critical angle along the boundary between two media and is totally reflected from the medium with the lower refractive index. The GIXD is highly surface sensitive because a monochromatic X-ray beam with a well-defined wavelength is used to focus the water surface at an angle  $\alpha_i$  (a value below the critical angle  $\alpha_c$  of total external reflection). The evanescent wave propagates along a top layer of only 8 nm. For a crystalline monolayer, the evanescent wave may be scattered from the lattice planes as in a Bragg scattering<sup>45</sup>. The types of information that may be obtained with GIXD include molecular organization in terms of unit cell dimensions and orientation of the molecules in relation to the interface.

In addition to GIXD, two other techniques have been important for the study of Langmuir monolayers: specular X-ray reflectivity (XR) and total reflection X-ray fluorescence (TRXF). With XR, one may probe non-structured liquid monolayers, which is not possible with GIXD. From XR experiments, the vertical structure of the monolayer may be determined, regardless of the phase state. The incident angle  $\alpha_i$  can

vary from 0.01 to  $0.8 \text{ \AA}^{-1}$  of the vertical scattering vector component (Eq. 4).

$$Q_z = (4\pi/\lambda) \sin(\alpha_f) \quad (4)$$

The background scattering from the subphase is measured at  $2\theta = 0.7^\circ$  and subtracted from the specular signal measured at  $2\theta = 0$ <sup>45</sup>.

Total reflection X-ray fluorescence is a simple method to characterize quantitatively the monolayers<sup>46</sup>. For the coupling between electron and X-ray to be efficient, the gap between the energy of the X-ray beam and the edge energy should not be too large, which means that the X-ray energy depends on the type of element to be detected. However, in some cases, the fluorescence process is inefficient and the radiation is much weaker than the primary beam. Hence, light elements cannot be detected because of instrumental limitations and low X-ray fluorescence yields. In TRXF, the measurement does not depend on the structure and monolayer composition, it depends on the experimental conditions, the fluorescence yield for a line and the X-ray absorbance of an element. The fluorescence intensity ( $I_i^f$ ) of an element  $I$  with a concentration profile  $c_i(z)$  (in the directional normal to the interface) is given in Eq. 5:

$$I_i^f = b_i \int I_{ex}(z) c_i(z) dz \quad (5)$$

where  $I_{ex}(z)$  corresponds to the exciting X-ray intensity at a distance  $z$  from the surface and  $b_i$  is a constant<sup>45</sup>.

### 3. Summary of recent results

The use of Langmuir monolayers as cell membrane models has continued as a popular topic, with more than 500 papers in indexed journals (in the Web of Science in July, 2020) over the last five years. For this review paper, we have chosen a few topics associated with drugs and biopolymers, which interactions with cell membranes are essential for their physiological action<sup>47</sup>.

The first topic is associated with pharmaceutical drugs which physiological action may be correlated with the ways they interact with cell membranes. Rodrigues et al.<sup>48</sup> investigated bacitracin, a drug used for treating minor wounds. Bacitracin is able to disrupt membrane models representing gram-positive and gram-negative bacteria. They observed that bacitracin is incorporated in 1,2-dipalmitoyl-*sn*-glycero-3-phospho-L-choline (DPPC), 1,2-dipalmitoyl-*sn*-glycero-3-phospho-(1'-*rac*-glycerol) (DPPG) and 1,2-

dipalmitoyl-*sn*-glycero-3-phospho-L-serine (DPPS) monolayers, and affects the monolayer morphology, as they showed in BAM images. The effects from bacitracin depended on the nature and microenvironment of the monolayer, as well as on the lipid polar head. For DPPC and DPPG, bacitracin expands the lipid monolayer, while for DPPS the drug condenses it. The observation that bacitracin interacted with the phospholipid monolayers at a surface pressure typical of a real membrane model (i.e. 30 – 35 mN/m) was of biological relevance<sup>48</sup>.

Węder et al.<sup>49</sup> studied 2-hydroxyoleic acid (2OHOA or Minerval) and its interaction with different membrane components, such as cholesterol, sphingomyelin and phosphatidylcholine<sup>50</sup>. They observed that the interactions between the lipids and the 2OHOA in the monolayer are more favorable when the monolayer is more fluid. The effects of 2OHOA depended on the condensation of monolayers mimicking lipid rafts; the ability of 2OHOA to destabilize and modify the morphology of the monolayers was suggested to be linked to its activity. Some classes of peptides are promising for killing bacteria, especially as they can disrupt bacteria membrane. This has motivated a number of studies with Langmuir monolayers<sup>51</sup>, including those from Prof. João Ruggiero<sup>52</sup>. In the latter study, the interaction of peptides was studied with Langmuir monolayers of DPPC, which was used to verify the influence of a peptide on lipid packing during the LE-LC coexistence plateau. Their results permitted to confirm that the subphase pH is an important parameter which modulates the peptide surface activity. Also relevant was the conclusion that the mutual lateral interaction could stabilize the peptides in the hydrophobic region of the membrane.

The importance of immobilizing enzymes in Langmuir and Langmuir-Blodgett films arises from the possible monitoring of catalytic activity at the molecular level<sup>13,53</sup>. Also significant is the finding that the environment provided by the lipid-enzyme architecture could conserve the catalytic activity for a long time<sup>54,55</sup>, which is interesting for biosensors. Rocha Junior and Caseli<sup>56</sup> studied the surface activity of the enzyme asparaginase at the air-water interface. Asparaginase is responsible for catalyzing the hydrolysis of asparagine to aspartic acid and ammonia and serves as an antitumorigenic agent<sup>57</sup>. They detected the formation of mixed asparaginase-DPPC monolayers using surface pressure and surface potential measurements and vibrational spectroscopy. Asparaginase decreased the lipid surface elasticity, increased the surface potential and condensed the

monolayer. When asparaginase was immobilized in phospholipid LB films, its activity was better preserved than in a homogeneous medium<sup>56</sup>.

An increased use of emerging pollutants with Langmuir monolayers has been noted for two main reasons. These pollutants have attracted considerable attention and their study in *in vivo* systems is difficult<sup>58</sup>. Alessio et al. investigated the interactions of the pollutants amoxicillin (AMX) and methylene blue (MB) with a simple membrane model consisting of DPPC monolayers<sup>59</sup>. Amoxicillin is an antibiotic of the penicillin family used to treat bacteria-related infections, and MB is a phenothiazine derivative used

as a medicine<sup>60</sup>, among other applications<sup>61</sup>. Amoxicillin and MB shifted the surface pressure of DPPC monolayers to larger areas and made these monolayers more compressible, as observed in Fig. 1. Even more important was the observation that a stronger effect occurred when the two pollutants were mixed, which was corroborated with PM-IRRAS data. This synergistic effect is in line with the problems reported about cooperative action of pollutants effects<sup>59</sup>.

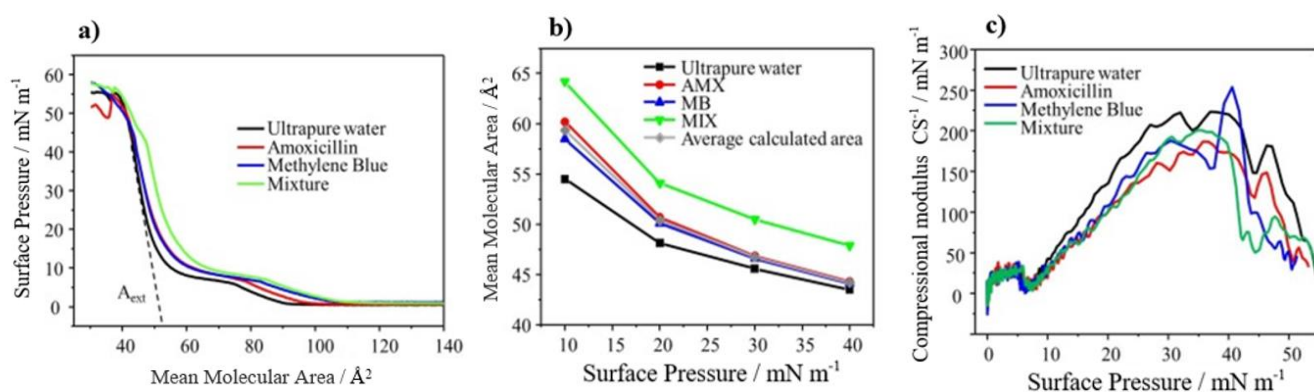


**Figure 1.** (a) Surface pressure isotherms of DPPC for  $10^{-4}$  mol/L subphases with AMX, MB and the mixture at 23 °C. (b) Modifications of the area induced by the subphases of AMX, MB and the mixture. (c) Compressional modulus versus surface pressure for DPPC monolayers obtained from the  $\pi$ -A isotherms. Reproduced from Maximino et al.<sup>59</sup> with Elsevier permission.

Another work related to pollutants by Węder et al.<sup>62</sup> involved the persistent organic pollutants polycyclic aromatic hydrocarbons (PAHs)<sup>63</sup> that can easily migrate in the environment. One way to eliminate PAHs is through bioremediation by using soil decomposer consortia in bacterial species capable of PAHs degradation<sup>64,65</sup>. However, the surface of the soil bacteria is hydrophilic, while PAHs are hydrophobic, so the direct contact between them is very limited. With this problem in mind, the authors proposed to study Langmuir monolayers from bacterial phospholipids as model membranes, as the studies in the literature are predominantly based on phosphatidylcholines (PC)<sup>66</sup>, which do not occur in this type of membrane. The lipid mixtures they used contained cardiolipin, phosphatidylglycerol and phosphatidyl ethanolamine. Six PAH molecules were employed, which showed different behaviors in contact with the monolayers. The results do not depend on the kind of the polar headgroup of the lipids. Polycyclic aromatic hydrocarbon molecules do not have any polar

groups and, therefore, they are incorporated between the hydrophobic chains of the phospholipid and interact with them, avoiding the hydrated regions of the monolayers. Based on the results for the various monolayers, Węder et al.<sup>62</sup> suggested that the toxicity of PAH molecules is directly related to their interactions with the membrane phospholipids.

One of the major challenges in the use of Langmuir monolayers as cell membrane models is to mimic the rich variety of membrane composition. For decades, most studies employed only neat phospholipids in the monolayers in order to make it simple. In recent years, attempts have been made to better mimic the membrane composition by using mixtures of lipids. Herein, we mention some contributions from the last four years in this topic. Sun et al.<sup>67</sup> used the mixtures of POPC/DPPC and POPC/DPPC/Chol (POPC is 1-palmitoyl-2-oleoyl-*sn*-glycero-3-phosphocholine and Chol is cholesterol) to investigate interactions with *Lycium barbarum* polysaccharides (LBP), natural biopolymers used in medicine and in the food industry<sup>68</sup>. A fewer number of LBP molecules

interacted with POPC/DPPC/Chol monolayers in comparison to POPC/DPPC monolayers, and  $C_S^{-1}_{max}$  was higher for the ternary mixture. These results indicated that the presence of cholesterol led to a more rigid, more stable membrane at the air-water interface. They were interpreted as considering that cholesterol protected the cell membrane from the effects of LBP. Another example of lipid mixtures in Langmuir monolayers included different proportions of Chol and sphingomyelin (SM) in a study of effects from the antimalarial drug cyclosporine A<sup>69</sup>. Cholesterol is known to affect membrane fluidity<sup>70,71</sup> and forms the so-called lipid rafts along with SM<sup>72,73</sup>. Wnętrzak et al.<sup>69</sup> observed that cyclosporine A was distributed on the monolayers in different ways, depending on the Chol-SM proportion. Cyclosporine A induces modifications in SM-Chol model membranes, especially in their mechanical properties. These modifications could affect the antimalarial activity of cyclosporine A, since this drug may disorganize SM-rich domains, which destabilizes the vacuolar membrane, preventing the development of parasites.

As already mentioned, Chol affects the conformational order and membrane permeability, thus regulating the lateral organization of membrane components<sup>13,70,72,74</sup>. This has been studied in detail on aminophospholipid membranes<sup>75</sup>. The isotherms and compressibility modulus depend on the Chol concentration, and the same applies to the molecular organization inferred from X-ray reflectivity measurements (XRR).

The third type of representative study of cell membrane models involves chitosans, which applications in medicine depend on their interactions with biomembranes. Owing to their biocompatibility and biodegradability, chitosans have been used in drug delivery<sup>76</sup> and as bactericidal agents<sup>77</sup>. Pavinatto et al.<sup>78</sup> investigated the interaction between two samples of chitosan with different molecular weights and zwitterionic (DPPC) and negatively charged (DPPG) phospholipids. The action of chitosan depends on three factors: degree of acetylation<sup>79,80</sup>, molecular weight<sup>81</sup> and functionalization<sup>82</sup>. The goal of this study was to show that smaller chitosan chains are more capable of penetrating into the membranes<sup>83</sup>. Both chitosans expanded the DPPC and DPPG monolayers and reduced their compressibility modulus, but the effects were more pronounced for the low molecular weight sample, as shown in Fig. 2. Furthermore, interaction was stronger with DPPG, owing to its negative charge. The reason why chitosans with lower molecular weight had more access to the monolayer was identified by dynamic light scattering measurements with the

chitosan solutions. Larger aggregates were observed for the high molecular weight chitosan, which hampered the access to the phospholipid hydrophobic tails<sup>78</sup>.

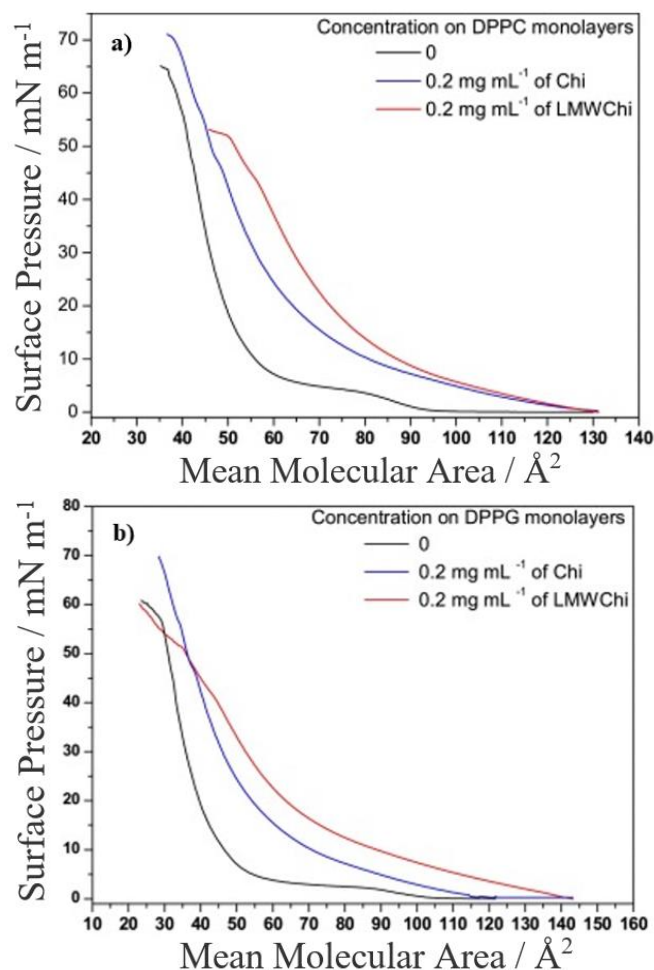


**Figure 2.** Surface pressure-area isotherms for (a) DPPC and (b) DPPG monolayers. Subphase: TS buffer pH 3.0 and 0.2 mg mL<sup>-1</sup> commercial chitosan (Chi) and lower molecular weight chitosan (LMWChi). Reproduced from Pavinatto et al.<sup>78</sup> with Elsevier permission.

Until recently, all the experiments with Langmuir monolayers were made with chitosans that were only soluble at acidic subphases. This has changed with the development of a novel strategy to produce chitosans soluble at a wide pH range with controllable degree of acetylation<sup>84</sup>. A chitosan with 35% acetylation degree (Ch35%) was made to interact with Langmuir monolayers of equimolar mixtures of (SM/DPPC/Chol) to mimic lipid rafts in cell membranes<sup>85</sup>. The most important observation was that interaction with such lipid rafts occurred at chitosan concentrations much



lower than reported in the literature, as shown in Fig. 3 for a subphase of phosphate buffer saline (PBS) solution. In fact, interaction with the SM/DPPC/Chol was always stronger than for the pure DPPC, and this applied not only to the high molecular weight Ch35%, but also for other types of chitosan. It is also worth noting that the interactions with SM/DPPC/Chol monolayers are even more pronounced for acidic subphases.

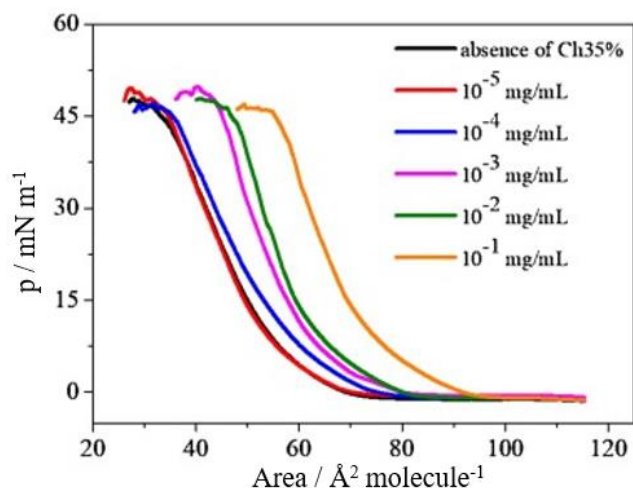


**Figure 3.** Surface pressure-area isotherms for monolayers of SM-DPPC-chol (1:1:1). Subphase: PBS (pH 7.4) containing Ch35% at different concentrations. Reproduced from Pereira et al.<sup>85</sup> with Elsevier permission.

#### 4. Final Remarks

The mimicking of cell membranes is, today, one of the most noble uses for Langmuir monolayers. In spite of the simplifications in the modeling, these monolayers are useful to obtain molecular-level information, which is virtually impossible with any other method. One may, for instance, identify the reasons why a peptide is effective against gram-positive bacteria, but not for gram-negative bacteria by simply verifying that the peptide cannot disrupt a Langmuir monolayer of lipopolysaccharide<sup>51</sup>. With the *in situ* vibrational spectroscopy techniques, on the other hand, it is possible to determine the chemical groups involved in the interactions between biologically-relevant molecules and the model membranes. While recent achievements in modeling are promising, some of which were discussed in this review paper, there are important challenges to move the field forward. In our view, the two most relevant hurdles are the need to use more complex mixtures of

lipids and other compounds to better mimic a real cell membrane and the need to understand the molecular-level interactions based on theoretical models. The latter has been addressed with molecular dynamics simulations<sup>86</sup>, but the results are still limited, owing to computational resources and to phenomena involving charge transfer that is difficult to simulate with classical methods.

#### Acknowledgments

The authors gratefully acknowledge the financial support from CNPq and FAPESP (project number 2018/22214-6) and the post-doctoral fellowship of A. R. Pereira (2018/00878-0).

#### References

- [1] Giner-Casares, J. J., Brezesinski, G., Möhwald, H., Langmuir monolayers as unique physical models, *Current Opinion in Colloid & Interface Science* 19 (3) (2014) 176-182. <https://doi.org/10.1016/j.cocis.2013.07.006>.
- [2] Stefaniu, C., Brezesinski, G., Möhwald, H., Langmuir monolayers as models to study processes at membrane surfaces, *Advances in Colloid and Interface Science* 208 (2014) 197-213. <https://doi.org/10.1016/j.cis.2014.02.013>.
- [3] Dynarowicz-Łatka, P., Dhanabalan, A., Oliveira Junior, O. N., Modern physicochemical research on Langmuir monolayers, *Advances in Colloid and Interface Science* 91 (2) (2001) 221-293. [https://doi.org/10.1016/S0001-8686\(99\)00034-2](https://doi.org/10.1016/S0001-8686(99)00034-2).
- [4] Yeagle, P., *The membrane of cells*, Academic Press, San Diego, 1993.
- [5] Petty, H. R., *Molecular biology of membranes: structure and function*, Springer, Boston, 1993. <https://doi.org/10.1007/978-1-4899-1146-9>.
- [6] RAYLEIGH, Surface tension, *Nature* 43 (1891) 437-439. <https://doi.org/10.1038/043437c0>.
- [7] Langmuir, I., The constitution and fundamental properties of solids and liquids. II. Liquids., *Journal of the American Chemical Society* 39 (9) (1917) 1848-1906. <https://doi.org/10.1021/ja02254a006>.
- [8] Nandi, N., Vollhardt, D., Chiral discrimination and recognition in Langmuir monolayers, *Current Opinion in Colloid & Interface Science*, 13 (1-2) (2008) 40-46. <https://doi.org/10.1016/j.cocis.2007.07.016>.
- [9] Blodgett, K. B., Langmuir, I., Built-Up Films of Barium Stearate and Their Optical Properties, *Physical Review* 51 (1937) 964-982. <https://doi.org/10.1103/PhysRev.51.964>.

- [10] Möbius, D., Kuhn, H., Monolayer assemblies of dyes to study the role of thermal collisions in energy-transfer, *Israel Journal of Chemistry* 18 (3-4) (1979) 375-384. <https://doi.org/10.1002/ijch.197900058>.
- [11] Phan, M. D., Shin, K., A Langmuir Monolayer: Ideal Model Membrane to Study Cell, *Journal of Chemical and Biological Interfaces* 2 (1) (2014) 1-5. <https://doi.org/10.1166/jcibi.2014.1028>.
- [12] Brockman, H., Lipid monolayers: why use half a membrane to characterize protein-membrane interactions? *Current Opinion in Structural Biology* 9 (4) (1999) 438-443. [https://doi.org/10.1016/S0959-440X\(99\)80061-X](https://doi.org/10.1016/S0959-440X(99)80061-X).
- [13] Nobre, T. M., Pavinatto, F. J., Caseli, L., Barros-Timmons, A., Dynarowicz-Łatka, P., Oliveira Junior, O. N., Interactions of bioactive molecules & nanomaterials with Langmuir monolayers as cell membrane models, *Thin Solid Films* 593 (2015) 158-188. <https://doi.org/10.1016/j.tsf.2015.09.047>.
- [14] Ferreira, M., Caetano, W., Itri, R., Tabak, M., Oliveira Junior, O. N., Técnicas de caracterização para investigar interações no nível moléculas em filmes de Langmuir e Langmuir-Blodgett (LB), *Química Nova* 28 (3) (2005) 502-510. <https://doi.org/10.1590/S0100-40422005000300024>.
- [15] Petty, M. C., *Langmuir-blodgett films: an introduction*, Cambridge University Press, Cambridge, 1996. <https://doi.org/10.1017/CBO9780511622519>.
- [16] Stenhagen, E., *Determination of organic structures by physical methods*, Academic Press, New York, 1955.
- [17] Wydro, P., Krajewska, B., Hąc-Wydro, K., Chitosan as a Lipid Binder: A Langmuir Monolayer Study of Chitosan-Lipid Interactions, *Biomacromolecules* 8 (2007) 2611-2617. <https://doi.org/10.1021/bm700453x>.
- [18] Demchak, R. J., Fort Junior, T., Surface dipole moments of close-packed monolayers at the air-water interface, *Journal of Colloid and Interface Science* 46 (1974) 191-202. [https://doi.org/10.1016/0021-9797\(74\)90002-2](https://doi.org/10.1016/0021-9797(74)90002-2).
- [19] Loschek, R., Möbius, D., Metalation of porphyrins in lipid monolayers at the air-water interface, *Chemical Physics Letters* 151 (1-2) (1988) 176-182. [https://doi.org/10.1016/0009-2614\(88\)80091-5](https://doi.org/10.1016/0009-2614(88)80091-5).
- [20] Rice, P. A., McConnell, H. M., Critical shape transitions of monolayer lipid domains, *Proceedings of the National Academy of Sciences of the United States of America* 86 (17) (1989) 6445-6448. <https://doi.org/10.1073/pnas.86.17.6445>.
- [21] Hénon, S., Meunier, J., Microscope at the Brewster angle: direct observation of first-order phase transitions in monolayers, *Review of Scientific Instruments* 62 (4) (1991) 936-939. <https://doi.org/10.1063/1.1142032>.
- [22] Hönig, D., Möbius, D., Brewster angle microscopy of LB films on solid substrates, *Chemical Physics Letters* 195 (1992) 50-52. [https://doi.org/10.1016/0009-2614\(92\)85909-T](https://doi.org/10.1016/0009-2614(92)85909-T).
- [23] Hönig, D., Möbius, D., Direct visualisation of monolayers at the air-water interface by Brewster angle microscopy, *The Journal of Physical Chemistry* 95 (12) (1991) 4590-4592. <https://doi.org/10.1021/j100165a003>.
- [24] Vollhardt, D., Brewster angle microscopy: A preferential method for mesoscopic characterization of monolayers at the air/water interface, *Current Opinion in Colloid & Interface Science* 19 (3) (2014) 183-197. <https://doi.org/10.1016/j.cocis.2014.02.001>.
- [25] Möbius, D., Light microscopy of organized monolayers, *Current Opinion in Colloid & Interface Science* 1 (2) (1996) 250-256. [https://doi.org/10.1016/S1359-0294\(96\)80012-4](https://doi.org/10.1016/S1359-0294(96)80012-4).
- [26] Kaercher, T., Hönig, D., Möbius, D., Brewster angle microscopy: a new method of visualizing the spreading of Meibomian lipids, *International Ophthalmology* 17 (6) (1993) 341-348. <https://doi.org/10.1007/BF00915741>.
- [27] Möbius, D., Morphology and structural characterization of organized monolayers by Brewster angle microscopy, *Current Opinion in Colloid & Interface Science* 3 (2) (1998) 137-142. [https://doi.org/10.1016/S1359-0294\(98\)80005-8](https://doi.org/10.1016/S1359-0294(98)80005-8).
- [28] Dluhy, R. A., Stephens, S. M., Widayati, S., Williams, A. D., Vibrational spectroscopy of biophysical monolayers. Applications of IR and Raman spectroscopy to biomembrane model systems at interfaces, *Spectrochimica Acta Part A-Molecular and Biomolecular Spectroscopy* 51 (8) (1995) 1413-1447. [https://doi.org/10.1016/0584-8539\(94\)00241-X](https://doi.org/10.1016/0584-8539(94)00241-X).
- [29] Mann, J. A., Dynamics, structure, and function of interfacial regions, *Langmuir* 1 (1) (1985) 10-23. <https://doi.org/10.1021/la00061a002>.
- [30] Blaudez, D., Turlet, J.-M., Dufourcq, J., Bard, D., Buffeteau, T., Desbat, B., Investigations at the air/water interface using polarization modulation IR spectroscopy, *Journal of the Chemical Society-Faraday Transactions* 92 (4) (1996) 525-530. <https://doi.org/10.1039/FT9969200525>.
- [31] Blaudez, D., Castano, S., Desbat, B., PM-IRRAS at liquid interfaces. In: *Biointerface Characterization by Advanced IR Spectroscopy*, Pradier, C. M., Chabal, Y. J., ed., Elsevier: Oxford, 2011, Ch. 2. <https://doi.org/10.1016/B978-0-444-53558-0.00002-3>.
- [32] Urakawa, A., Bürgi, T., Baiker, A., Modulation excitation PM-IRRAS: A new possibility for simultaneous monitoring of surface and gas species and surface properties,

- CHIMIA International Journal for Chemistry 60 (4) (2006) 231-233. <https://doi.org/10.2533/00094290677674949>.
- [33] Hunt, J. H., Guyot-sionnest, P., Shen, Y. R., Observation of C-H stretch vibrations of monolayers of molecules optical Sum-frequency generation, *Chemical Physics Letters* 133 (3) (1987) 189-192. [https://doi.org/10.1016/0009-2614\(87\)87049-5](https://doi.org/10.1016/0009-2614(87)87049-5).
- [34] Rasing, T., Shen, Y. R., Kim, M. W., Valint Junior, P., Bock, J., Orientation of surfactant molecules at a liquid-air interface measured by optical second-harmonic generation, *Physical Review A* 31 (1) (1985) 537-539. <https://doi.org/10.1103/PhysRevA.31.537>.
- [35] Shen, Y. R., *The principles of nonlinear optics*, Wiley and Sons, Hoboken, 2003.
- [36] Boyd, R. R., *Nonlinear optics*, Academic Press, San Diego, 2003.
- [37] Sung, W., Kim, D., Shen, Y. R. Sum-frequency vibrational spectroscopic studies of Langmuir monolayers, *Current Applied Physics* 13 (4) (2013) 619-632. <https://doi.org/10.1016/j.cap.2012.12.002>.
- [38] Miranda, P. B., Du, Q., Shen, Y. R., Interaction of water with a fatty acid Langmuir film, *Chemical Physics Letters* 286 (1-2) (1998) 1-8. [https://doi.org/10.1016/S0009-2614\(97\)01476-0](https://doi.org/10.1016/S0009-2614(97)01476-0).
- [39] Sung, W., Seok, S., Kim, D., Tian, C. S., Shen, Y. R., Sum-Frequency Spectroscopic Study of Langmuir Monolayers of Lipids Having Oppositely Charged Headgroups, *Langmuir* 26 (23) (2010) 18266-18272. <https://doi.org/10.1021/la103129z>.
- [40] Miranda, P. B., Shen, Y. R., *Liquid Interfaces: A Study by Sum-Frequency Vibrational Spectroscopy*, *Journal of Physical Chemistry B* 103 (17) (1999) 3292-3307. <https://doi.org/10.1021/jp9843757>.
- [41] Shultz, M. J., Baldelli, S., Schnitzer, C., Simonelli, D., Aqueous Solution/Air Interfaces Probed with Sum Frequency Generation spectroscopy, *Journal of Physical Chemistry B* 106 (21) (2002) 5313-5324. <https://doi.org/10.1021/jp014466v>.
- [42] Lambert, A. G., Davies, P. B., Neivandt, D. J., Implementing the theory of sum frequency generation vibrational spectroscopy: A tutorial review, *Applied Spectroscopy Reviews* 40 (2) (2005) 103-145. <https://doi.org/10.1081/ASR-200038326>.
- [43] Adamson, A. W., Gast, A. P., *Physical Chemistry of Surfaces*, John Wiley and Sons, New York, 1999.
- [44] Stefaniu, C., Brezesinski, G., Grazing incidence X-ray diffraction studies of condensed double-chain phospholipid monolayers formed at the soft air/water interface, *Advances in Colloid and Interface Science* 207 (2014) 265-279. <https://doi.org/10.1016/j.cis.2014.01.005>.
- [45] Stefaniu, C., Brezesinski, G., X-ray investigation of monolayers formed at the soft air/water interface, *Current Opinion in Colloid & Interface Science* 19 (3) (2014) 216-227. <https://doi.org/10.1016/j.cocis.2014.01.004>.
- [46] Shapovalov, V. L., Ryskin, M. E., Konovalov, O. V., Hermelink, A., Brezesinski, G., Elemental analysis within the electrical double layer using total reflection X-ray fluorescence technique, *Journal of Physical Chemistry B* 111 (15) (2007) 3927-3934. <https://doi.org/10.1021/jp066894c>.
- [47] Fischer, H. C., Chan, W. C. W., Nanotoxicity: the growing need for in vivo study, *Current Opinion in Biotechnology* 18 (6) (2007) 565-571. <https://doi.org/10.1016/j.copbio.2007.11.008>.
- [48] Rodrigues, J. C., Caseli, L., Incorporation of bacitracin in Langmuir films of phospholipids at the air-water interface, *Thin Solid Films* 622 (2017) 95-103. <https://doi.org/10.1016/j.tsf.2016.12.019>.
- [49] Węder, K., Mach, M., Hac-Wydro, K., Wydro, P., Studies on the interactions of anticancer drug - Minerval - with membrane lipids in binary and ternary Langmuir monolayers, *Biochimica et Biophysica Acta (BBA) - Biomembranes* 1860 (11) (2018) 2329-2336. <https://doi.org/10.1016/j.bbamem.2018.05.019>.
- [50] Torgersen, M. L., Klock, T. I., Kavaliauskiene, S., Klose, C., Simons, K., Skotland, T., Sandvig, K., The anti-tumor drug 2-hydroxyoleic acid (Minerval) stimulates signaling and retrograde transport, *Oncotarget* 7 (2016) 86871-86888. <https://doi.org/10.18632/oncotarget.13508>.
- [51] Barbosa, S. C., Nobre, T. M., Volpati, D., Cilli, E. M., Correa, D. S., Oliveira Junior, O. N., The cyclic peptide labaditin does not alter the outer membrane integrity of *Salmonella enterica* serovar Typhimurium, *Scientific Reports* 9 (2019) 1993. <https://doi.org/10.1038/s41598-019-38551-5>.
- [52] Alvares, D. S., Viegas, T. G., Ruggiero Neto, J., Lipid-packing perturbation of model membranes by pH-responsive antimicrobial peptides, *Biophysical Reviews* 9 (5) (2017) 669-682. <https://doi.org/10.1007/s12551-017-0296-0>.
- [53] Girard-Egrot, A. P., Godoy, S., Blum, L. J., Enzyme association with lipidic Langmuir-Blodgett films: Interests and applications in nanobioscience, *Advances in Colloid and Interface Science* 116 (1-3) (2005) 205-225. <https://doi.org/10.1016/j.cis.2005.04.006>.
- [54] Scholl, F. A., Caseli, L., Langmuir and Langmuir-Blodgett films of lipids and penicillinase: Studies on adsorption and enzymatic activity, *Colloids and Surfaces B:*

- Biointerfaces 126 (2015) 232-236. <https://doi.org/10.1016/j.colsurfb.2014.12.033>.
- [55] Araújo, F. T. de, Caseli, L., Rhodanese incorporated in Langmuir and Langmuir-Blodgett films of dimyristoylphosphatidic acid: Physical chemical properties and improvement of the enzyme activity, *Colloids and Surfaces B: Biointerfaces* 141 (2016) 59-64. <https://doi.org/10.1016/j.colsurfb.2016.01.037>.
- [56] Rocha Junior, C., Caseli, L., Adsorption and enzyme activity of asparaginase at lipid Langmuir and Langmuir-Blodgett films, *Materials Science & Engineering: C* 73 (2017) 579-584. <https://doi.org/10.1016/j.msec.2016.12.041>.
- [57] Broome, J. D., L-asparaginase: discovery and development as a tumor-inhibitory agent, *Cancer Treatment Reports* 65 (Suppl. 4) (1981) 111-114.
- [58] Makyla, K., Paluch, M., The linoleic acid influence on molecular interactions in the model of biological membrane, *Colloids and Surfaces B: Biointerfaces* 71 (1) (2009) 59-66. <https://doi.org/10.1016/j.colsurfb.2009.01.005>.
- [59] Maximino, M. D., Constantino, C. J. L., Oliveira Junior, O. N., Alessio, P., Synergy in the interaction of amoxicillin and methylene blue with dipalmitoyl phosphatidyl choline (DPPC) monolayers, *Applied Surface Science* 476 (2019) 493-500. <https://doi.org/10.1016/j.apsusc.2019.01.065>.
- [60] Tawfik, A. A., Noaman, I., El-Elsayyad, H., El-Mashad, N., Soliman, M., A study of the treatment of cutaneous fungal infection in animal model using photoactivated composite of methylene blue and gold nanoparticle, *Photodiagnosis and Photodynamic Therapy* 15 (2016) 59-69. <https://doi.org/10.1016/j.pdpdt.2016.05.010>.
- [61] Zakaria, A., Hamdi, N., Abdel-Kader, R. M., Methylene Blue Improves Brain Mitochondrial ABAD Functions and Decreases A $\beta$  in a Neuroinflammatory Alzheimer's Disease Mouse Model, *Molecular Neurobiology* 53 (2) (2016) 1220-1228. <https://doi.org/10.1007/s12035-014-9088-8>.
- [62] Broniatowski, M., Binczycka, M., Wójcik, A., Flasiński, M., Wydro, P., Polycyclic aromatic hydrocarbons in model bacterial membranes - Langmuir monolayer studies, *Biochimica et Biophysica Acta (BBA) – Biomembranes* 1859 (12) (2017) 2402-2412. <https://doi.org/10.1016/j.bbamem.2017.09.017>.
- [63] Purcaro, G., Moret, S., Conte, L. S., Overview on polycyclic aromatic hydrocarbons: Occurrence, legislation and innovative determination in foods, *Talanta* 105 (2013) 292-305. <https://doi.org/10.1016/j.talanta.2012.10.041>.
- [64] Macrae, J. D., Hall, K. J., Comparison of methods used to determine the availability of polycyclic aromatic hydrocarbons in marine sediment, *Environmental Science & Technology* 32 (23) (1998) 3809-3815. <https://doi.org/10.1021/es980165w>.
- [65] Kanaly, R. A., Harayama, S., Advances in the field of high-molecular-weight polycyclic aromatic hydrocarbon biodegradation by bacteria, *Microbial Biotechnology* 3 (2) (2010) 136-164. <https://doi.org/10.1111/j.1751-7915.2009.00130.x>.
- [66] Korchowiec, B., Corvis, Y., Viitala, T., Feidt, C., Guiavarch, Y., Corbier, C., Rogalska, E., Interfacial Approach to Polyaromatic Hydrocarbon Toxicity: Phosphoglyceride and Cholesterol Monolayer Response to Phenanthrene, Anthracene, Pyrene, Chrysene, and Benzo[a]pyrene, *Journal of Physical Chemistry B* 112 (43) (2008) 13518-13531. <https://doi.org/10.1021/jp804080h>.
- [67] Zhang, Z. Y., Hao, C. C., Liu, H. Y., Zhang, X. G., Sun, R. G., Cholesterol mediates spontaneous insertion of *Lycium barbarum* polysaccharides in biomembrane model, *Adsorption* 26 (6) (2020) 855-862. <https://doi.org/10.1007/s10450-019-00180-9>.
- [68] Ahn, M., Park, J. S., Chae, S., Kim, S., Moon, C., Hyun, J. W., Shin, T., Hepatoprotective effects of *Lycium chinense* Miller fruit and its constituent betaine in CCl<sub>4</sub>-induced hepatic damage in rats, *Acta Histochemica* 116 (6) (2014) 1104-1112. <https://doi.org/10.1016/j.acthis.2014.05.004>.
- [69] Wnętrzak, A., Makyła-Juzak, K., Chachaj-Brekiesz, A., Lipiec, E., Romeu, N. V., Dynarowicz-Latka, P., Cyclosporin A distribution in cholesterol-sphingomyelin artificial membranes modeled as Langmuir monolayers, *Colloids and Surfaces B: Biointerfaces* 166 (2018) 286-294. <https://doi.org/10.1016/j.colsurfb.2018.03.031>.
- [70] Barenholz, Y., Cholesterol and other membrane active sterols: from membrane evolution to "rafts", *Progress in Lipid Research* 41 (1) (2002) 1-5. [https://doi.org/10.1016/S0163-7827\(01\)00016-9](https://doi.org/10.1016/S0163-7827(01)00016-9).
- [71] Ohvo-Rekilä, H., Ramstedt, B., Leppimäki, P., Slotte, J. P., Cholesterol interactions with phospholipids in membranes, *Progress in Lipid Research* 41 (1) (2002) 66-97. [https://doi.org/10.1016/S0163-7827\(01\)00020-0](https://doi.org/10.1016/S0163-7827(01)00020-0).
- [72] Crane, J. M., Tamm, L. M., Role of cholesterol in the formation and nature of lipid rafts in planar and spherical model membranes, *Biophysical Journal* 86 (5) (2004) 2965-2979. [https://doi.org/10.1016/S0006-3495\(04\)74347-7](https://doi.org/10.1016/S0006-3495(04)74347-7).
- [73] Fan, J., Sammalkorpi, M., Haataja, M., Formation and regulation of lipid microdomains in cell membranes: Theory, modeling, and speculation, *FEBS Letters* 584 (9) (2010) 1678-1684. <https://doi.org/10.1016/j.febslet.2009.10.051>.

- [74] Leslie, M., Do lipid rafts exist? *Science* 334 (6059) (2011) 1046-1047. <https://doi.org/10.1126/science.334.6059.1046-b>.
- [75] Giri, R. P., Chakrabarti, A., Mukhopadhyay, M. K., Cholesterol-Induced Structural Changes in Saturated Phospholipid Model Membranes Revealed through X-ray Scattering Technique, *Journal of Physical Chemistry B* 121 (16) (2017) 4081-4090. <https://doi.org/10.1021/acs.jpcc.6b12587>.
- [76] Gupta, K. C., Kumar, M. N. V. R., An Overview on Chitin and Chitosan Applications with an Emphasis on Controlled Drug Release Formulations, *Journal of Macromolecular Science, Part C* 40 (4) (2000) 273-308. <https://doi.org/10.1081/MC-100102399>.
- [77] Liu, H., Du, Y., Wang, X., Sun, L., Chitosan kills bacteria through cell membrane damage, *International Journal of Food Microbiology* 95 (2) (2004) 147-155. <https://doi.org/10.1016/j.ijfoodmicro.2004.01.022>.
- [78] Pavinatto, A., Delezuk, J. A. M., Souza, A. L., Pavinatto, F. J., Volpati, D., Miranda, P. B., Campana-Filho, S. P., Oliveira Junior, O. N., Experimental evidence for the mode of action based on electrostatic and hydrophobic forces to explain interaction between chitosans and phospholipid Langmuir monolayers, *Colloids and Surfaces B: Biointerfaces* 145 (2016) 201-207. <https://doi.org/10.1016/j.colsurfb.2016.05.001>.
- [79] Younes, I., Sellimi, S., Rinaudo, M., Jellouli, K., Nasri, M. Influence of acetylation degree and molecular weight of homogeneous chitosans on antibacterial and antifungal activities, *International Journal of Food Microbiology* 185 (2014) 57-63. <https://doi.org/10.1016/j.ijfoodmicro.2014.04.029>.
- [80] Mellegård, H., Strand, S. P., Christensen, B. E., Granum, P. E., Hardy, S. P., Antibacterial activity of chemically defined chitosans: Influence of molecular weight, degree of acetylation and test organism, *International Journal of Food Microbiology* 148 (1) (2011) 48-54. <https://doi.org/10.1016/j.ijfoodmicro.2011.04.023>.
- [81] Krajewska, B., Wydro, P., Janczyk, A., Probing the Modes of Antibacterial Activity of Chitosan. Effects of pH and Molecular Weight on Chitosan Interactions with Membrane Lipids in Langmuir Films, *Biomacromolecules* 12 (11) (2011) 4144-4152. <https://doi.org/10.1021/bm2012295>.
- [82] Badawy, M. E. I., Rabea, E. I., Taktak, N. E. M., Antimicrobial and inhibitory enzyme activity of N-(benzyl) and quaternary N-(benzyl) chitosan derivatives on plant pathogens, *Carbohydrate Polymers* 111 (2014) 670-682. <https://doi.org/10.1016/j.carbpol.2014.04.098>.
- [83] Pavinatto, A., Pavinatto, F. J., Delezuk, J. A. D., Nobre, T. M., Souza, A. L., Campana-Filho, S. P., Oliveira Junior, O. N., Low molecular-weight chitosans are stronger biomembrane model perturbants, *Colloids and Surfaces B: Biointerfaces* 104 (2013) 48-53. <https://doi.org/10.1016/j.colsurfb.2012.11.047>.
- [84] Fiamingo, A., Oliveira Junior, O. N., Campana-Filho, S. C., Tuning the properties of high molecular weight chitosans to develop full water solubility within a wide pH range, *ChemRxiv* (2020). Preprint. <https://doi.org/10.26434/chemrxiv.11854293.v1>.
- [85] Pereira, A. R., Fiamingo, A., Pedro, R. O., Campana-Filho, S. P., Miranda, P. B., Oliveira Junior, O. N., Enhanced chitosan effects on cell membrane models made with lipid raft monolayers, *Colloids and Surfaces B: Biointerfaces* 193 (2020) 111017. <https://doi.org/10.1016/j.colsurfb.2020.111017>.
- [86] Mendonca, C. M. N., Balogh, D. T., Barbosa, S. C., Sintra, T. E., Ventura, S. P. M., Martins, L. F. G., Morgado, P., Filipe, E. J. M., Coutinho, J. A. P., Oliveira Junior, O. N., Barros-Timmons, A., Understanding the interactions of imidazolium-based ionic liquids with cell membrane models, *Physical Chemistry Chemical Physics* 20 (47) (2018) 29764-29777. <https://doi.org/10.1039/C8CP05035J>.

## Dengue fusion peptides in interaction with model membranes – a fluorescence study

Danilo da Silva Olivier<sup>1,2</sup>, Graziely Ferreira Cespedes<sup>3</sup>, Wallance Moreira Pazin<sup>1,4</sup>, Eduardo Maffud Cilli<sup>3</sup>, Amando Siuiti Ito<sup>1+</sup>

1. University of São Paulo, Faculty of Philosophy, Sciences and Letters of Ribeirão Preto, Ribeirão Preto, Brazil.
2. Universidade Federal do Tocantins, Araguaína Campus, Araguaína, Brazil.
3. São Paulo State University, Institute of Chemistry, Araraquara, Brazil.
4. São Paulo State University, School of Technology and Applied Sciences, Presidente Prudente, Brazil.

**+Corresponding author:** Amando Siuiti Ito, **Phone:** +55 11 3021-4574, **Email address:** [amandosi@ffclrp.usp.br](mailto:amandosi@ffclrp.usp.br)

### ARTICLE INFO

#### Article history:

**Received:** July 01, 2020

**Accepted:** October 19, 2020

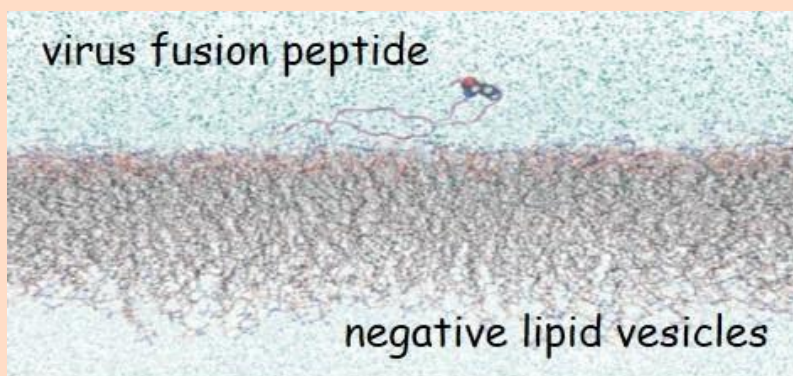
**Published:** April xx, 2021

#### Keywords

1. dengue virus peptide
2. lipid peptide interaction
3. fluorescence spectroscopy
4. vesicles diffusion coefficient

**ABSTRACT:** Dengue fever is a widespread infectious disease caused by Dengue viruses and responsible for millions of cases per year. One of the key steps during the infection is the fusion between the cell membrane and the lipidic bilayer of the virus, done by the glycoprotein envelope. At the tip of the envelope there is a fusion peptide widely conserved among the four known virus serotypes. Here dengue fusion peptides were studied in buffer solution and interacting with

model membranes using fluorescence techniques. Peptides have the tryptophan residue exposed to aqueous environment when in buffer, while is exposed to a hydrophobic environment when interacting with negatively charged vesicles, as shown by the blue shift of fluorescence emission and increase in the lifetime decay. Fluorescence anisotropy results confirm that the residue is in a more restrictive environment when interacting with vesicles. Finally, fluorescence correlation spectroscopy results support the importance of electrostatic interaction, showing that dengue peptide promotes a significant increase in diameter of negatively charged vesicles, compared to the absence of effect in the size of neutral vesicles.



## 1. Introduction

Dengue fever is an infectious disease spread in tropical and subtropical areas of the world, affecting around 2 billion people and causing as many as 100 million cases each year<sup>1,2</sup>. The disease is caused by the dengue virus, a member of the Flaviviridae family, a group of enveloped viruses containing a positive-sense single-stranded RNA genome. The viral particle contains three structural proteins – capsid, membrane precursor and envelope glycoprotein protein (E) – and seven non-structural proteins<sup>3,4</sup>. As for other enveloped viruses, dengue virus infection depends on a step involving the fusion of the viral envelope with the cell membrane promoted by the envelope glycoprotein E<sup>5,6</sup>.

The glycoprotein E is a dimer complex with 495 amino acids in each subunit, which, under acidic conditions, undergoes a structural change, exposing the fusion peptide and forming a trimer<sup>7–10</sup>. The segment between residues 98 and 112, called fusion peptide, forms a loop in domain II of glycoprotein E and inserts into the cell membrane<sup>7,9,11,12</sup> in the interaction step between the flavivirus and the host cell. The same sequence is present in the four dengue virus serotypes, which differ by the amino acid sequences flanking the fusion peptide. Dengue virus serotype II is associated with severe symptoms in humans, and the extended sequence 88–123, has been studied, trying to understand the process of fusion with membranes (Fig. 1).

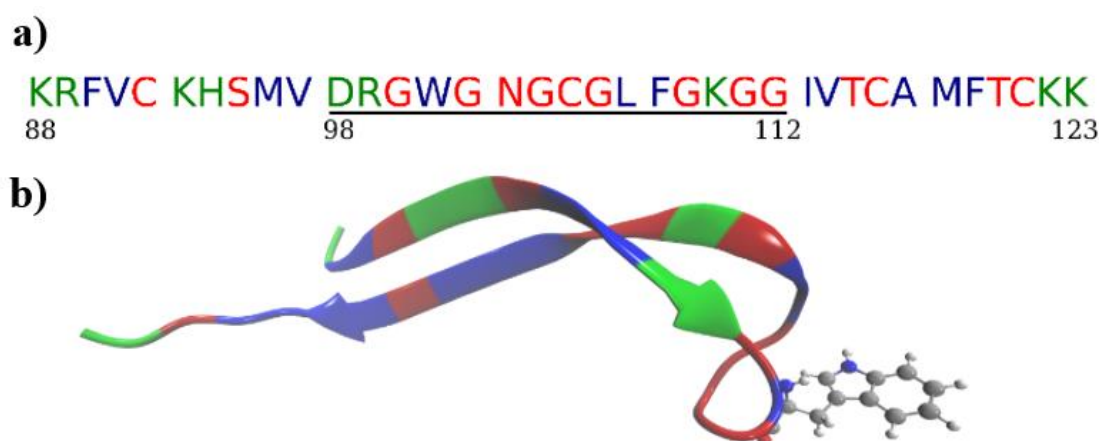


**Figure 1.** (a) Amino acid sequence of serotype II dengue virus fusion peptide (88–123); the sequence 98–112 is underlined, charged polar residues are indicated in green, hydrophobic residues are in blue and non-charged polar are in red. (b) Dengue peptide and tryptophan in new cartoon and CPK representation, respectively. Color code is the same as presented in (a). PDB ID:1OK8<sup>3</sup>.

The peptide has a Trp residue in position 101 of the sequence, allowing its direct observation by fluorescence spectroscopy. In this study, we examined the fusion loop peptide and three other peptides from dengue virus serotype II: the long sequence 88–123, the amino flank 88–111 and the carboxy flank 98–123. Due to the involvement in the process of virus fusion with cell membranes, we report here the analysis of the peptides in a buffer medium and interacting with model membranes using fluorescence spectroscopy techniques. As model membranes, we used small unilamellar vesicles (SUVs) of neutral lipid 1,2-dimyristoyl-*sn*-glycero-3-phosphocoline (DMPC) and negative 1,2-dimyristoyl-*sn*-glycero-3-phosphoglycerol (DMPG). We also used large unilamellar vesicles (LUVs) of neutral lipid 1,2-dipalmitoyl-*sn*-glycero-3-phosphocoline (DPPC) and negatively charged 1,2-dipalmitoyl-*sn*-glycero-3-phosphoglycerol (DPPG).

## 2. Experimental

### 2.1 Peptides synthesis

Peptides were manually prepared using solid phase peptide synthesis by the 9-fluorenylmethoxycarbonyl (Fmoc) procedure<sup>13</sup>. Ninhydrin test was used to monitor each coupling/deprotection steps. Amino acids were purchased in Nova Biochem Corp Synpep or Advanced Chem Tech (USA). PA solvents were acquired from LabSynth and Acros Organics (USA). Purification of products of synthesis was performed by preparative high performance liquid chromatography (HPLC) using C18 Phenomenex column. After the purification, peptides were characterized by analytical HPLC and mass spectrometry.

## 2.2 Preparation of model membranes

The lipids DMPC, DMPG, DPPC and DMPG were purchased from Avanti Polar Lipids (Alabaster, AL, USA) as powder. The fluorescent probe 1,19-dioctadecyl-3,3,39,39-tetramethylindocarbocyanine perchlorate (DiIC18) was from Molecular Probes (Eugene, OR, USA). All the reagents were used without further purification.

Small unilamellar vesicles films of DMPC and DMPG were prepared in standard test tubes by diluting the lipid in 20–30  $\mu\text{L}$  of chloroform, followed by evaporation of the solvent in a stream of  $\text{N}_2$ . After this step, the tube is left under reduced pressure for 2 h. Lipid dispersions were prepared by adding citrate buffer up to final concentration equal to 1  $\text{mmol L}^{-1}$  lipid in 2 mL citrate buffer (10  $\text{mmol L}^{-1}$ , pH 5.4). After vortexing in temperature above the lipid gel-fluid transition, the content was transferred into a Falcon with volume of 50 mL.

The SUVs were prepared by sonication of the lipid dispersion using the Vibracell VC-600 sonicator, with 1/2 in (13 mm) probe tip. The amplitude used during the sonication was set to 37%. To measure the particle size, we used the Beckman coulter - N5 submicron particle size analyzer. The analysis was made by counts to obtain the percentage distribution and size of the particles.

Large unilamellar vesicles were prepared from stock solutions of DPPC and DPPG in chloroform at 40  $\text{mmol L}^{-1}$ . Dry films emerged by evaporating the solvent under a  $\text{N}_2$  flow and eliminating the remaining traces of organic solvent under reduced pressure for at least 3 h. Multilamellar vesicles (MLVs) were prepared by adding Milli-Q water onto the films and vortexing them at 45  $^\circ\text{C}$  for 2 min above the phase transition temperature of DPPC. Subsequent extrusion afforded the LUVs, as described elsewhere<sup>14,15</sup>. The MLVs suspension was passed through a polycarbonate membrane with pores measuring 0.1  $\mu\text{m}$  (Whatman, Sigma Aldrich) at least 21 times.

## 2.3 Optical absorption and fluorescence apparatus

An Amersham Ultrospec 2100 pro spectrophotometer was used to obtain optical absorption spectra. Steady-state fluorescence measurements were made in a Hitachi F-7000 spectrofluorometer; internal calibration was performed to correct the emission spectra intensity, and polarizer filters were employed for anisotropy experiments.

Fluorescence intensity decays, and time-resolved anisotropy measurements were recorded on a picosecond laser system operating in the time-correlated single-photon counting mode. The excitation source was a mode-locked Ti:sapphire laser (Tsunami 3950, pumped by Millennia X, Spectra Physics), which produced laser pulses with 5.0-ps Full Width at Half Maximum (FWHM). The pulse repetition rate was adjusted to 8.0 MHz using the 3980 Spectra Physics pulse picker. The laser wavelength was selected with a third harmonic generator (BBO crystal, GWN-23PL Spectra Physics), yielding 295 nm excitation pulses that were directed to an L-format Edinburgh FL900 spectrometer with a monochromator in the emission channel. Single photons were detected by a cooled Hamamatsu R3809U microchannel plate photomultiplier, and the instrument response function was  $\sim 100$  ps. In anisotropy experiments, a Soleil–Babinet compensator and a Glann–Taylor polarizer were used in the excitation and emission beam, respectively. Data were analyzed by using a commercial software (Edinburgh Instruments) based on nonlinear least squares method. The quality of the fit was judged by the reduced  $\chi^2$  values and the residuals distribution.

## 2.4 Fluorescence correlation spectroscopy

Fluorescence correlation spectroscopy (FCS) experiments were performed in the PicoQuant MicroTime 200 instrument, which combined confocal optics (Olympus IX-71 inverted microscope) with pulsed excitation and time resolved data acquisition along with a highly sensitive avalanche photodiode detector. A pulsed diode laser operating at an excitation wavelength of 530 nm was employed, and detection was accomplished using a bandpass filter to collect light with a wavelength above 550 nm to remove scattered light. The samples were examined in a microscope slide, where a very small fluorescent volume was selected, and fluctuations in emission were collected. Using the software provided by PicoQuant, FCS measurements allowed determination of the autocorrelation function  $G(t)$  for the fluorescence emission.

## 3. Results and discussion

### 3.1 Peptides synthesis

The sequence of the peptides obtained in the synthesis and used in this work are presented in [Tab. 1](#).



The peptides contain serine residues in substitution to cysteine in position 92, 105, 116 and 121. The cysteine residues were replaced by serine residues to avoid

dimerization. In previous study, it was verified that this modification did not promote difference in fusion activity<sup>16</sup>.

**Table 1.** Peptides sequence.

| Peptide          | Sequence                              |    |     |     |
|------------------|---------------------------------------|----|-----|-----|
|                  | 88                                    | 98 | 112 | 123 |
| DEN II 98-112    | DRGWGNGSGLFGKGG                       |    |     |     |
| DEN II 98-123    | DRGWGNGSGLFGKGG VTSAMFRSKK            |    |     |     |
| DEN2NC II 88-123 | KRFVSKHSMV DRGWGNGSGLFGKGG VTSAMFRSKK |    |     |     |
| DEN2N II 88-111  | KRFVSKHSMV DRGWGNGSGLFGKGG            |    |     |     |

### 3.2 Fluorescence of peptides in buffer

#### 3.2.1 Emission spectra

The peptides in citrate buffer (10 mM, pH 5.4) solution presented absorption centered in 280 nm due to the presence of tryptophan residue. Under excitation at 290 nm, the maximum of fluorescence emission was observed at 358 nm for DEN II 98–112 and DEN II 98–123 peptides and at 356 nm for DEN II 88–111 and DEN II 88–123 peptides. The fluorescence spectra are typical of emission from tryptophan immersed in a polar environment (Fig. 2). Thus, the spectra observed for all peptides in citrate buffer solution indicate that the tryptophan residue in DEN II is exposed to the aqueous environment, independent of the sequences flanking the 98–112 fusion loop peptide.

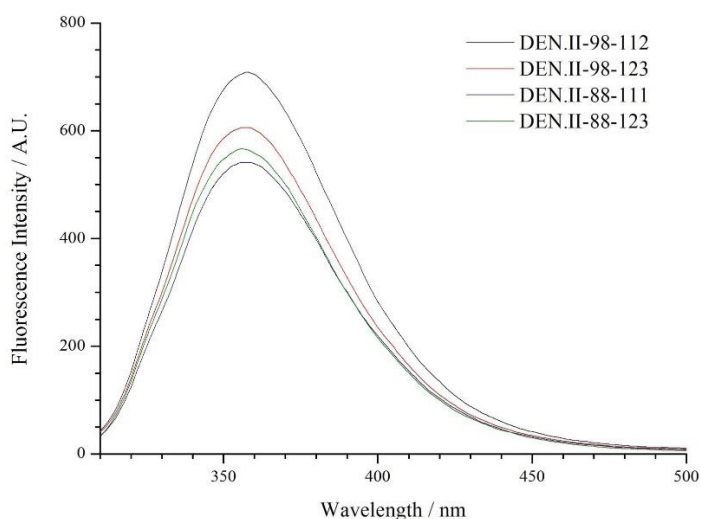


**Figure 2.** Fluorescence emission of dengue peptides in citrate buffer pH 5.4. Peptide concentration 15  $\mu\text{mol L}^{-1}$ , excitation 290 nm.

#### 3.2.2 Time-resolved emission

Time-intensity  $I(t)$  decays of all peptides measured at 350 nm were complex, and the experimental data were fitted to multi-exponential curves (Eq. 1):

$$I(t) = I_0 \sum_i \alpha_i e^{-\frac{t}{\tau_i}} \quad (1)$$

where  $I_0$  is the initial intensity, and  $\alpha_i$  and  $\tau_i$  are the normalized pre-exponential factor and the lifetime of component  $i$  of the intensity decay, respectively. The best fit of intensity decay profiles of peptides in citrate buffer pH 5.4 was obtained using three exponential functions, as usually found in peptides containing tryptophan (Fig. 3).

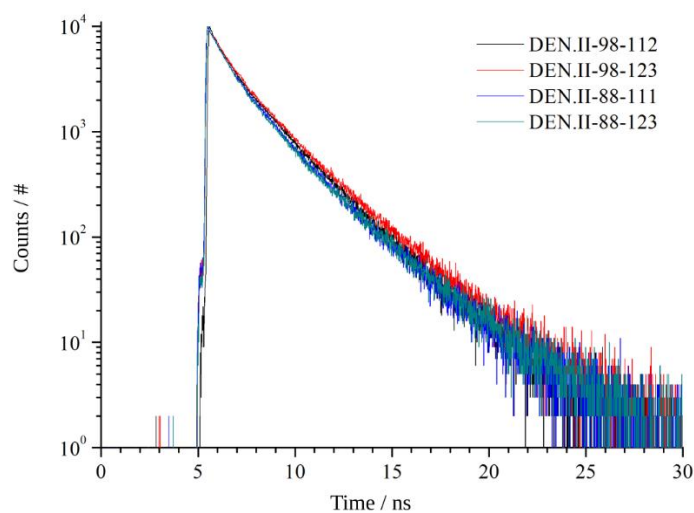


**Figure 3.** Time-resolved fluorescence decay for dengue II fusion peptides in citrate buffer pH 5.4. Excitation 290 nm, temperature 45 °C.

The occurrence of three lifetimes in the decay of peptides was attributed to the presence of different rotational conformers of the indole ring around the  $C_\alpha$ - $C_\beta$  bond of the alanyl side chain: in the  $g^+$  (gauche plus) rotamers of Trp in the peptide chain, electron

transfer processes predominate over fluorescence emission<sup>17</sup>, leading to sub-nanosecond lifetime component. In the fitted curve for DEN II peptides, the value of the long lifetime component was around 3.0 ns, and the intermediate component was circa 1.5 ns;

the sub-nanosecond component around 0.3 ns was necessary to fit the experimental decay (Tab. 2). The values are within those usually found in peptides, where the Trp residue is exposed to aqueous solvent<sup>18-21</sup>.

**Table 2.** Time-resolved data from fit of intensity decay to three exponential curves: lifetime components ( $\tau_i$ ) and normalized pre-exponential factors ( $\alpha_i$ ). Peptides in citrate buffer solution, pH 5.4. Concentration 15  $\mu\text{mol L}^{-1}$  excitation 290 nm, emission at 350 nm. Temperature 45 °C.

| Peptide       | Lifetime      |               |               | Norm. pre-exponential |            |            | Average                   |
|---------------|---------------|---------------|---------------|-----------------------|------------|------------|---------------------------|
|               | $\tau_1$ / ns | $\tau_2$ / ns | $\tau_3$ / ns | $\alpha_1$            | $\alpha_2$ | $\alpha_3$ | $\langle\tau\rangle$ / ns |
| DEN II 98-112 | 2.88          | 1.47          | 0.25          | 0.15                  | 0.49       | 0.36       | 1.87                      |
| DEN II 98-123 | 3.23          | 1.56          | 0.39          | 0.15                  | 0.58       | 0.27       | 2.02                      |
| DEN II 88-111 | 3.62          | 1.53          | 0.26          | 0.05                  | 0.63       | 0.32       | 1.75                      |
| DEN II 88-123 | 3.77          | 1.45          | 0.28          | 0.06                  | 0.64       | 0.30       | 1.79                      |

The normalized pre-exponential factor for the short component was around 0.30 for all peptides. However, we can notice that the long lifetime component of the peptides with the amino flanking sequence (88–111 and 88–123) presents lower contribution to the decay (normalized pre-exponential around 0.05) compared to the fusion loop peptide (98–112) and the peptide with carboxy flanking sequence (98–123).

From the definition of mean values, the average lifetime  $\langle\tau\rangle$  was calculated from individual lifetimes and corresponding pre-exponential factors according to Eq. 2:

$$\langle\tau\rangle = \frac{\sum_i \alpha_i \tau_i^2}{\sum_i \alpha_i \tau_i} \quad (2)$$

It is observed that smaller values of average lifetime correspond to the amino flanking peptides. The interaction of Trp with charged residues Arg, Lys and His may contribute to nonradiative de-excitation rate and subsequent decrease in fluorescent emission lifetime.

### 3.2.3 Quenching of fluorescence emission

The steady-state fluorescence emission intensity of peptides tryptophan decreased upon the addition of acrylamide into the solution. The decrease in intensity with increase in the concentration of quencher can be described by the Stern–Volmer equation (Eq. 3):

$$\frac{F_o}{F} = 1 + K_{SV}[Q] \quad (3)$$

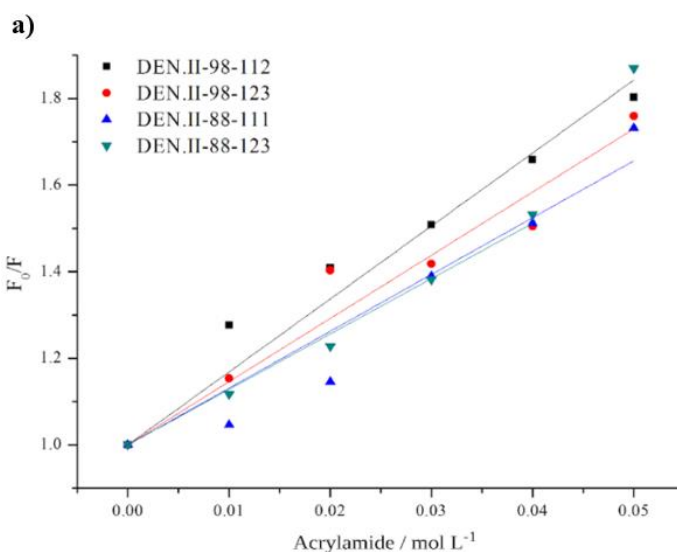
where  $F_o$  is the intensity in the solution without quencher,  $F$  is the intensity in the presence of quencher at concentration  $[Q]$ , and  $K_{SV}$  is the proportionality constant known as Stern–Volmer constant.

From time-resolved measurements, an equivalent equation can be written as Eq. 4.

$$\frac{\tau_o}{\tau} = 1 + K_{din}[Q] \quad (4)$$

where  $\tau_o$  is the lifetime of the fluorescent molecule in the absence of quencher and  $\tau$  is the lifetime in the presence of quencher at concentration  $[Q]$ , and  $K_{din}$  is the proportionality constant known as dynamic constant for quenching.

Quenching of peptides emission was examined through the Stern–Volmer plot (Fig. 4). Both parameters  $F_o/F$  and  $\tau_o/\tau$  increased linearly with the quencher concentration and the Stern–Volmer constants ( $K_{SV}$ ) and the dynamic constant ( $K_{din}$ ), obtained from the respective plots, present good agreement (Tab. 3), demonstrating the collisional nature of quenching without the formation of nonfluorescent species.



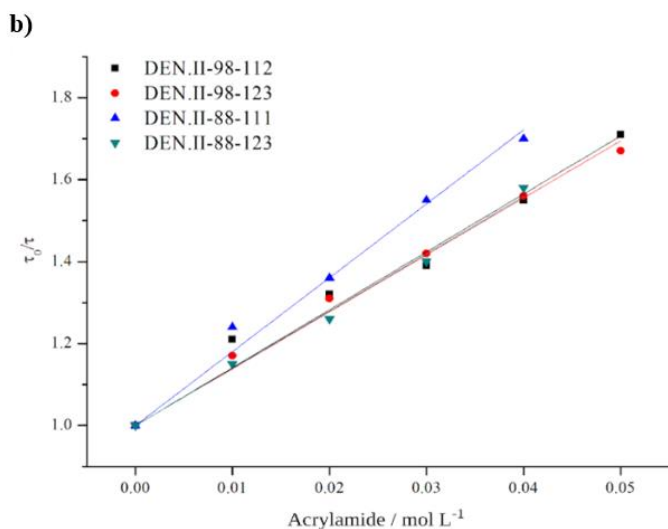


**Figure 4.** Quenching, by acrylamide, of tryptophan fluorescence in dengue II peptides. (a) Stern–Volmer plot using steady-state fluorescence emission. (b) Stern–Volmer plot from time-resolved data. Straight lines are best fits of experimental data to Stern–Volmer equation.

Results indicated that Trp residues in the peptides are exposed to the solvent, allowing the interaction with the quencher molecules. The quenching results from collisions between acrylamide molecules and tryptophan residues in the peptides are a process dependent on the diffusion of the interacting species in the medium. The collisional constant  $K_q$  is proportional to the diffusion coefficients of acrylamide and peptides and is determined with Eq. 5.

$$K_q = \frac{K_{din}}{\tau} \quad (5)$$

In order to calculate the constant, we used the results of average lifetimes obtained according to Eq. 2. The values of collisional constant calculated for all the peptides (Tab. 3) are comparable to the results of observations made in antimicrobial and

melanotropic peptides<sup>21,22</sup> and are consistent with the dimensions of the molecules involved in the process.

The collisional constant is proportional to the sum of diffusion coefficients of fluorophore and quencher. We must consider that, in our experiments, the fluorophore is the tryptophan residue bound to the peptide chain, and there is another component in the process, related to the accessibility of the quencher to the indol group of tryptophan. Thus, the slightly higher value of  $K_q$  observed for 88–111 peptide indicates an increased accessibility of the indol group to the quencher, suggesting that the tryptophan in the peptide has a high degree of exposure to the solvent.

**Table 3.** Steady state ( $K_{sv}$ ) and time-resolved ( $K_{din}$ ) constants for quenching of tryptophan emission by acrylamide. The collisional constants ( $K_q$ ) were calculated from Eq. 5.

| Peptide       | $K_{sv} / L$<br>$mol^{-1}$ | $K_{din} / L$<br>$mol^{-1}$ | $K_q / 10^6 L$<br>$mol^{-1} s^{-1}$ |
|---------------|----------------------------|-----------------------------|-------------------------------------|
| DEN II 98–112 | 16.9                       | 14.1                        | 7.6                                 |
| DEN II 98–123 | 14.6                       | 13.9                        | 6.9                                 |
| DEN II 88–111 | 13.1                       | 18.0                        | 10.1                                |
| DEN II 88–123 | 12.8                       | 14.0                        | 7.7                                 |

### 3.2.4 Fluorescence anisotropy

Values of steady-state fluorescence anisotropy ( $A_{SS}$ ) of the peptides measured in citrate buffer solution pH 5.4, around 0.020 (Tab. 4), are comparable to those observed in peptides with similar number of residues, like melanocyte stimulating hormone (MSH) and adrenocorticotropin hormone fragment (ACTH 1–24)<sup>20,22</sup>. As the fluorescence anisotropy originates from the rotational movement of the fluorophore, the relatively low values of anisotropy reflect the rotational freedom of the peptides in aqueous medium. Slightly higher values were observed for the sequence 88–123 of the larger peptide.

**Table 4.** Steady-state anisotropy ( $A_{SS}$ ) and time-resolved components of anisotropy decay: rotational correlation time ( $\varphi_i$ ) and time-zero anisotropy ( $\beta_i$ ) of component i. Peptides in citrate buffer, pH 5.4, concentration  $15 \mu mol L^{-1}$ , excitation 290 nm, emission set at 350 nm.

| Peptide      | $A_{SS}$ | $\varphi_1 / ns$ | $\varphi_2 / ns$ | $\beta_1$ | $\beta_2$ | $r_\infty$ | $r_0$ | $r_{mean}$ |
|--------------|----------|------------------|------------------|-----------|-----------|------------|-------|------------|
| 98–112 45 °C | 0.017    | 0.03             | 0.40             | 0.21      | 0.08      | -0.006     | 0.27  | 0.023      |
| 98–123 45 °C | 0.019    | -                | -                | -         | -         | -          | -     | -          |
| 88–111 45 °C | 0.018    | 0.06             | 0.56             | 0.19      | 0.08      | -0.012     | 0.25  | 0.019      |
| 88–123 45 °C | 0.021    | 0.08             | 0.55             | 0.15      | 0.11      | -0.014     | 0.25  | 0.027      |
| 88–123 25 °C | 0.023    | 0.06             | 0.65             | 0.17      | 0.08      | 0.006      | 0.26  | 0.029      |

Time-resolved data can offer elements for the analysis of steady-state results and the experimental anisotropy decays  $r(t)$  were fitted to multi-exponential curves (Eq. 6):

$$r(t) = \sum_i \beta_i e^{-\frac{t}{\tau_i}} + r_\infty \quad (6)$$

where  $\beta_i$  and  $\tau_i$  are the time-zero anisotropy and rotational correlation time of component  $i$  of the anisotropy decay, respectively, and  $r_\infty$  stands for the residual anisotropy at long time  $t$ .

The fitted function for anisotropy decay relates to the theoretically derived expression<sup>23</sup> (Eq. 7):

$$r(t) = (r_0 - r_\infty) \sum_i f_i e^{-\frac{t}{\tau_i}} + r_\infty \quad (7)$$

where  $r_0$  is the initial anisotropy obtained from the experimental fit of anisotropy decay through (Eq. 8)

$$r_0 = \sum_i \beta_i + r_\infty \text{ and } f_i = \frac{\beta_i}{\sum_i \beta_i} \quad (8)$$

From the usual definition of mean value, it is possible to calculate the mean anisotropy from the temporal dependence of intensity and anisotropy<sup>14</sup>, written from the fitted parameters as Eq. 9.

$$r_m = \frac{\int_0^\infty r(t)I(t)dt}{\int_0^\infty I(t)dt} = r_\infty + \frac{1}{\sum_i \alpha_i \tau_i} \sum_{i,j} \frac{\alpha_i \beta_j \tau_i \tau_j}{(\tau_i + \tau_j)} \quad (9)$$

Anisotropy decay profiles, as illustrated in Fig. 5 for DEN II 98-112, were best fitted to two rotational correlation times in the sub-nanosecond region (Tab. 4). For peptides, the short correlation time is ascribed to rotation of the Trp residue around its bonding to the peptide chain, and the longer correlation time corresponds to the whole peptide rotations<sup>21</sup>. The mean anisotropy, calculated from time-resolved data, has values comparable to the results of steady-state measurements. The calculated mean anisotropy contains contributions from fluorescence intensity decay and rotational movement of the fluorophore (Eq. 9). As the lifetime of Trp did not show large variation in the different peptides, the slightly higher value of anisotropy observed for the sequence 88-123 is consistent with the decrease in rotational diffusion of the longer peptide, associated to its larger dimension.

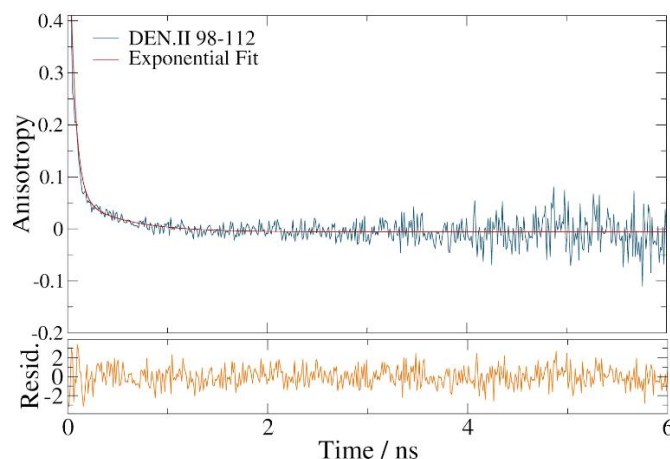


**Figure 5.** Fluorescence anisotropy decay for DEN.II 98-112 in buffer at 45 °C. Also shown best fit to a two exponential decay and graphic of residuals.

### 3.3 Interaction with lipid vesicles

The fluorescence of the long peptide 88-123 was measured in the presence of SUVs and LUVs. SUVs of neutral (DMPC) and charged (DMPG) vesicles were prepared by sonication at 25 °C. LUVs of neutral (DPPC) and charged (DPPG) lipids were prepared by extrusion at 45 °C, above the vesicles thermal transition temperature.

In the presence of neutral PC vesicles, the spectral position of maximum emission did not change compared to the observations in aqueous buffer. In contrast, in the presence of negatively charged PG vesicles, we observed a ~10 nm blue shift in the emission of tryptophan, accompanied by ~25% increase in intensity, indicating the positioning of the fluorescent residue in a less polar environment in the acidic lipid vesicle. However, the extent of the spectral changes is not very large, indicating that the tryptophan is not inserted deep inside the bilayer. As the interaction occurs with negative lipids, there is also contribution of electrostatic effects, suggesting the positioning of the peptide in the region near to the negative charged phosphate groups of the lipids.

The results of the experiments of intensity time decay of the peptides emission in the presence of negatively charged DMPG and DPPG vesicles showed that the long lifetime component increased considerably, yielding to mean lifetime remarkably high compared to the values obtained in buffer (Tab. 5). The steady-state anisotropy changed markedly in the presence of vesicles, the more pronounced effect observed for the negatively charged LUVs or SUVs (Tab. 6). Furthermore, the long rotational correlation time attained values as high as

3.2 ns in DMPG SUVs at 25 °C and 1.47 ns in DPPG LUVs at 45 °C, showing that the rotational diffusion of the peptides greatly slowed down due to the interaction with negative vesicles. The increase in anisotropy and

lifetimes is consistent with the insertion of the peptide in the interface region of the negatively charged vesicles<sup>20,21</sup>, with consequent restriction to the rotational diffusion of tryptophan.

**Table 5.** Time-resolved data for emission of peptide 88-123 in the presence of lipid vesicles. Parameters obtained from fit of intensity decay to three exponential curves: lifetime components ( $\tau_i$ ) and normalized pre-exponential factors ( $\alpha_i$ ). Peptides in citrate buffer solution, pH 5.4. Concentration 20  $\mu\text{mol L}^{-1}$ , excitation 290 nm, emission set at 350 nm. Temperature 45 °C.

| System           | Lifetime      |               |               | Norm pre-exponential |            |            | Mean                      |
|------------------|---------------|---------------|---------------|----------------------|------------|------------|---------------------------|
|                  | $\tau_1$ / ns | $\tau_2$ / ns | $\tau_3$ / ns | $\alpha_1$           | $\alpha_2$ | $\alpha_3$ | $\langle\tau\rangle$ / ns |
| Buffer 25 °C     | 4.6           | 2.3           | 0.71          | 0.09                 | 0.54       | 0.37       | 2.58                      |
| DMPC – SUV 25 °C | 4.8           | 2.3           | 0.86          | 0.09                 | 0.56       | 0.35       | 2.62                      |
| DMPG – SUV 25 °C | 7.1           | 3.2           | 1.20          | 0.05                 | 0.58       | 0.36       | 3.40                      |
| Buffer 45 °C     | 3.8           | 1.5           | 0.28          | 0.06                 | 0.64       | 0.30       | 1.81                      |
| DPPC – LUV 45 °C | 8.0           | 1.7           | 0.14          | 0.05                 | 0.50       | 0.45       | 3.54                      |
| DPPG – LUV 45 °C | 8.1           | 2.5           | 0.17          | 0.05                 | 0.58       | 0.36       | 3.66                      |

**Table 6.** Steady-state anisotropy ( $A_{ss}$ ) and time-resolved components of anisotropy decay: rotational correlation time ( $\phi_i$ ) and time-zero anisotropy ( $\beta_i$ ) of component i. Peptides in citrate buffer, pH 5.4, in medium containing suspension of lipid unilamellar vesicles. Peptide concentration 20  $\mu\text{mol L}^{-1}$ , lipid concentration 1  $\text{mmol L}^{-1}$ , excitation 290 nm, emission at 350 nm.

| System         | $A_{ss}$ | $\phi_1$ / ns | $\phi_2$ / ns | $\beta_1$ | $\beta_2$ | $r_\infty$ | $r_0$ | $r_{mean}$ |
|----------------|----------|---------------|---------------|-----------|-----------|------------|-------|------------|
| Buffer 25 °C   | 0.023    | 0.06          | 0.65          | 0.17      | 0.08      | 0.002      | 0.260 | 0.029      |
| DMPC/SUV 25 °C | 0.034    | 0.06          | 0.67          | 0.14      | 0.07      | 0.010      | 0.253 | 0.035      |
| DMPG/SUV 25 °C | 0.083    | 0.07          | 3.20          | 0.21      | 0.02      | 0.020      | 0.250 | 0.067      |
| Buffer 45 °C   | 0.021    | 0.08          | 0.55          | 0.15      | 0.11      | -0.014     | 0.246 | 0.024      |
| DPPC/LUV 45 °C | 0.042    | 0.04          | 0.45          | 0.18      | 0.10      | 0.018      | 0.296 | 0.042      |
| DPPG/LUV 45 °C | 0.065    | 0.06          | 1.47          | 0.16      | 0.07      | 0.015      | 0.246 | 0.049      |

An interesting result was that increase in lifetime was not observed for the peptide in the presence of neutral SUVs of DMPC at 25 °C. However, at the temperature of 45 °C the long lifetime component increased in the presence of neutral vesicles of DPPC. Thus, at high temperature the bilayer structure allows those neutral lipids to interact with the peptide with a significant increase in the calculated mean lifetime of Trp emission. The increase in temperature promotes thermal disorganization of the bilayer. At 25 °C the bilayers are in the gel phase and at 45 °C, above the thermal phase transition temperature, the bilayers are in the liquid crystalline phase. In the high temperature the bilayer of the neutral lipids is less packed, making possible the positioning of the peptides so that the tryptophan residue can span regions in the bilayer with decreased polarity compared to the aqueous environment.

### 3.4 Fluorescence correlation spectroscopy - effects of the peptide on the size of vesicles

In FCS measurements, software (SymPho Time 64) provided by PicoQuant, allowed determination of the auto-correlation function  $G(t)$  for the fluorescence emission. The algorithm employed for data analysis, adequate to the low intensity emission from microscopic volumes, is based in a combination of time-correlated single-photon counting (TCSPC) technique and data acquisition following a specific time-tagged event, or TTTR (time-tagged time-resolved) mode<sup>24</sup>.

The time evolution of the fluctuations in intensity can be described by the autocorrelation function  $G(t)$ , which is dependent on the fluctuations in the concentration of the fluorophores. It was shown that, in the case of emission forming a single fluorescent species, the autocorrelation function relates to the diffusion of the fluorophore within a tiny sampling volume through Eq. 10.

$$G(t) = \frac{1}{N} \frac{1}{1+t/\tau_D} \quad (10)$$

where  $N$  and  $\tau_D$  are the mean number of molecules and the diffusion time within the illuminated volume, respectively<sup>25</sup>.

The diffusion coefficient  $D$  of the emitting subject is inversely proportional to  $\tau_D$  and was determined from the experimental autocorrelation function. From  $D$  values, the hydrodynamic radius  $R_H$  of the fluorescent subject was calculated from the Stokes–Einstein equation (Eq. 11):

$$R_H = \frac{kT}{6\pi\eta D} \quad (11)$$

where  $k$  is the Boltzmann constant, and  $\eta$  is the viscosity of the solution. In our experiments, the emitting species was the fluorescent probe DiIC<sub>18</sub>. As the probe is bound to the vesicles, the diffusion coefficient and the hydrodynamic radius refer to the whole vesicles.

Fluorescence correlation spectroscopy experiments were performed in small unilamellar vesicles of DMPC and DMPG containing the fluorescent probe DiIC<sub>18</sub> located in the surface vesicles, using a probe to lipid concentration below 1/100. From the measurements, we observed that the SUVs dimensions in buffer, calculated from the correlation curves, were comparable to those obtained from DLS (Tab. 7). After the addition of peptides, the FCS data for the neutral vesicles changed slightly, indicating the small extent of interaction that could not be observed through changes in the vesicle's diffusion. However, in the case of negative DMPC vesicles, the vesicles diffusion coefficient was significantly modified due to interaction with the peptides, resulting in a drastic increase in the diameter of the negative SUVs (Fig. 6).

**Table 7.** Diameter ( $\Phi$ ) of small unilamellar vesicles of DMPC and DMPG determined from DLS and FCS measurements in citrate buffer pH 5.4, in the absence and in presence of DEN II 88–123 peptide. Also shown diffusion coefficient ( $D$ ) of the vesicles determined from FCS experiments.

| System                              | $\Phi$ / nm - DLS | $D$ / $\mu\text{m}^2 \text{s}^{-1}$ - FCS | $\Phi$ / nm - FCS |
|-------------------------------------|-------------------|---|-------------------|
| DMPC                                | 32.5              | -   | -                 |
| DMPC + DiIC <sub>18</sub>           | 32.8              | 7.51                                      | 28.8              |
| DMPC + DiIC <sub>18</sub> + Peptide | nd                | 8.18                                      | 26.4              |
| DMPG                                | 46.0              | -   | -                 |
| DMPG + DiIC <sub>18</sub>           | 47.5              | 8.43                                      | 25.6              |
| DMPG + DiIC <sub>18</sub> + Peptide | nd                | 3.24                                      | 67.0              |

The FCS provides an experimental verification, independent of Trp fluorescence, revealing that the interaction between the DEN II 88–123 fusion peptide and the lipids vesicles has an electrostatic component,

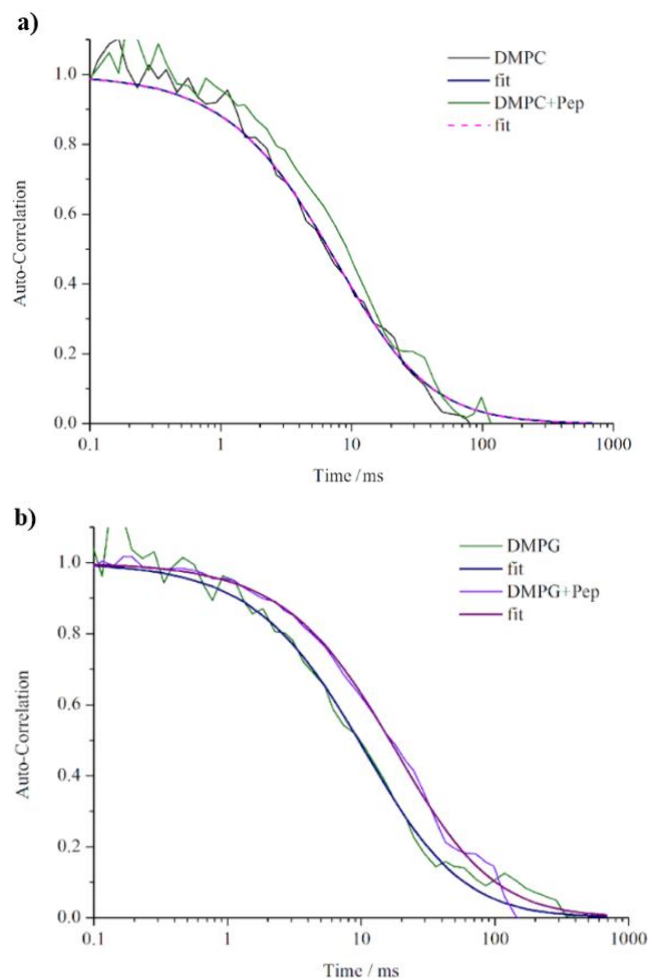


**Figure 6.** Autocorrelation function obtained from FCS experiments performed in small unilamellar vesicles of neutral DMPC and negative DMPG containing the fluorescent probe DiIC<sub>18</sub>. Experiments in citrate buffer pH 5.4, at 45 °C, in the presence and in absence of DEN II 88–123 peptide.

involving the charged residues of the peptide and the negatively charged head groups of DMPG vesicles. As a result of the interaction, the vesicles drastically

changed shape and dimension, as revealed by the increase in the diffusion coefficient.

#### 4. Conclusions

The fluorescence spectroscopy gives information about the local environment around the tryptophan residue in the dengue fusion peptides. The changes in fluorescence characteristics (emission spectrum, time-resolved intensity decay, quenching by acrylamide, steady-state and time-resolved anisotropy) are similar to observations performed in different peptides containing tryptophan, like melanocyte stimulating hormone, adrenocorticotropin hormone and antimicrobial peptides. Despite the local character of the information obtained from tryptophan fluorescence, it is possible to draw conclusions concerning the peptides. In buffer solution, intensities and lifetimes are smaller for the amino flanking peptides 88–111 and 88–123, due to the presence of positively charged amino acids Lys, Arg and His in the sequence that promotes nonradiative pathways to the de-excitation of the tryptophan excited state.

The dengue fusion peptides in the buffer have the tryptophan residue exposed to the aqueous environment, interacting with molecules dissolved in the medium. The extent of interaction with the quencher acrylamide depends on the size of the peptides, which affects their translational diffusion. The rotational diffusion was monitored by fluorescence anisotropy measurements and are resulted from the rotation of the Trp residue around its bonding to the peptide chain, combined with the rotation of the whole peptide. The model is consistent with the dependence of anisotropy on the size of the peptides.

The interaction with lipid vesicles was assessed by changes in spectral position, intensity and time-resolved parameters. Compatible with the role that the fusion loop peptide exerts in the process of entry in the cell, the fluorescence of tryptophan residue gives information about the insertion of the nonpolar sequence of fusion peptide into the nonpolar region of lipid vesicles. Noticeably, the effect is enhanced in the aggregates containing negatively charged phospholipids. The presence of positive residues in the amino flanking peptides indicates that the electrostatic and hydrophobic interactions are relevant to the process of interaction of serotype II dengue virus fusion peptide with the membrane. Results of FCS experiments using the membrane probe DiIC<sub>18</sub> reveal changes in the size of negative vesicles due to interaction with fusion peptides and are consistent with those obtained from tryptophan fluorescence.

#### Acknowledgments

EMC is a senior researcher of CNPq (grant 301975/2018–3). ASI is recipient of CNPq research grant (305771/2016-7). This study was financed in part by the Coordenação de Aperfeiçoamento de Pessoal de Nível Superior - Brasil (CAPES) - Finance Code 001.

#### References

- [1] Bhatt, S., Gething, P. W., Brady, O. J., Messina, J. P., Farlow, A. W., Moyes, C. L., Drake, J. M., Brownstein, J. S., Hoen, A. G., Sankoh, O., Myers, M. F., George, D. B., Jaenisch, T., Wint, G. R. W., Simmons, C. P., Scott, T. W., Farrar, J. J., Hay, S. I., The global distribution and burden of dengue, *Nature* 496 (2013) 504-507. <https://doi.org/10.1038/nature12060>.
- [2] Barrows, N. J., Campos, R. K., Liao, K.-C., Prasanth, K. R., Soto-Acosta, R., Yeh, S.-C., Geraldine Schott-Lerner, G., Pompon, J., Sessions, O. M., Bradrick, S. S., Garcia-Blanco, M. A., *Biochemistry and Molecular Biology of Flaviviruses, Chemical Reviews* 118 (8) (2018) 4448-4482. <https://doi.org/10.1021/acs.chemrev.7b00719>.
- [3] Modis, Y., Ogata, S., Clements, D., Harrison, S. C., Structure of the dengue virus envelope protein after membrane fusion, *Nature* 427 (2004) 313-319. <https://doi.org/10.1038/nature02165>.
- [4] Zonetti, L. F. C., Coutinho, M. C., Araujo, A. S. de, Molecular Aspects of the Dengue Virus Infection Process: A Review, *Protein & Peptide Letters* 25 (8) (2018) 712-719. <https://doi.org/10.2174/0929866525666180709115506>.
- [5] Smit, J. M., Moesker, B., Rodenhuis-Zybert, I., Wilschut, J., Flavivirus Cell Entry and Membrane Fusion, *Viruses* 3 (2) (2011) 160-171. <https://doi.org/10.3390/v3020160>.
- [6] Rice, C. M., Linderbach, B. D., Theil, H., Flaviviridae: the viruses and their replication, In: Fields Virology 5th edition., Knipe, D. M., Howley PM, ed., Lippincott-Raven, Philadelphia, 2007, Ch. 33.
- [7] Harrison, S. C., The pH sensor for flavivirus membrane fusion, *Journal of Cell Biology* 183 (2) (2008) 177-179. <https://doi.org/10.1083/jcb.200809175>.
- [8] Hrobowski, Y. M., Garry, R. F., Michael, S. F., Peptide inhibitors of dengue virus and West Nile virus infectivity, *Virology Journal* 2 (2005) 49. <https://doi.org/10.1186/1743-422X-2-49>.
- [9] Seligman, S. J., Constancy and diversity in the flavivirus fusion peptide, *Virology Journal* 5 (2008) 27. <https://doi.org/10.1186/1743-422X-5-27>.

- [10] Stauffer, F., Melo, M. N., Carneiro, F. A., Sousa, F. J. R., Juliano, M. A., Juliano, L., Mohana-Borges, R., Poian, A. T. da, Castanho, M. A. R. B., Interaction between dengue virus fusion peptide and lipid bilayers depends on peptide clustering, *Molecular Membrane Biology* 25 (2) (2008) 128-138. <https://doi.org/10.1080/09687680701633091>.
- [11] Melo, M. N., Sousa, F. J. R., Carneiro, F. A., Castanho, M. A. R. B., Valente, A. P., Almeida, F. C. L., Poian, A. T. da, Mohana-Borges, R., Interaction of the Dengue Virus Fusion Peptide with Membranes Assessed by NMR: The Essential Role of the Envelope Protein Trp101 for Membrane Fusion, *Journal of Molecular Biology* 392 (3) (2009) 736-746. <https://doi.org/10.1016/j.jmb.2009.07.035>.
- [12] Carpio, L. E., Villalaín, J., Identification of the phospholipid binding regions of the envelope E protein of flaviviruses by molecular dynamics, *Journal of Biomolecular Structure and Dynamics* 38 (17) (2020) 5136-5147. <https://doi.org/10.1080/07391102.2019.1697368>.
- [13] Fields, G. B., Noble, R. L., Solid phase peptide synthesis utilizing 9-fluorenylmethoxycarbonyl amino acids, *International Journal of Peptide and Protein Research* 35 (3) (2009) 161-214. <https://doi.org/10.1111/j.1399-3011.1990.tb00939.x>.
- [14] Ito, A. S., Rodrigues, A. P., Pazin, W. M., Barioni, M. B., Fluorescence depolarization analysis of thermal phase transition in DPPC and DMPG aqueous dispersions, *Journal of Luminescence* 158 (2015) 153-159. <https://doi.org/10.1016/j.jlumin.2014.09.051>.
- [15] Ristori, S., Di Cola, E., Lunghi, C., Richichi, B., Nativi, C., Structural study of liposomes loaded with a GM3 lactone analogue for the targeting of tumor epitopes, *Biochimica et Biophysica Acta (BBA) - Biomembranes* 1788 (12) (2009) 2518-2525. <https://doi.org/10.1016/j.bbamem.2009.10.005>.
- [16] Cespedes, G. F., Nobre, T. M., Oliveira Junior, O. N., Bong, D., Cilli, E. M., On the role of surrounding regions in the fusion peptide in dengue virus infection, *Virology* 557 (2021) 62-69. <https://doi.org/10.1016/j.virol.2021.02.012>.
- [17] Goldman, C., Pascutti, P. G., Piquini, P., Ito, A. S., On the contribution of electron transfer reactions to the quenching of tryptophan fluorescence, *The Journal of Chemical Physics* 103 (24) (1995) 10614-10620. <https://doi.org/10.1063/1.469846>.
- [18] Marquezin, C. A., Hirata, I. Y., Juliano, L., Ito, A. S., Tryptophan as a probe for acid-base equilibria in peptides, *Peptide Science* 71 (5) (2003) 569-576. <https://doi.org/10.1002/bip.10535>.
- [19] Fernandez, R. M., Vieira, R. F. F., Nakaie, C. R., Lamy, M. T., Ito, A. S., Acid-base titration of melanocortin peptides: Evidence of Trp rotational conformers interconversion, *Biopolymers* 80 (5) (2005) 643-650. <https://doi.org/10.1002/bip.20210>.
- [20] Romani, A. P., Ito, A. S., Interaction of adrenocorticotropin peptides with microheterogeneous systems — A fluorescence study, *Biophysical Chemistry* 139 (2-3) (2009) 92-98. <https://doi.org/10.1016/j.bpc.2008.10.009>.
- [21] Zanin, L. M. P., Alvares, D. dos S., Juliano, M. A., Pazin, W. M., Ito, A. S., Ruggiero Neto, J., Interaction of a synthetic antimicrobial peptide with model membrane by fluorescence spectroscopy, *European Biophysics Journal* 42 (11-12) (2013) 819-831. <https://doi.org/10.1007/s00249-013-0930-0>.
- [22] Souto, A. L. C. F., Ito, A. S., Tryptophan fluorescence studies of melanotropins in the amphiphile-water interface of reversed micelles, *European Biophysics Journal* 29 (1) (2000) 38-47. <https://doi.org/10.1007/s002490050249>.
- [23] Kawato, S., Kinoshita Junior, K., Ikegami, A., Effect of cholesterol on the molecular motion in the hydrocarbon region of lecithin bilayers studied by nanosecond fluorescence techniques, *Biochemistry* 17 (23) (1978) 5026-5031. <https://doi.org/10.1021/bi00616a026>.
- [24] Wahl, M., Gregor, I., Patting, M., Enderlein, J., Fast calculation of fluorescence correlation data with asynchronous time-correlated single-photon counting, *Optics Express* 11 (26) (2003) 3583-3591. <https://doi.org/10.1364/OE.11.003583>.
- [25] Krishevsky, O., Bonnet, G., Fluorescence correlation spectroscopy: the technique and its applications, *Reports on Progress in Physics* 65 (2) (2002) 251-297. <https://doi.org/10.1088/0034-4885/65/2/203>.



# Purification and characterization of embryo-specific soy urease (*Glycine max*) and its antifungal potential against *Paracoccidioides brasiliensis*

Elisângela Andrade Ângelo<sup>1</sup>, Tainá Michelle da Cruz<sup>2</sup>, José Renato Pattaro Júnior<sup>2</sup>, Daniele Maria Zanzarin<sup>3</sup>, Franciele Abigail Vilugron Rodrigues<sup>4</sup>, Eduardo Jorge Pilau<sup>3</sup>, Érika Seki Kioshima<sup>4</sup>, Maria Aparecida Fernandez<sup>5</sup>, Flavio Augusto Vicente Seixas<sup>2+</sup>

1. Federal Institute of Paraná, Biology laboratory, Umuarama, Brazil.
2. State University of Maringá, Department of Technology, Umuarama, Brazil.
3. State University of Maringá, Department of Chemistry, Maringá, Brazil.
4. State University of Maringá, Department of Clinical Analysis and Biotechnology, Maringá, Brazil.
5. State University of Maringá, Department of Biotechnology, Genetics and Cell Biology, Maringá, Brazil.

**+Corresponding author:** Flavio Augusto Vicente Seixas, **Phone:** +55 44 3621-9300, **Email address:** favseixas@uem.br

## ARTICLE INFO

Article history:

**Received:** June 01, 2020

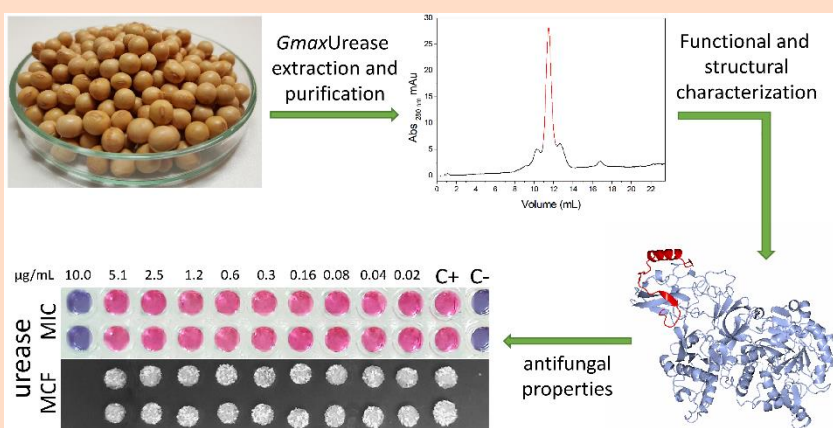
**Accepted:** October 26, 2020

**Published:** April xx, 2021

## Keywords

1. urease
2. *Glycine max*
3. fungitoxic
4. *Paracoccidioides brasiliensis*

**ABSTRACT:** Ureases are amidohydrolases that catalyze the hydrolysis of urea to ammonia and carbamate. In addition to the enzymatic function, ureases have fungitoxic and insecticidal function, which are independent of their catalytic activity. Soy (*Glycine max*) has two main urease isoforms: ubiquitous and embryo-specific, the latter is present in beans. In view of the potential applications of ureases, this work aimed to extract, purify, characterize the structure, activity and fungitoxic activity of soy urease against *Paracoccidioides brasiliensis*. The biochemical characterization was performed, in terms of optimal pH and temperature, as well as the determination of the Michaelis–Menten constant ( $K_M$ ) and maximum



After purification and structural-functional characterization, the embryo-specific soybean urease shows antifungal properties against *Paracoccidioides brasiliensis*.

velocity ( $V_{max}$ ). The protein sequence was identified by mass spectrometry and used in computational modeling of the biological structure. The optimum pH and temperature of the enzyme were 6.5 and 65 °C, respectively,  $K_M$  526 mmol L<sup>-1</sup> and  $V_{max}$  7.4 mmol L<sup>-1</sup> NH<sub>3</sub>·μg<sub>urease</sub><sup>-1</sup>·s<sup>-1</sup> and biological unity as a trimer. The antifungal activity assays (*in vitro*) were promising, showing a fungicidal profile of the urease, with a minimum inhibitory concentration of 10 μg·mL<sup>-1</sup>. This work demonstrated, for the first time, the fungitoxic activity of embryo-specific soy urease against the Pb18 strain of *P. brasiliensis*.

## 1. Introduction

Ureasas are nickel-dependent amidohydrolases (EC.3.5.1.5) that catalyze the breakdown of the urea amide group into ammonia and carbamate, which decomposes spontaneously in a neutral environment to ammonia and carbon dioxide<sup>1,2</sup>. Ureasas are present in bacteria, fungi and vegetables, but are absent in animals<sup>3</sup>. Vegetable ureasas play an important role in using urea as a source of nitrogen for the plant. This substrate can originate both from the internal plant metabolism and from an external source, when used as a fertilizer. This substrate can originate either from the internal plant metabolism or from external source when used as fertilizer. In the latter situation, urea is used as nitrogen source, and it can be directly absorbed by the plant or may be used in the form of ammonia or nitrate. When absorbed in the form of ammonia, urea is hydrolyzed outside the plant by ureasas present in the soil, which can be of either from vegetable or microbial origin. When absorbed as nitrate, the ammonia hydrolyzed from urea is converted into nitrate by microorganisms present in the soil<sup>4-6</sup>.

The discovery of ureasas in vegetables occurred in 1909 by Takeuchi, when studying soybeans, since then, it was discovered that these enzymes are present in all vegetables, in their most diverse tissues<sup>6</sup>. However, such enzymes are especially abundant in vegetables of the families Fabaceae (vegetables), Cucurbitaceae, Asteraceae and Pinaceae<sup>7,8</sup>. The soy (*Glycine max*) has three urease isoforms: ubiquitous, embryo-specific and SBU-3. Ubiquitous urease is found in the various tissues of soy, while embryo-specific urease is found only in the seed and SBU-3 is found in small amounts, at specific moments of plant development<sup>7</sup>.

More recent studies indicate a new property of plant ureasas, related to its toxic role against fungi and insects. It is noteworthy that these toxic activities do not depend on the catalytic activity of this enzyme<sup>3,9</sup>. Due to this property, plant ureasas have come to be considered multi proteins<sup>2</sup>, and studies have been carried out in order to explore their fungitoxic<sup>10,11</sup> and entomotoxic potential<sup>12</sup>. Regarding the fungitoxic potential, studies are mainly focused on phytopathogenic filamentous fungi, such as species from the genera *Fusarium* and *Penicillium*<sup>2,3</sup>. There are also some studies with pathogenic mammalian yeasts, such as those of the genus *Candida*<sup>10,13</sup>. However, there are no studies with dimorphic fungi pathogenic to humans, such as *Paracoccidioides brasiliensis*.

*Paracoccidioides brasiliensis* is one of those responsible for causing paracoccidioidomycosis (PCM), an endemic systemic mycosis in Latin

America, frequent in Brazil, Argentina, Colombia and Venezuela. This dimorphic fungus is common at filamentous form in the environment, especially in the soil. Hyphae may contain propagating-infective structures (microconidia) that become yeast-like when inhaled. This form multiplies in the body, causing pathogenesis, which can compromise the functions of several systems, especially the respiratory system<sup>14,15</sup>. In the chronic form, lesions on the oral mucosa, lymph node involvement and, rarely, dermatological lesions may be observed<sup>16</sup>. It is estimated that 10 million people in Latin America are infected by *Paracoccidioides* spp., with 1–2% presenting clinical manifestations<sup>17</sup>. Brazil has a high incidence of PCM and annual estimates of its occurrence vary from 0.71 to 3.7 cases for every 100,000 inhabitants. However, there are Brazilian regions where the incidence of PCM is even higher, as in two municipalities in Rondônia, where the incidence rate is 40 cases for every 100,000 inhabitants<sup>18</sup>. Paracoccidioidomycosis is the main responsible for death due to systemic mycoses in Brazil, corresponding to 51.2% of deaths in this category, between the years 1996 to 2006<sup>19</sup>. Even so, it is considered by the World Health Organization (WHO) as a neglected disease<sup>17</sup>.

Regarding the treatments available for human fungal diseases, many antifungals promote adverse effects on the patient, which makes the treatment difficult to continue<sup>20</sup>. In the case of PCM, this situation is aggravated, as the treatments tend to be long, reaching up to 24 months<sup>15,18</sup>.

Thus, in view of the antifungal potential of ureasas, as well as the need to develop new drugs against PCM, this work aims to extract and characterize embryo-specific soy urease (*GmaxUrease*), as well as to evaluate its activity (*in vitro*) against *P. brasiliensis*. Thus, this work can contribute to the development of future technologies based on urease (natural product), aimed at the treatment of topical manifestations of PCM.

## 2. Experimental

### 2.1 Extraction of embryo-specific soy urease

The protocol for enzyme extraction was guided by the method proposed by Bracco et al.<sup>21</sup> with modifications. The soy flour was obtained from the soybean seed Bayer 26B42 ground. Then, 25 g of the flour was defatted by double washing with chloroform in an ice bath under stirring for 30 min, followed by filtration on Whatman paper. The defatted extract was

used for protein extraction by means of constant agitation with 20% (w/v) of 20 mmol L<sup>-1</sup> phosphate buffer with 1 mmol L<sup>-1</sup> β-mercaptoethanol, pH 7.5 at 4 °C for 12 h. The soluble protein fraction (supernatant) was separated by centrifugation at 30,000 g for 30 min. This fraction was considered the crude extract and 10 μL of the cocktail of a plant protease inhibitor was added to it (Sigma P9599, USA).

## 2.2 Purification of embryo-specific soy urease

Purification of *GmaxUrease* was done using chromatography and centrifugation techniques. Initially, a gel filtration chromatography column containing Sephadex G-25 resin (25.0 × 1.5 cm) and phosphate buffer (20 mmol L<sup>-1</sup>) with 100 mmol L<sup>-1</sup> NaCl and pH 7.5 as mobile phase and elution flow of 1.0 mL·min<sup>-1</sup> monitored by spectrophotometer at 280 nm. The fraction that showed ureolytic activity was concentrated by means of ultrafiltration using Amicon filter 30 kDa cutoff, at 1,000 g for 20 min. This fraction was called G25 and 10% glycerol (*q.s.*) was added to it.

The G-25 fraction was subjected to a new size exclusion chromatography in a column with Sephacryl HS-200 resin (60.0 × 1.5 cm), in a fast protein liquid chromatography (FPLC) system model Äkta Prime (GE Lifesciences, USA). The protein fractions were eluted using the phosphate buffer described in the previous step, with a flow rate of 0.5 mL·min<sup>-1</sup>. The fraction that showed ureolytic activity was collected and concentrated by means of ultracentrifugation. At the end, 10% glycerol was added to the concentrate (*q.s.*), which was identified as the Sephacryl fraction.

Finally, the Sephacryl fraction was subjected to a third size exclusion chromatography, using a Superdex-200 10/300 column (GE Lifesciences, USA), using other FPLC filtration system model Äkta Pure M (GE Lifesciences, USA). The elution and concentration conditions were the same as in the previous steps. At the end, the concentrate received 10% glycerol (*q.s.*) again and was called Superdex fraction.

## 2.3 Verification of purity and molecular weight

The purity of the eluted fractions was verified using 12% SDS-PAGE electrophoresis, stained with Coomassie blue<sup>22</sup>. Electrophoresis was also used to estimate the molecular weight of the bands, using the marker Sigma-Marker ColorBurst (Sigma, C1992, USA) by means of ImageQuant-TL 8.1 program (GE-

lifescience, USA). This program was also used to estimate the percentage of urease in the sample.

The molecular weight (MW) of the biological unity of soybean urease, under nondenaturing conditions, was calculated using the gel filtration method by a Superdex-200 10/300 column (GE Lifesciences). The calibration curve was constructed with the low and high MW gel filtration calibration kit standards (GE Lifesciences), following the manufacturer's recommendations. The proteins were eluted in isocratic mode using 50 mmol L<sup>-1</sup> phosphate buffer + 150 mmol L<sup>-1</sup> NaCl, pH 7.2 at room temperature, in a flow rate of 0.5 mL·min<sup>-1</sup>. The absorbances were monitored at 214 and 280 nm and elution volumes for each protein were measured and converted to  $K_{av}$  (Eq. 1) and plotted against the logarithm of the respective molecular weights ( $\log MW$ ).

$$K_{av} = \frac{v_e - v_o}{v_c - v_o} \quad (1)$$

where  $V_e$  = elution volume,  $V_o$  = column void volume and  $V_c$  = geometric column volume.

## 2.4 Determination of protein concentration and ureolytic activity

The protein concentration of the crude extract, as well as of the G-25, Sephacryl and Superdex fractions, was determined according to Bradford<sup>23</sup>, using bovine serum albumin as a standard. The assays were done in duplicate and triplicate if necessary. The measurement of ureolytic activity was performed by quantifying the ammonia (product) using Nessler's reagent<sup>24</sup>. An enzyme unit (U) was considered to be the amount of enzyme needed to produce 1 μmol L<sup>-1</sup> of ammonia per minute<sup>25</sup>.

## 2.5 Protein identification by liquid chromatography-mass spectrometry (LC-MS<sup>E</sup>)

To determine whether the protein obtained was embryo-specific soy urease (*GmaxUrease*), peptide sequence identification was performed by liquid chromatography-mass spectrometry (LC-MS<sup>E</sup>) analysis. The protein band extracted from the SDS-PAGE, which had molecular mass corresponding to the estimated theoretical value for urease, was digested in the cropped gel band with trypsin, according to the Shevchenko protocols<sup>26,27</sup>.

The analysis was performed using Acquity UPLC M-Class System ultra-high performance liquid chromatography (Waters, Milford, MA) coupled a time-of-flight high resolution mass spectrometry (Xevo G2, Waters) equipped with an electrospray ionization source. Chromatographic separation was performed on an Acquity UPLC M-Class HSS T3 column, with particle size 1.8  $\mu\text{m}$ , 300  $\mu\text{m} \times 150 \text{ mm}$  (Waters, UK), and flux of 6  $\mu\text{L}\cdot\text{min}^{-1}$ . The solvent gradient mixture: A ( $\text{H}_2\text{O}/0.1\%$  formic acid; v:v) and B (acetonitrile/ $0.1\%$  formic acid; v:v) was: 3% B 0–1 min, 40% B 1–80 min, 97% B 80–90 min, holding 97% B for 90–97 min, 3% B for 97–100 min, and holding 3% B for 100–103 min at 40 °C. The capillary voltage was operated in the positive mode at 3.0 kV. In the cone, the voltage was adjusted to 40 V and the gas to 600  $\text{L}\cdot\text{h}^{-1}$  at 400 °C. Data were collected in the range between 50 to 2000  $m/z$  using  $\text{MS}^E$  acquisition mode, scan time 0.5 sec and collision energy ramp 15–45 V.

After analysis, the data (.raw) were processed/analyzed using the ProteinLynx Global ServerTM 3.0.3 software, and the revised soy database (*Glycine max*, Uniprot). The parameters used for searching the database were: cleavage specificity, trypsin with 1 missed cleavage allowed, min fragment ion matches per peptide = 2, min fragment ion matches per protein = 5, min peptide matches per protein = 1, fixed modifier reagent: carbamidomethyl C, variable modifier reagents: oxidation M.

## 2.6 Structural modeling of embryo-specific soy urease

The amino acid sequence of soy urease identified by LC- $\text{MS}^E$  deposited in Uniprot (id: i1k3k3) was used to search for template structures in the protein data bank (PDB), by BlastP program. The urease structure of *Canavalia ensiformis* (pdb id: 3la4)<sup>28</sup> was chosen and used as a template. The modeling was performed using the Modeller v9.24 software package<sup>29</sup>, where 2,100 models of urease were generated in the presence of the nickel cofactor and four residues with post-transcriptional modifications. Only one chain was modeled, and the homotrimer and homohexamer structures generated by symmetry operations. The final model was chosen based on the Modeller DOPE score and also by stereochemical quality using the Procheck program<sup>30</sup>.

## 2.7 Effect of pH and temperature on enzyme activity

The effect of pH on ureolytic activity was estimated using the Britton–Robinson 0.04  $\text{mol L}^{-1}$  buffer<sup>31</sup>, in the range of 5.0 to 9.0. Firstly, a single buffer was made in the presence of 3% urea and the pH adjusted according to the test. Subsequently, incubation was performed with 2.7  $\mu\text{g}\cdot\text{mL}^{-1}$  of urease at 55 °C for 15 min.

The effect of temperature on the rate of urea production was determined at constant enzyme concentrations. An amount of 2.7  $\mu\text{g}\cdot\text{mL}^{-1}$  urease was incubated in 0.2  $\text{mol L}^{-1}$  phosphate buffer, 3% urea, pH 6.5, for 15 min. The incubation temperatures ranged between 25 to 85 °C, the experiments were carried out in duplicate, discounting the urea degradation due to temperature, using a negative control. The ammonia generated was quantified using the Nessler methodology, in a NanoDrop system (Thermo Scientific) in all activity assays.

## 2.8 Effect of different substrate concentrations

The assays were performed at urea concentrations ranging from 0 to 235  $\text{mmol L}^{-1}$ , pH 6.5, temperature of 65 °C and incubation time of 5 min, followed by the determination of ureolytic activity. The enzyme concentration used in these assays was 2.7  $\mu\text{g}\cdot\text{mL}^{-1}$ . The results were plotted as function of substrate concentration (Michaelis–Menten plot) and double-reciprocal (Lineweaver–Burk plot), through which was possible to calculate the Michaelis–Menten apparent constant ( $K_M$ ) and  $V_{\text{max}}$ .

## 2.9 Antifungal activity against *P. brasiliensis*

The fungitoxic activity of urease was evaluated against *P. brasiliensis*, Pb18 strain, by means of serial broth microdilution assay, according to the methodology of Clinical and Laboratory Standards Institute<sup>32,33</sup>, with modifications as described by Rodrigues–Vendramini<sup>34</sup>. The urease concentration ranged between 0.02 to 10  $\mu\text{g}\cdot\text{mL}^{-1}$ . The antifungal agent itraconazole was used as a negative control at a concentration of 1  $\mu\text{g}\cdot\text{mL}^{-1}$ . An assay containing only the microorganism and the culture medium was used as positive control, in order to verify the viability of the strain. In addition, bovine serum albumin (BSA) was evaluated at concentrations between 0.2 to 104.4  $\mu\text{g}\cdot\text{mL}^{-1}$ , to assess whether any inhibitory activity could be due to osmotic origin. The inoculum

for the assays were grown in RPMI 1640 medium, prepared with a concentration of  $105 \text{ UFC}\cdot\text{mL}^{-1}$ , standardized by counting in a Neubauer chamber and diluted 1:2 in the wells of a 96-well microplate. After inoculation, the microplates were incubated at  $37^\circ\text{C}$  for 7 days, and on the sixth day  $20 \mu\text{L}$  of 0.02% resazurin was added to each well, as an indicator of metabolic activity. Then, the plates were again incubated for 24 h.

To identify the minimum inhibitory concentration (MIC), a visual reading of the color change of the wells was performed. To identify the minimum fungicidal concentration (MFC), growth was evaluated in solid medium. For this purpose,  $20 \mu\text{L}$  aliquots of the wells were transferred to plates containing brain heart infusion agar, followed by superficial inoculation (spread plate). The plates were kept at  $35^\circ\text{C}$  for 48 h and, after this period, the possible formation of colonies was observed. The MFC was considered the lowest concentration in which there was no growth in the plate<sup>35</sup>.

### 3. Results and discussion

#### 3.1 Protein purification

The extraction of proteins from defatted soy flour resulted in a sample containing  $18.79 \text{ mg}\cdot\text{mL}^{-1}$  of total proteins. The purification carried out using centrifugation and chromatographic methods of gel filtration resulted in a yield of 18.23% and a purification factor of 5.92, for which steps are summarized in Tab. 1. Although the yield was lower than reported by other authors<sup>25</sup>, the specific activity was about 5 times higher. This is because the soy used probably had a high initial urease content. Enzyme unit values are compatible with other study with embryo-specific soy urease, which showed values between 24,630 and 141,350 of enzyme units<sup>36</sup>. It is interesting to note that even in studies with heterologous expression of urease, the concentration in the culture medium is around  $2 \mu\text{g}\cdot\text{mL}^{-1}$  and  $5 \mu\text{g}\cdot\text{mL}^{-1}$  after purification and concentration respectively<sup>13</sup>. Thus, the results presented here are promising.

**Table 1.** Summary of *Gmax*Urease purification steps from soybean seeds.

| Step          | Proteins / $\text{mg}\cdot\text{mL}^{-1}$ | Enzyme unity / U | Specific activity / $\text{U}\cdot\text{mg}^{-1}$ | Yield / % | Purification factor |
|---------------|---|------------------|---|-----------|---------------------|
| Crude extract | 18.79                                     | 96,764.72        | 5,149.80  | 100.00    | 1.00                |
| G25           | 3.96                                      | 36,130.19        | 9,123.79  | 37.34     | 1.77                |
| Sephacryl     | 1.69                                      | 25,150.22        | 14,881.78   | 25.99     | 2.89                |
| Superdex      | 0.58                                      | 17,638.42        | 30,411.07   | 18.23     | 5.90                |

The urease purification chromatograms in the Sephadex G25, Sephacryl HS-200 and Superdex S-200 columns, pointing the peaks that showed ureolytic activity, are shown in Fig. 1a–c. It is noteworthy that, in the step performed using Superdex S-200 column, which has analytical grade, only the maximum point of the eluted peak was collected in the process, in order to ensure better purification. However, this fact may have contributed to the lower yield, when compared to another urease purification studies<sup>25</sup>.

The SDS-PAGE showed a band with approximately 90 kDa. According to data in the literature, ureases

correspond to 0.2 to 0.3% of soluble proteins that can be extracted<sup>37</sup>. Additional attempts to purify urease in a Q-Sepharose anion exchange column (GE Lifesciences) resulted in almost total loss of ureolytic activity, even after supplementation of the eluted fraction with nickel. Thus, the purification process was all carried out using different gel filtration columns. The calculated MW for the protein in solution using the elution volume of the Superdex S-200 column was 272.2 kDa, compatible as a trimer in solution (Fig. 1d).

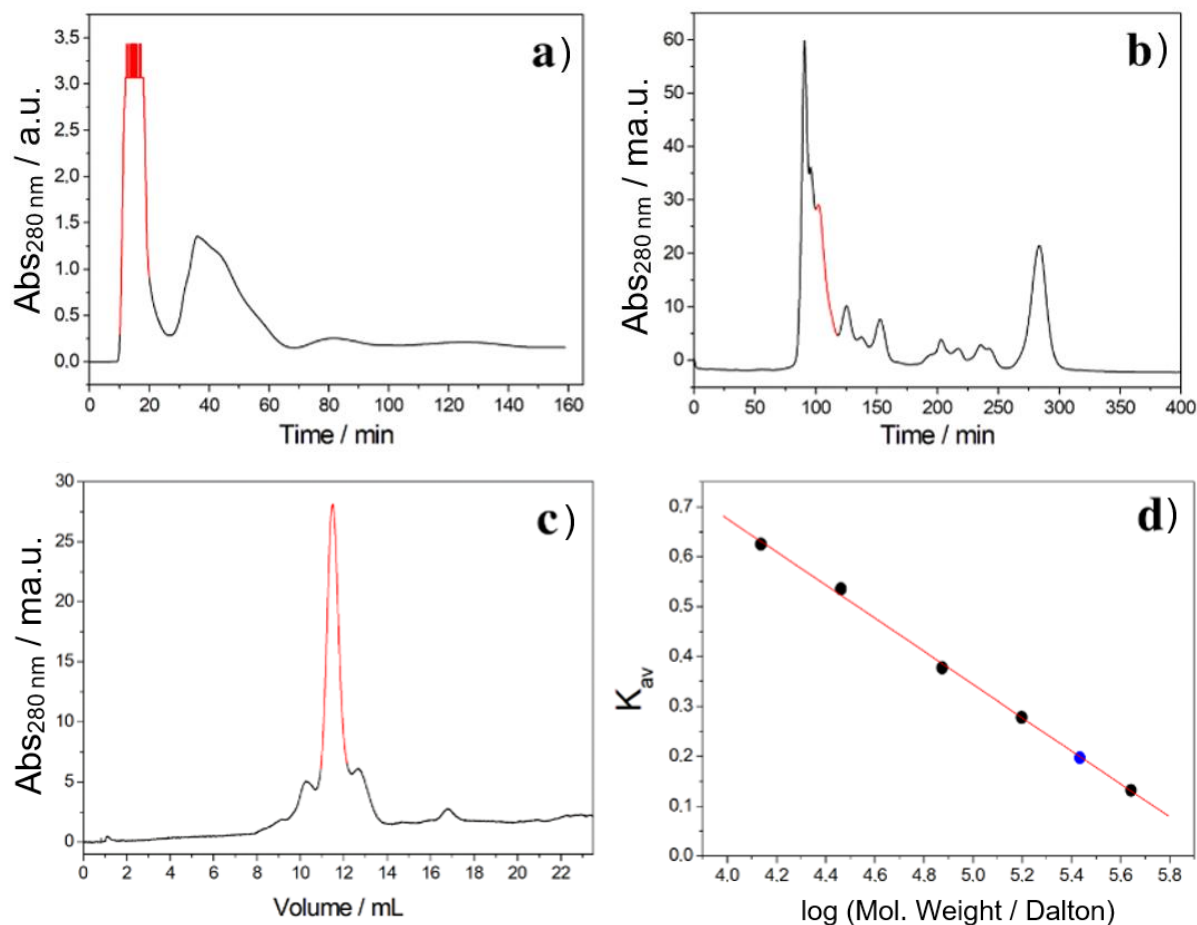


**Figure 1.** Chromatograms of the *GmaxUrease* purification steps. The red lines indicate the peaks that showed ureolytic activity and were collected. (a) Sephadex G25, (b) Sephacryl HS-200, (c) Superdex S-200. The volume referring to the peak of the Superdex S-200 column was used to estimate the molecular weight of *GmaxUrease* in figure (d). In this assay, 500  $\mu\text{L}$  of the protein mix with known molecular weights (black dots) was applied: Ferritin (440 kDa), aldolase (158 kDa), canalbumin (75 kDa), carbonic anhydrase (29 kDa) and ribonuclease (13.7 kDa), in the Superdex-200 10/300 column. To estimate the MW of *GmaxUrease*, 500  $\mu\text{L}$  of protein was applied at a concentration of  $1 \text{ mg}\cdot\text{min}^{-1}$ , and its elution volume converted to  $K_{av}$  (blue dot). The elution flow was  $0.5 \text{ mg}\cdot\text{min}^{-1}$  at room temperature of  $\sim 23 \text{ }^\circ\text{C}$ . The estimated MW was  $\sim 272.2 \text{ kDa}$ , compatible with a trimer in solution. The linear regression ( $y = a + bx$ ) parameters are:  $a = 2.00381$ ,  $b = -0.33196$  and  $R = -0.99912$ . The  $K_{av}$  for *GmaxUrease* is ( $y = 0.19961$ ).

### 3.2 Protein identification using data-independent analysis (MSE)

Mass spectrometry was performed using an electrospray ionization source and time of flight (TOF) analyzer, which allow proteomic analysis, since it is possible to form fragments with various charges and there is no molecular weight limitation for the analyzer. Thus, the protein on the electrophoresis gel band was digested by trypsin to obtain peptides for injection into the mass spectrometer, followed by comparative analysis using Uniprot database. The processing results data showed different levels of

coverage of urease sequences (several Uniprot ids) without occurrence of false positives. In view of the high molecular weight of this protein, the percentage found is suitable for its identification, considering that in other study the percentage of 20% was sufficient for this identification<sup>13</sup>. Table 2 summarizes the results of the mass spectrometry analysis and shows that all ranked proteins resulting from processing refer to soy urease. The alignment of the resulting sequences, let to the identification of the protein with Uniprot id: i1k3k3 with theoretical molecular mass of 90,338 Da being the most conserved, therefore, being used for modeling the protein structure.

**Table 2.** Results from mass spectrometry analysis of the band considered as *Gmax*Urease extracted from SDS-PAGE.

| Protein description (Uniprot)  | Uniprot id  | Score | Aligned peptides / % | Theoretical molecular weight / Da |
|--|---|-------|----------------------|-----------------------------------|
| Urease OS= <i>Glycine soja</i>   | a0a0b2rjr9  | 1211  | 28.11                | 90,046                            |
| Urease OS= <i>Glycine max</i>  | i1k3k3  | 1209  | 26.22                | 90,338                            |
| Urease OS= <i>Glycine soja</i>   | a0a445kny1  | 1209  | 26.22                | 90,360                            |
| Urease OS= <i>Glycine max</i>  | q7xac5  | 1026  | 18.62                | 90,157                            |
| Urease (Fragment) OS= <i>Glycine max</i>   | q41214  | 726   | 21.37                | 14,091                            |
| <b>Protein</b>   | Urease OS= <i>Glycine soja</i> ; Uniprot ID i1k3k3      |       |                      |                                   |
| <b>Species</b>   | <i>Glycine max</i> (Soybean) ( <i>Glycine hispida</i> ) |       |                      |                                   |
| <b>Peptide numbers</b>   | 17  |       |                      |                                   |
| <b>Peptide sequences</b>   | LGDTDLFAK   |       |                      |                                   |
|  | LNIAAGTAVR  |       |                      |                                   |
|  | GPLQGESDNDNFR   |       |                      |                                   |
|  | GGVVAWADMGDPNASIPTPEPVK                                 |       |                      |                                   |
|  | NYFLF   |       |                      |                                   |
|  | GSSSKPDELHDIK   |       |                      |                                   |
|  | DGLIVSIGK   |       |                      |                                   |
|  | EGTIAAEDILDIGAISSSDSQAMGR                               |       |                      |                                   |
|  | GGNGIADGQVNETNLR  |       |                      |                                   |
|  | NAVILK  |       |                      |                                   |
|  | YGPTTGDK  |       |                      |                                   |
|  | ADIGIK  |       |                      |                                   |
|  | ATTCTPAPSQMK  |       |                      |                                   |
|  | VEAVGNVR  |       |                      |                                   |
|  | EEEDASEGITGDPDSPFTTIIPREEYANK                           |       |                      |                                   |
|  | EDNRIPGEIYGDGSLVLPNGK                                   |       |                      |                                   |
|  | RVEAVGNVR   |       |                      |                                   |
| <b>Protein mass (MW)</b>   | 90,338  |       |                      |                                   |
| <b>Sequence coverage*</b>  | 26.22%  |       |                      |                                   |
| MKLSPREVEKLGHLNAGYLAQKRLARGLRLNYTEAVALIATQIMEFARDGEKTVQALMCIGKHLGRRQVLPEVQHLLNAVQV<br>EATFPDGTGLVTVHDPI SCEHGDGALFGSFLPVPVSLDKFAENK <b>EDNRIPGEIYGDGSLVLPNGKNAVILK</b> VVSNDRPIQ<br>VGSHYHFIEVNPYLTFDRRKAYGMR <b>LNIAAGTAVR</b> FEPGDSKSVKLVIRIGGNKVI <b>GGNGIADGQVNETNLR</b> EAMEAVCKRGF<br>GH <b>EEEDASEGITGDPDSPFTTIIPREEYANKYGPTTGDKIRLGDTDLFAK</b> IEKDFALYGDCEVFGGKVLDRDGMGQSCGHPP<br>AISLDTVITNAVIDYSGI <b>IKADIGIKDGLIVSIGK</b> AGNPDIMDDVFFNMIIGANTEVIAGEGLIVTAGAIDCHVHYICPQLV<br>DEAISSGITTLVGGGTGPTAGTR <b>ATTCTPAPSQMK</b> LMLQSTDDLPLNFGFTG <b>GSSSKPDELHDIK</b> AGAMGLKLHEDWGSTP<br>AAIDSCLTVADQYDIQINIHTDTLNEAGFVEHSIAAFKGRITHTYHSEGAGGGHAPDIIKVCGMKNVLPSSSTNPTPLTLNTI<br>DEHLDMVMVCHHLNREIPEDLAFACSR <b>IEGTIAAEDILDIGAISSSDSQAMGR</b> VGEVISRWTQANKMKVQR <b>GPLQGESDNDNFR</b><br><b>IKRYIAKYTINPAIANGFSQYVGSVEVGKLDLVMWKPSFFGAKPEMVIKGGVVAWADMGDPNASIPTPEPVK</b> MRP<br>MFGTLGKAGGALSIAFAAVDQRVHALYGLN <b>KRVEAVGNVR</b> KLTKLDMKLNDSLPQITVDPDNYTVTADGEVLTSEATTFVPLS<br><b>RNYFLF</b> |   |       |                      |                                   |

\*functional protein without N-terminal signal peptide.

### 3.3 Analysis of enzyme activity

Different enzyme batches were extracted from different soy samples, which guaranteed biological reproducibility. Then, in order to characterize the functional parameters of the protein, activity assays were carried out under different pH and temperature conditions (Fig. 2). The enzyme showed better activity at pH 6.5 and temperature close to 65 °C. Literature reports that the optimal pH for ureases, in general,

ranges between 5.0 and 8.0, depending on the species and even the isoform<sup>4</sup>. However, for ubiquitous soy urease, there are two peaks of activity, one around 5.5 and the other at 9.0<sup>21,38</sup>; however, there is a study that reports optimal activity for embryo-specific soy urease at pH 6.1<sup>39</sup>. Regarding the temperature, literature also reports variation, however, it is usually around 0 °C<sup>38</sup>.

The substrate concentration at maximum urease activity was close to 190 mmol L<sup>-1</sup> (Fig. 3a). Beyond this concentration, activity begins to decrease

gradually, a fact that can be explained by a mechanism of substrate inhibition<sup>40</sup>. Thus, the Michaelis–Menten equation was adjusted to the experimental points and provided  $K_M$  of  $109 \pm 23 \text{ mmol L}^{-1}$  and  $V_{\max}$  of  $2.5 \pm 0.4 \text{ mmol L}^{-1} \text{ NH}_3 \cdot \mu\text{g}_{\text{urease}}^{-1} \cdot \text{s}^{-1}$  (Fig. 3a). Values quite different from those obtained by the double-reciprocal plot (Fig. 3b), which presented  $K_M$  of  $\sim 526 \text{ mmol L}^{-1}$  and  $V_{\max}$  of  $7.4 \text{ mM NH}_3 \cdot \mu\text{g}_{\text{urease}}^{-1} \cdot \text{s}^{-1}$ . However, *Pisum sativum* urease showed the same substrate inhibitory effect, and its  $K_M$  found by adjusting the Michaelis–Menten equation to data points was close to  $100 \text{ mmol L}^{-1}$  but was  $500 \text{ mmol L}^{-1}$  when calculated by the double-reciprocal plot at pH 7.5<sup>25</sup>. These values are very similar to those found in this work.

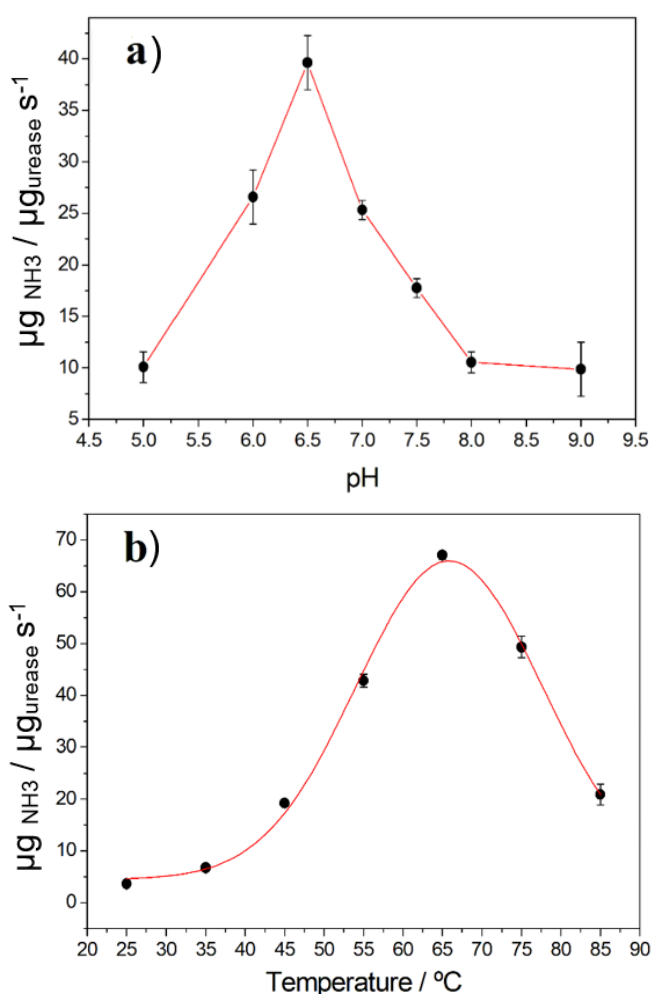


**Figure 2.** Effects of changes in the experimental conditions on the catalytic activity of *GmaxUrease*. (a) Effect of pH using  $0.04 \text{ mol L}^{-1}$  Britton–Robinson buffer, with 3% urea and a temperature of  $55 \text{ }^\circ\text{C}$ . (b) Effect of temperature using  $0.2 \text{ mol L}^{-1}$  phosphate buffer, 3% urea, pH 6.5. In both assays, the enzyme concentration was  $2.7 \mu\text{g}\cdot\text{mL}^{-1}$ . Each point on the graph represents the average of two repetitions.

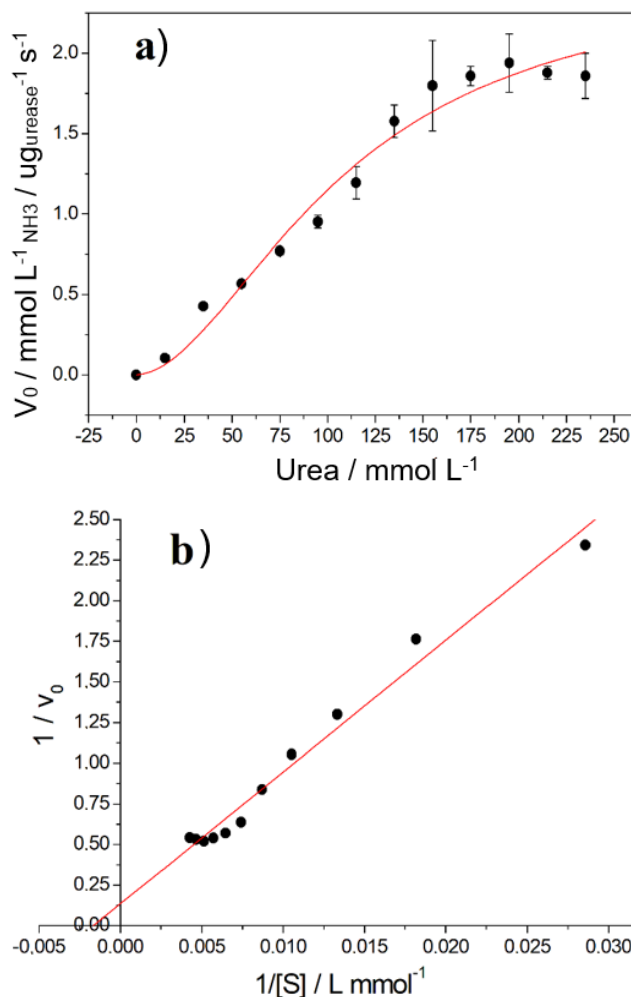


**Figure 3.** Effect of the substrate (urea) concentration on the catalytic activity of *GmaxUrease*, using  $0.2 \text{ mol L}^{-1}$  phosphate buffer, pH of 6.5 at  $65 \text{ }^\circ\text{C}$  temperature. (a) Michaelis–Menten plot showing a tendency of decrease in velocity at urea concentrations higher than  $195 \text{ mmol L}^{-1}$ . The red line represents the best fit of Michaelis–Menten equation to the experimental data points. (b) Double-reciprocal plot for estimating  $K_M$  and  $V_{\max}$  values. Each point on the graphs represents the average of two repetitions.

### 3.4 Evaluation of antifungal activity

We carried out microbiological assays aiming to evaluate the antifungal property of *GmaxUrease* against the human pathogenic fungus *P. brasiliensis*. Until then, this property of urease was never evaluated against this fungal. The MIC and MFC values obtained were  $\sim 10 \mu\text{g}\cdot\text{mL}^{-1}$  of urease. Bovine serum albumin was used as negative control in order to verify a possible inhibitory osmotic effect due to protein concentration; however, such influence did not occur



(Fig. 4). The MIC/MFC values found are promising, because, although this is the first study that demonstrates the urease antifungal activity against *P. brasiliensis*, when comparing this result to similar ones that used other fungi, such as the yeast *Candida albicans*, the MIC values ranged between 240 to 150  $\mu\text{g}\cdot\text{mL}^{-1}$  of urease<sup>11,13</sup>.

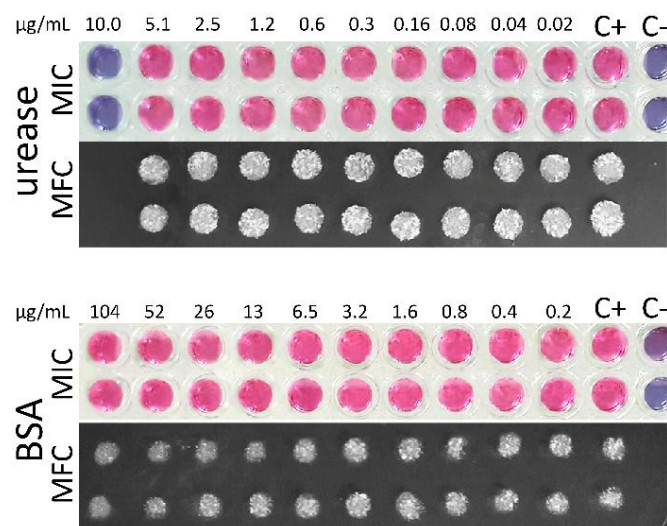


**Figure 4.** The experimental values of MIC and MFC of *GmaxUrease* against Pb18 strain of *P. brasiliensis*. The inoculum concentration was  $10^5$  CFU and *GmaxUrease* concentration ranged between  $0.02 \mu\text{g}\cdot\text{mL}^{-1}$  to  $10 \mu\text{g}\cdot\text{mL}^{-1}$ . The concentration of BSA ranged between  $0.2$  to  $104.4 \mu\text{g}\cdot\text{mL}^{-1}$ . Minimal inhibitory concentration is displayed in color and MFC in black/white. Negative control (C-) and positive control (C+).

### 3.5 Modeled structure

The final model of *GmaxUrease* shares 92.3% identity with template from *Canavalia ensiformis* and presents excellent stereochemical quality with 91.9% of the residues in the most favored, 7.8% in the additional allowed and only 0.3% of the residues in the generously allowed regions of Ramachandran plot, a much better quality than template (88.3%, 11.1% and 0.6% respectively). The Fig. 5a and b shows the embryo-specific soy urease modeled in this study. The pdb file is provided as supplementary material. Ureases have high homology between different organisms, which indicates common genetic ancestry and similar catalytic action<sup>3,6</sup>. This may justify all residues of catalytic site conserved in *GmaxUrease* regarding *Canavalia ensiformis*. However, the three-dimensional structure of ureases varies between organisms and many still need to be clarified<sup>10</sup>. Plants have ureases

formed by a single kind of chain with ~90 kDa, which form complex trimers ( $\alpha_3$ ), hexamers ( $\alpha_6$ ) and, more rarely, dodecamers ( $\alpha_{12}$ ), located in the cytosol of plant and fungal cells<sup>2,6,10</sup>. There are studies indicating that fungitoxic activity of ureases is independent of the catalytic activity<sup>1,11</sup>, being related to the release of peptides with antimicrobial activity when hydrolyzed. It is noteworthy that *P. brasiliensis* has close to 30 to 35 extracellular proteases<sup>41</sup>, which could act on urease, resulting in polypeptides that could be toxic to the fungus. The Fig. 5c shows the alignment of part of the amino acid sequences of plant and microorganisms ureases, plus the recombinant jaburetox peptide identified in the urease of *Canavalia ensiformis*, considered responsible for the antifungal effect<sup>12</sup>. In *GmaxUrease*, the homologous sequence corresponds to residues 229 to 269. It is noteworthy that microorganisms do not have this sequence in their ureases. There are several hypotheses to explain the antifungal mechanism of these peptides, the most likely being due to the reorganization of membrane lipids<sup>12</sup>; however, for *GmaxUrease*, this mechanism still needs validation assays.

Regardless of the action mechanism, the antifungal property of *GmaxUrease* against Pb18, the most virulent strain of *P. brasiliensis*, was clearly demonstrated in this work. Due to the low yield of the protein obtained, it was not possible to perform additional tests in this work. However, the results presented here demonstrate the feasibility for carrying out future studies, aiming at the expression of recombinant *GmaxUrease*. The soybean is a feedstock widely used in human and animal nutrition and there are no reports of toxic effects in humans regarding the ingestion of urease present in soy. The possibilities for biotechnological use of ureases are wide and can be explored in topical creams formulations for antifungal medicines, especially for oral manifestations of PCM, dermatophytes, as well as a natural preservative in industrialized foods, replacing possible antimicrobial products. This work allows to envision a wide range of research possibilities for the biotechnological applications of soy urease. In addition, despite being an organism of economic and agricultural interest, the notation of soy proteins in the proteomic databases is still very incipient. Many proteins do not have status (sequence of amino acids) confirmed by means of sequencing studies, which include urease. This work helps to improve this notation.

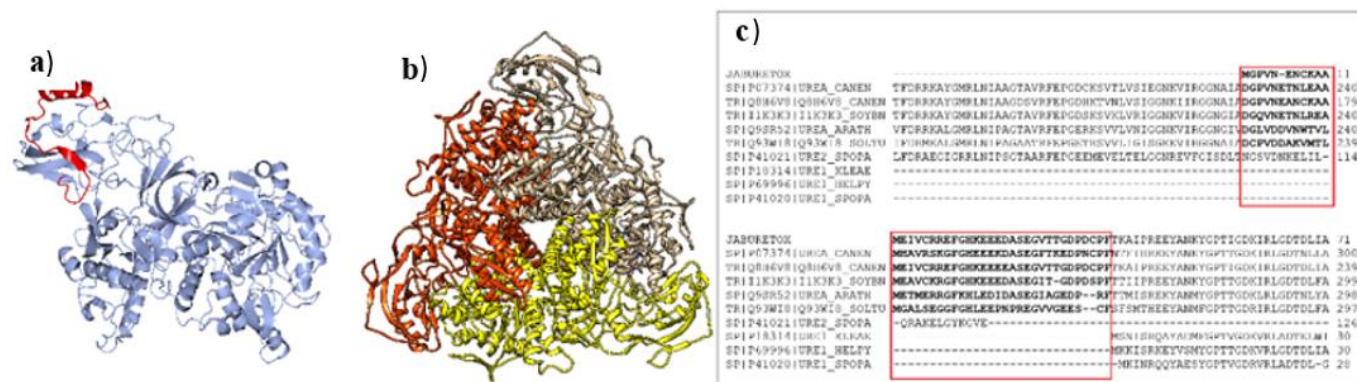


**Figure 5.** *GmaxUrease* as structure models and homologs alignment. **(a)** Ribbon model (blue) of the modeled structure of *GmaxUrease*. The red segment represents the peptide homolog to jaburetox. **(b)** Ribbon representation of the biological unit (trimer). **(c)** Alignment of plant urease sequences: Jaburetox, *Canavalia ensiformis* (P07374), *Canavalia ensiformis* JBURE-II (Q8H6V8), *Glycine max*, this work (I1K3K3), *Arabidopsis thaliana* (Q9SR52), *Solanum tuberosum* (Q93WI8). Microorganisms ureases: *Sporosarcina pasteurii* (P41021), *Klebsiella aerogenes*, alpha subunit (P18314), *Helicobacter pylori*, beta subunit (P69996) and *Sporosarcina pasteurii*, alpha subunit (P41020). The jaburetox peptide present in plant ureases, but absent in bacterial ureases, is highlighted by a red rectangle.

#### 4. Conclusions

The embryo-specific soybean urease was extracted and kept its functional properties after centrifugation, gel filtration chromatography and ultrafiltration membrane separation techniques. The results obtained from structural analysis by LC-MS<sup>E</sup>, as well as the characterization of the functional catalytic activity, were compatible with those of embryo-specific soy urease. The enzyme has homotrimer as biological unit and, therefore, the structure was modeled by homology in this assembly. In terms of kinetic parameters, the enzyme presented  $K_M$  of  $\sim 526 \text{ mmol L}^{-1}$  and  $V_{\max}$  of  $7.4 \text{ mmol L}^{-1} \text{NH}_3 \mu\text{g}_{\text{urease}}^{-1} \text{ s}^{-1}$ , similar to those from *Pisum sativum* urease. The extracted protein fraction showed, for the first time, an activity compatible with fungicidal profile (*in vitro*) against *P. brasiliensis*. We hope to contribute to better understanding the antifungal property of this enzyme, in order to glimpse other possible biotechnological applications.

#### Acknowledgments

This work was funded by Fundação Araucária (grant numbers: 40/16 and 53/19), CAPES cod 001, National Council for Scientific and Technological Development (CNPq), Federal Foundation for the Brazilian Research and Development (0673/13-CT-Infra-FINEP) and Complex of Research Support Centers of State University of Maringá (COMCAP-UEM). In particular, we thank professor Márcio Francisco Colombo and João Ruggiero Neto, for their

contribution in guiding and training part of the authors of this work, which allowed us to create a research group in biochemistry and molecular biophysics at UEM.

#### References

- [1] Balasubramanian, A., Durairajpandian, V., Elumalai, S., Mathivanan, N., Munirajan, A. K., Ponnuraj, K., Structural and functional studies on urease from pigeon pea (*Cajanus cajan*), *International Journal of Biological Macromolecules* 58 (2013) 301-309. <https://doi.org/10.1016/j.ijbiomac.2013.04.055>.
- [2] Carlini, C. R., Ligabue-Braun, R., Ureases as multifunctional toxic proteins: A review, *Toxicon* 110 (2016) 90-109. <https://doi.org/10.1016/j.toxicon.2015.11.020>.
- [3] Kappaun, K., Piovesan, A. R., Carlini, C. R., Ligabue-Braun, R., Ureases: Historical aspects, catalytic, and non-catalytic properties – A review, *Journal of Advanced Research* 13 (2018) 3-17. <https://doi.org/10.1016/j.jare.2018.05.010>.
- [4] Fisher, K. A., Yarwood, S.A., James, B. R., Soil urease activity and bacterial ureC gene copy numbers: Effect of pH, *Geoderma* 285 (2017) 1-8. <https://doi.org/10.1016/j.geoderma.2016.09.012>.
- [5] Wessén, E., Nyberg, K., Jansson, J. K., Hallin, S., Responses of bacterial and archaeal ammonia oxidizers to soil organic and fertilizer amendments under long-term management, *Applied Soil Ecology* 45 (2010) 193-200. <https://doi.org/10.1016/j.apsoil.2010.04.003>.

- [6] Krajewska, B., Ureases I. Functional, catalytic and kinetic properties: A review, *Journal of Molecular Catalysis B: Enzymatic* 59 (2009) 9–21. <https://doi.org/10.1016/j.molcatb.2009.01.003>.
- [7] Wiebke-Strohm, B., Ligabue-Braun, R., Rechenmacher, C., De Oliveira-Busatto, L. A., Carlini, C. R., Bodanese-Zanettini, M. H., Structural and transcriptional characterization of a novel member of the soybean urease gene family, *Plant Physiology and Biochemistry* 101 (2016) 96–104. <https://doi.org/10.1016/j.plaphy.2016.01.023>.
- [8] Polacco, J. C., Mazzafera, P., Tezotto, T., Opinion – Nickel and urease in plants: Still many knowledge gaps, *Plant Science* 199–200 (2013) 79–90. <https://doi.org/10.1016/j.plantsci.2012.10.010>.
- [9] Follmer, C., Barcellos, G. B. S., Zingali, R. B., Machado, O. L. T., Alves, E. W., Barja-Fidalgo, C., Guimarães, J. A., Carlini, C. R., Canatoxin, a toxic protein from jack beans (*Canavalia ensiformis*), is a variant form of urease (EC 3.5.1.5): biological effects of urease independent of its ureolytic activity, *Biochemical Journal* 360 (2001) 217–224. <https://doi.org/10.1042/0264-6021:3600217>.
- [10] Postal, M., Martinelli, A. H. S., Becker-Ritt, A. B., Ligabue-Braun, R., Demartini, D. R., Ribeiro, S. F. F., Pasquali, G., Gomes, V. M., Carlini, C. R., Antifungal properties of *Canavalia ensiformis* urease and derived peptides, *Peptides* 38 (2012) 22–32. <https://doi.org/10.1016/j.peptides.2012.08.010>.
- [11] Becker-Ritt, A. B., Martinelli, A. H. S., Mitidieri, S., Feder, V., Wassermann, G.E., Santi, L., Vainstein, M. H., Oliveira, J. T. A., Fiuza, L. M., Pasquali, G., Carlini, C. R., Antifungal activity of plant and bacterial ureases, *Toxicon* 50 (2007) 971–983. <https://doi.org/10.1016/j.toxicon.2007.07.008>.
- [12] Martinelli, A. H. S., Kappaun, K., Ligabue-Braun, R., Defferrari, M. S., Piovesan, A. R., Stanisçuaski, F., Demartini, D. R., Dal Belo, C. A., Almeida, C. G. M., Follmer, C., Verli, H., Carlini, C. R., Pasquali, G., Structure–function studies on jaburetox, a recombinant insecticidal peptide derived from jack bean (*Canavalia ensiformis*) urease, *Biochimica et Biophysica Acta (BBA) - General Subjects* 1840 (2014) 935–944. <https://doi.org/10.1016/j.bbagen.2013.11.010>.
- [13] Martinelli, A. H. S., Lopes, F. C., Broll, V., Defferrari, M. S., Ligabue-Braun, R., Kappaun, K., Tichota, D. M., Fruttero, L. L., Moyetta, N. R., Demartini, D. R., Postal, M., Medeiros-Silva, M., Becker-Ritt, A. B., Pasquali, G., Carlini, C. R., Soybean ubiquitous urease with purification facilitator: An addition to the moonlighting studies toolbox, *Process Biochemistry* 53 (2017) 245–258. <https://doi.org/10.1016/j.procbio.2016.12.003>.
- [14] Wanke, B., Aidê, M.A., Capítulo 6 - Paracoccidioidomicose, *Jornal Brasileiro de Pneumologia* 35 (2009) 1245–1249. <https://doi.org/10.1590/S1806-37132009001200013>.
- [15] Ferreira, M. S., Paracoccidioidomycosis, *Paediatric Respiratory Reviews* 10 (2009) 161–165. <https://doi.org/10.1016/j.prrv.2009.08.001>.
- [16] Ricci, C.D., Evangelista, C., Tomaz, B.C.A., da Silva, M.V., Barbo, M.L.P., Paracoccidioidomicose: forma crônica cutânea, *Revista da Faculdade Ciências Médicas Sorocaba* 20 (2018) 51. <https://doi.org/10.23925/1984-4840.2018v20i1a12>.
- [17] Queiroz-Telles, F., Fahal, A. H., Falci, D. R., Caceres, D. H., Chiller, T., Pasqualotto, A. C., Neglected endemic mycoses, *The Lancet Infectious Disease* 17 (2017) e367–e377. [https://doi.org/10.1016/S1473-3099\(17\)30306-7](https://doi.org/10.1016/S1473-3099(17)30306-7).
- [18] Shikanai-Yasuda, M. A., Mendes, R. P., Colombo, A. L., Telles, F. de Q., Kono, A., Paniago, A. M. M., Nathan, A., do Valle, A. C. F., Bagagli, E., Benard, G., Ferreira, M.S., Teixeira, M. de M., Vergara, M. L. S., Pereira, R. M., Cavalcante, R. de S., Hahn, R., Durlacher, R.R., Khoury, Z., de Camargo, Z.P., Moretti, M. L., Martinez, R., II Consenso Brasileiro em Paracoccidioidomicose - 2017, *Epidemiologia e Serviços Saúde*. 27 (2018). <https://doi.org/10.5123/S1679-49742018000500001>.
- [19] Borba, J. V. V. B., Tauhata, S. B. F., de Oliveira, C. M. A., Marques, M. F., Bailão, A. M., Soares, C. M. de A., Pereira, M., Chemoproteomic identification of molecular targets of antifungal prototypes, thiosemicarbazide and a camphene derivative of thiosemicarbazide, in *Paracoccidioides brasiliensis*, *PLoS One*. 13 (2018) e0201948. <https://doi.org/10.1371/journal.pone.0201948>.
- [20] Nicola, A. M., Albuquerque, P., Paes, H. C., Fernandes, L., Costa, F. F., Kioshima, E. S., Abadio, A. K. R., Bocca, A. L., Felipe, M. S., Antifungal drugs: New insights in research & development, *Pharmacology & Therapeutics* 195 (2019) 21–38. <https://doi.org/10.1016/j.pharmthera.2018.10.008>.
- [21] Bracco, L. F., Levin, G. J., Urtasun, N., del Cañizo, A. A. N., Wolman, F. J., Miranda, M. V., Cascone, O., Covalent immobilization of soybean seed hull urease on chitosan mini-spheres and the impact on their properties, *Biocatalysis and Agricultural Biotechnology* 18 (2019) 101093. <https://doi.org/10.1016/j.bcab.2019.101093>.
- [22] Laemmli, U. K., Cleavage of Structural Proteins during the Assembly of the Head of Bacteriophage T4, *Nature* 227 (1970) 680–685. <https://doi.org/10.1038/227680a0>.
- [23] Bradford, M. M., A rapid and sensitive method for the quantitation of microgram quantities of protein utilizing the

principle of protein-dye binding, *Analytical Biochemistry* 72 (1976) 248–254. <https://doi.org/10.1006/abio.1976.9999>.

[24] Bzura, J., Koncki, R., A mechanized urease activity assay, *Enzyme and Microbial Technology* 123 (2019) 1–7. <https://doi.org/10.1016/j.enzmictec.2019.01.001>.

[25] El-Hefnawy M. E., Sakran, M., Ismail, A. I., Aboelfetoh, E., Extraction, purification, kinetic and thermodynamic properties of urease from germinating *Pisum Sativum* L. seeds, *BMC Biochemistry* 15 (2014) 15. <https://doi.org/10.1186/1471-2091-15-15>.

[26] Shevchenko, A., Jensen, O. N., Podtelejnikov, A. V., Sagliocco, F., Wilm, M., Vorm, O., Mortensen, P., Shevchenko, A., Boucherie, H., Mann, M., Linking genome and proteome by mass spectrometry: Large-scale identification of yeast proteins from two dimensional gels, *Proceedings of the National Academy of Sciences of the United States of America* 93 (1996) 14440–14445. <https://doi.org/10.1073/pnas.93.25.14440>.

[27] Shevchenko, A., Wilm, M., Vorm, O., Mann, M., Mass Spectrometric Sequencing of Proteins from Silver-Stained Polyacrylamide Gels, *Analytical Chemistry* 68 (1996) 850–858. <https://doi.org/10.1021/ac950914h>.

[28] Balasubramanian, A., Ponnuraj, K., Crystal Structure of the First Plant Urease from Jack Bean: 83 Years of Journey from Its First Crystal to Molecular Structure, *Journal of Molecular Biology* 400 (2010) 274–283. <https://doi.org/10.1016/j.jmb.2010.05.009>.

[29] Webb, B., Sali, A., Comparative Protein Structure Modeling Using MODELLER, *Current Protocols in Bioinformatics* 54 (2016). <https://doi.org/10.1002/cpbi.3>.

[30] Collaborative Computational Project Number 4, The CCP4 suite: programs for protein crystallography, *Acta Crystallographica Section D Structural Biology* 50 (1994) 760–763. <https://doi.org/10.1107/S0907444994003112>.

[31] Britton, H. T. S., Robinson, R. A., CXC VIII—Universal buffer solutions and the dissociation constant of veronal, *Journal of the Chemical Society* (1931) 1456–1462. <https://doi.org/10.1039/JR9310001456>.

[32] CLSI, Método de Referência para Testes de Diluição em Caldo para a Determinação da Sensibilidade a Terapia Antifúngica das Leveduras, 22 (2002) 1–50.

[33] Wayne, P. A., CLSI. Performance Standards for Antimicrobial Susceptibility Testing; Twenty-second Informational supplement. CLSI document M100-S22. Clinical and Laboratory Standards Institute, 2015.

[34] Rodrigues-Vendramini, F. A. V., Faria, D. R., Arita, G. S., Capoci, I. R. G., Sakita, K. M., Caparroz-Assef, S. M., Becker, T. C. A., Bonfim-Mendonça, P. S., Felipe, M. S.,

Svidzinski, T. I. E., Maigret, B., Kioshima, É. S., Antifungal activity of two oxadiazole compounds for the paracoccidioidomycosis treatment, *PLoS Neglected Tropical Diseases* 13 (2019) e0007441. <https://doi.org/10.1371/journal.pntd.0007441>.

[35] Rodrigues-Vendramini, F. A. V., Marschalk, C., Toplak, M., Macheroux, P., Bonfim-Mendonça, P. S., Svidzinski, P. T. I. E., Seixas, F. A. V., Kioshima, E. S., Promising New Antifungal Treatment Targeting Chorismate Synthase from *Paracoccidioides brasiliensis*, *Antimicrobial Agents and Chemotherapy* 63 (2018) e01097-18. <https://doi.org/10.1128/AAC.01097-18>.

[36] Polacco, J. C., Havir, E. A., Comparisons of soybean urease isolated from seed and tissue culture., *Journal of Biological Chemistry*, 254 (1979) 1707-1715.

[37] Polacco, J. C., Thomas, A. L., Bledsoe, P. J., A Soybean Seed Urease-Null Produces Urease in Cell Culture, *Plant Physiology* 69 (1982) 1233-1240. <https://doi.org/10.1104/pp.69.5.1233>.








[38] Torisky, R. S., Polacco, J. C., Soybean Roots Retain the Seed Urease Isozyme Synthesized during Embryo Development, *Plant Physiology* 94 (1990) 681-689. <https://doi.org/10.1104/pp.94.2.681>.

[39] Polacco, J. C., Winkler, R. G., Soybean Leaf Urease: A Seed Enzyme?, *Plant Physiology* 74 (1984) 800-803. <https://doi.org/10.1104/pp.74.4.800>.

[40] Yoo, Y. J., Feng, Y., Kim, Y.-H., Yagonia, C. F. J., *Fundamentals of Enzyme Engineering*, New York, Springer, 2017. <https://doi.org/10.1007/978-94-024-1026-6>.

[41] Desjardins, C. A., Champion, M. D., Holder, J. W., Muszewska, A., Goldberg, J., Bailão, A. M., Brigido M. M., Ferreira, M. E. S., Garcia, A. M., Grynberg, M., Gujja, S., Heiman, D. I., Henn, M. R., Kodira, C. D., León-Narváez, H., Longo, L. V. G., Ma, L.-J., Malavazi, I., Matsuo, A. L., Morais, F. V., Pereira, M., Rodríguez-Brito, S., Sakthikumar, S., Salem-Izacc, S. M., Sykes, S. M., Teixeira, M. M., Vallejo, M. C., Walter, M. E. M. T., Yandava, C., Young, S., Zeng, Q., Zucker, J., Felipe, M. S., Goldman, G. H., Haas, B. J., McEwan, J. G., Nino-Vega, G., Puccia, R., San-Blas, G., Soares, C. M. A., Birres, B. W., Cuomo, C. A., Comparative Genomic Analysis of Human Fungal Pathogens Causing Paracoccidioidomycosis, *PLoS Genetics* 7 (2011) e1002345. <https://doi.org/10.1371/journal.pgen.1002345>.

# Production and biochemical characterization of xylanases synthesized by the thermophilic fungus *Rasamsonia emersonii* S10 by solid-state cultivation

Jéssica de Araujo Zanoni<sup>1</sup>, Isabela Brunozi de Oliveira<sup>1</sup>, Olavo Micali Perrone<sup>1</sup>, Julieth Orduña Ortega<sup>2</sup>, Maurício Boscolo<sup>1</sup>, Eleni Gomes<sup>1</sup>, Gustavo Orlando Bonilla-Rodriguez<sup>1+</sup>

1. São Paulo State University, Institute of Biosciences, Languages and Exact Sciences, São José do Rio Preto, Brazil.  
2. Universidad Santiago de Cali, Facultad de Ciencias Basicas, Cali, Colombia.

**+Corresponding author:** Gustavo Orlando Bonilla Rodriguez, **Phone:** +55 17 3221-2361, **Email address:** [gustavo.b.rodriguez@unesp.br](mailto:gustavo.b.rodriguez@unesp.br)

## ARTICLE INFO

### Article history:

**Received:** July 03, 2020

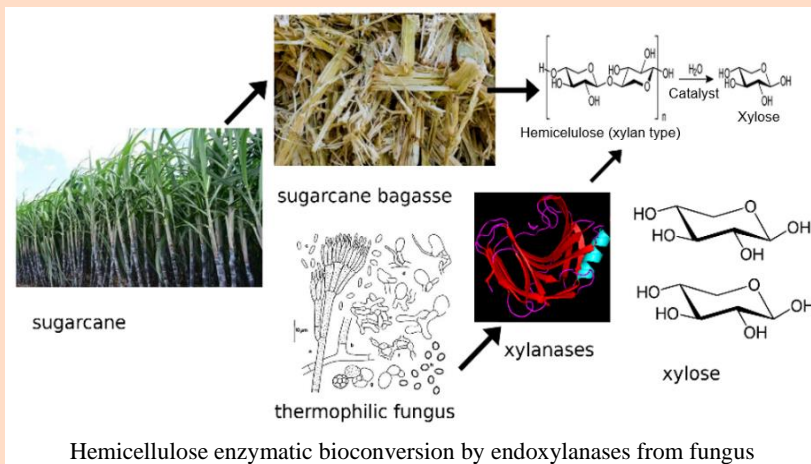
**Accepted:** November 11, 2020

**Published:** April xx, 2021

## Keywords

1. Endoxylanases
2. Thermostability
3. Sugarcane bagasse
4. Thermophilic fungus
5. Solid-state cultivation

**ABSTRACT:** The xylanolytic enzyme complex hydrolyzes xylan, and these enzymes have various industrial applications. The goal of this work was to characterize the endoxylanases produced by the thermophilic fungus *Rasamsonia emersonii* in solid-state cultivation. Tests were carried out to evaluate the effects of pH, temperature, glycerol and phenolic compounds on enzyme activity. Thermal denaturation of one isolated enzyme was evaluated. The crude extract from *R. emersonii* was applied to breakdown pretreated sugarcane bagasse, by quantifying the release of xylose and glucose. The optimum pH value for the crude enzymatic extract was 5.5, and 80 °C was the optimum temperature. Regarding the stability of the crude extract, the highest values occurred between the pH ranges from 4 to 5.5. Several phenolic compounds were tested, showing an increase in enzymatic activity on the crude extract, except for tannic acid. Zymography displayed four corresponding endoxylanase bands, which were isolated by extraction from a polyacrylamide gel. The thermodynamic parameters of isolated Xylanase C were evaluated, showing a half-life greater than 6 h at 80 °C (optimum temperature), in addition to high melting temperature (93.3 °C) and structural resistance to thermal denaturation. Pretreated sugarcane bagasse breakdown by the crude enzymatic extract from *R. emersonii* has good hemicellulose conversion to xylose.



Hemicellulose enzymatic bioconversion by endoxylanases from fungus

## 1. Introduction

The negative effects resulting from the growing demand for fossil fuel energy have mobilized the international community in the search for renewable fuels<sup>1,2</sup>. An alternative is the use of biofuels, and, among them bioethanol, or second-generation ethanol (2G), obtained by the fermentation of sugars present in plant residues<sup>3,4</sup>.

The plant cell wall matrix is lignocellulosic and composed of cellulose fibrils with a protective layer of hemicellulose and lignin. Covalent bonds ensure cell wall rigidity and high resistance to microbial degradation<sup>5</sup>. Cellulose is the primary constituent<sup>6</sup>, followed by hemicellulose, which is composed by different linked monomers, resulting in a branched heteropolysaccharide. These monomers include pentoses (D-xylose, L-arabinopyranose, L-arabinofuranose), hexoses (D-glucose, D-mannose, D-galactose), hexuronic acids (D-glycuronic, D-4-O-methylglycuronic, D-galacturonic) and deoxyhexoses (L-rhamnose and L-fucose)<sup>7</sup>. Xylan, a polymer of D-xylose, is the primary polymer constituent of hemicelluloses.

Xylanases degrade xylan by hydrolyzing the  $\beta$  1,4 glycosidic bonds producing xylooligosaccharides (XOS) and  $\beta$ -xylosidases convert them to xylose. However, xylan has more structural complexity, containing  $\beta$ -D-xylopyranoside residues linked by  $\beta$  1,4 glycosidic bonds associated with other sugars, forming glucuronoxylans, glucuronoarabinoxylans, glucomannans, arabinogalactans and galactoglucomannans<sup>8</sup>. Because of this heterogeneity, their complete hydrolysis requires several enzymes acting synergistically to convert their disaccharides and constituent monosaccharides into its subunits<sup>9,10</sup>.

Industry uses enzymes of the xylanolytic complex in different processes. For example, the paper industry uses enzymes in the bleaching stage to replace chlorine, as they promote the removal of xylan linked to the lignin, facilitating the bleaching of lignin<sup>11</sup>. They are also used in the pretreatment of arabinoxylan found in the substrate in beer production, reducing the viscosity and facilitating the process of filtration. These enzymes are employed in the production of bread, by increasing the volume of the product, making the dough soft and loose<sup>12</sup>.

Filamentous fungi are the major producers of enzymes of the xylanolytic complex, followed by macromycetes, bacteria, seaweed and some germinating plant seeds<sup>8</sup>. Fungal enzymes for biotechnological purposes can be produced in two main ways: by cultivation in solid-state (CSS) or by

submerged culture (CSm). The CSm is characterized by the high availability of free water in the culture medium<sup>13</sup>. To promote the aeration necessary for the growth of filamentous fungi, it is necessary to agitate the culture medium, but the constant agitation during the growth of the mycelium can cause morphological changes in the microorganism<sup>14</sup>, resulting in changes in the metabolite production.

Cultivation in solid-state is carried out without the presence of free water, and with the humidity necessary for fungal growth<sup>15</sup>, the material is incubated and the product is recovered at the end of the process. The solid substrate provides better conditions for mycelial growth and is similar to the natural environment of fungi, requiring a lower demand of energy<sup>16</sup>. Aeration of the medium does not require agitation when the fungus contact surface with the substrate is assured.

The biodegradation of xylan by enzymes from the xylanolytic complex allows to obtain several products, such as xylitol, xylooligosaccharides (XOS) and xylose<sup>8,17</sup>. In recent years, the use of these enzymes in saccharification of plant biomass has gained prominence, since in combination with other enzymes they facilitate the release of monosaccharides from the hemicellulose polymer, thus, yeasts can metabolize them for the production of second generation ethanol<sup>4</sup>. The enzymatic attack on the lignocellulosic material allows the conversion of polymers into carbohydrate monomers. For an efficient degradation, it is necessary to overcome the structural barrier of this material, and for that pretreatment strategies are adopted. Several options can be used; the main ones are physical, chemical and biological pretreatment. Also, the combination of these processes is described as more efficient in removing the noncellulosic fraction<sup>18</sup>.

Physical pretreatment (grinding, radiation, or heat treatment) is responsible for decreasing polymerization of the material, increasing the surface area. Among thermal methods, high temperatures are required, the biomass is mixed with water and are heated to the desired temperature and held at the pretreatment conditions for a controlled time before being cooled<sup>19</sup>. Higher temperatures require shorter treatment times, while lower temperatures require longer treatment times. In this context, it would be helpful to use thermostable enzymes for the next hydrolysis step, thus, the pretreated material could be hydrolyzed at high temperatures, saving refrigeration resources.

This study describes a biochemical characterization of endoxylanases from the crude extract of the thermophilic fungi *Rasamsonia emersonii*. In addition, it was investigated the effectiveness of this crude

extract to hydrolyze pretreated sugarcane bagasse to release products, like glucose and xylose. Endoxylanases isolation and the analysis of thermostability for the enzyme with the highest activity towards xylan were also carried out.

## 2. Experimental

### 2.1 Materials

All chemicals and solvents used for the procedures were analytical grade.

### 2.2 Enzyme production by *R. emersonii* S10 by solid-state cultivation

The thermophilic fungus *R. emersonii* S10, isolated and identified by a previous work<sup>20</sup>, was cultivated on Sabouraud dextrose agar. From this agar, 20 disks of 1 cm in diameter were extracted and cultivated at 55 °C for 6 days in individual polypropylene bags containing 5 g (1:1:1 w/w) of sugarcane bagasse, wheat bran and corn straw, these were previously washed on distilled water and dried at 47 °C until constant weight. To each bag were added 20 mL of nutrition solution (3.5 g L<sup>-1</sup> of (NH<sub>4</sub>)<sub>2</sub>SO<sub>4</sub>, 3 g L<sup>-1</sup> of KH<sub>2</sub>PO<sub>4</sub>, 0.5 g L<sup>-1</sup> of CaCl<sub>2</sub>, 0.5 g L<sup>-1</sup> of MgSO<sub>4</sub>·7H<sub>2</sub>O and 10 g L<sup>-1</sup> of tween 80) at pH 5.0.

To prepare the enzyme extract, 50 mL of deionized water was added, and the plastic bags were placed on an orbital shaker at 150 rpm for 40 min. The liquid extract containing the enzymes was transferred from the bag and it was vacuum filtered through a 0.45 μm nylon membrane. Subsequently, the filtrate was centrifuged at 10,000 xg for 30 min at 4 °C. The supernatant was the used as crude extract in the subsequent procedures.

### 2.3 Biochemical characterization of xylanases from the crude extract

To determine the xylanolytic activity, the sample was incubated in 1% (w/v) beechwood xylan at 55 °C for 10 min, and for endoglucanase activity, the sample was incubated with 4% (w/v) of carboxymethylcellulose (CMC) as substrate at 50 °C using a 1:9 enzyme:substrate volume ratio<sup>21</sup>. The released reducing sugars reacted with 3,5-dinitrosalicylic acid (DNS) and the activity was quantified using spectrophotometry, being expressed as the product concentration change over time (d[P]/dt)<sup>22</sup>, which was linear up to 4 min, time adopted for the

enzymatic assays. Experiments were carried out using a 0.1 mol L<sup>-1</sup> acetate buffer pH 5.5, with the exception of the determination of the optimal pH.

All experiments to determine the optimal pH (3.0–9.5) and temperature (30–90 °C) were conducted in three repetitions, and the pH stability of the crude extract was evaluated after 24 h of incubation in this range of pH, at the optimum temperature. For the optimal pH determination, the following buffers (0.1 mol L<sup>-1</sup>) were used: citrate (pH 3.0 and 3.5), acetate (pH 4, 4.5, 5.0 and 5.5), MES (pH 6.0, 6.5 and 7.0), tris (pH 7.5 and 8.0) and glycine (pH 8.5, 9.0 and 9.5). For the pH stability experiment, the enzyme activity was expressed as the relative activity between the activity before and after the 24 h treatment.

The effect of glycerol on the storage conditions of the xylanases was evaluated by their activity, performing every experiment in triplicate. Three aliquots of the crude extract were stored in liquid nitrogen (-196 °C), -80 °C freezer, freezer (-20 °C), refrigerator (4 °C) and room temperature (25 °C), with and without glycerol 50% (v/v). The enzyme activity was quantified before and after 24 h of storage.

### 2.4 Effect of phenolic compounds on the xylanolytic activity

The inhibition of xylanolytic activity by phenolic compounds was tested on the crude extract at room temperature (24 °C). The following compounds were tested individually at a final concentration of 10 mmol L<sup>-1</sup>: tannic acid, p-coumaric acid, syringic acid, gallic acid, ferulic acid, 4-hydroxybenzoic acid, vanillin, vanillic acid and syringaldehyde. The enzymatic activity was measured and expressed as percentage for the solutions incubated for 10 min, 24 and 48 h. The activity of the enzyme was compared with that measured prior to incubation, considered to be 100%.

### 2.5 Sugarcane bagasse pretreatment

The pretreatment was carried out by a combination of ozonolysis with an alkaline treatment<sup>23</sup>. After these procedures, the bagasse was either washed or left unwashed. The washed bagasse was rinsed several times with distilled water. Both washed and unwashed treated bagasses were dried in a convective oven at 40 °C until constant weight.

## 2.6 Enzymatic hydrolysis of sugarcane bagasse

Hydrolysis was performed using an orbital shaker at 150 rpm in glass flasks with rubber stoppers, containing 0.5 g of washed or unwashed bagasses, 2.5 mL of acetate buffer 0.1 mmol L<sup>-1</sup> pH 5.5 and 2.5 mL of crude extract of *R. emersonii* containing 22 U mL<sup>-1</sup> of xylanase (or 110 U per g of sugarcane bagasse) and 17 U mL<sup>-1</sup> of endoglucanases (or 85 U per g of sugarcane bagasse). All the tests were conducted in three repetitions.

A preliminary test to determine the optimal time and temperature for enzymatic hydrolysis was conducted with untreated sugarcane bagasse. The untreated sugarcane bagasse was hydrolyzed for 6, 12 and 24 h at 50, 60, 70 and 80 °C. Maximum hydrolysis was observed with 6 h at 60 °C.

The pretreated sugarcane bagasses, washed and unwashed, were hydrolyzed at 60 °C for 2, 4 and 6 h. The material was filtered after hydrolysis, and the soluble fraction was used for quantification of released sugars. Experiments were performed using sugarcane bagasse (untreated, washed and unwashed pretreated) with 5 mL of 0.1 mmol L<sup>-1</sup> pH 5.5 acetate buffer (without enzyme extract) as a control of hydrolysis.

The efficiency in converting hemicellulose (or cellulose) was calculated as in Eq. 1:

$$\% \text{ xylose} = \frac{c \times v \times 0.9}{m} \times 100\% \quad (1)$$

where *c* is the concentration (g L<sup>-1</sup>) of sugars in the soluble fraction hydrolyzed, *v* is the volume in liters of soluble fraction and *m* is the hemicellulose (or cellulose) mass in grams.

## 2.7 Quantification of the sugars from the breakdown of the sugarcane bagasse

The procedures were done according to Perrone et al.<sup>23</sup>. The obtained hydrolysates from washed and unwashed pretreated sugarcane bagasses were analyzed by chromatography. The quantification of glucose and xylose were carried out using high-performance liquid chromatography (HPLC) with a pulsed amperometric detector (HPAEC-PAD, Thermo Scientific, Dionex, ICS-5000). A Dionex CarboPac PA-1 column was used for separation at 25 °C, using a flow of 1 mL min<sup>-1</sup> with ultrapure water (solvent A) and 0.5 mol L<sup>-1</sup> NaOH (solvent B). Elution was carried from 0 to 12 min with 4.8% of solvent B, and from 12 to 16 min with 100% of the same solution. Before each injection, the sample was diluted and filtered through a

0.22 μm polyvinylidene fluoride (PVDF) filter unit (Merck).

## 2.8 Electrophoretic profile of endoxylanases produced by *R. emersonii*

Polyacrylamide gel electrophoresis was performed on the crude extract. The gel was immersed on 1% of triton X-100 at the end of the run to eliminate the residual SDS and washed with a 0.1 mmol L<sup>-1</sup> pH 5.5 acetate buffer.

One vertical strip was separated and used for zymogram analysis<sup>24</sup>. After that, the strip and the original unstained gel were put side by side and a strip of the gel was cut horizontally to compare the known gel isoforms with the zymogram, a technique used to isolate other enzymes<sup>25</sup>.

The enzymatic activity of the four isolated endoxylanase isoforms was analyzed against different substrates: the synthetic substrates pNPG (specific for β-xylanases) and pNPX (specific for β-glucanases), and the natural polymers CMC (for endoglucanases), beechwood xylan and oat spelt xylan (for endoxylanases).

## 2.9 Thermodynamic analysis of Xyl\_C isolated from the crude enzymatic extract of *R. emersonii*

Among the four isolated isoforms, was selected the xylanase that showed the highest affinity for the complex substrate, confirming the endoxylanase identity for these experiments.

The thermodynamic analysis of Xyl\_C thermal denaturation was done using xylan from beechwood at the optimum pH. After incubation at each temperature samples were cooled in ice overnight, followed by the enzyme assay for residual activity. The calculation of the activation energy *E<sub>a</sub>*, the temperature coefficient *Q<sub>10</sub>*, half-life *T<sub>1/2</sub>* and other parameters of the enzyme related to the thermal denaturation, including the activation energy *E<sub>a(D)</sub>*, melting temperature *T<sub>m</sub>*,  $\Delta H_{(D)}$ ,  $\Delta G_{(D)}$  and  $\Delta S_{(D)}$ , followed the method proposed in the literature<sup>26,27</sup> and done in previous studies with other enzymes<sup>28,29</sup>. The irreversible denatured “I” state is evaluated using the model N ↔ D → I, where N represents the native conformation and D the reversible denatured conformation.



### 3. Results and discussion

#### 3.1 Production and biochemical characterization of endoxylanases on the crude extract produced by *R. emersonii*

The production of endoxylanases by *R. emersonii* on solid state cultivation was  $473.86 \text{ U g}^{-1}$  after 144 h of cultivation at  $55 \text{ }^\circ\text{C}$ . The substrate combination of equal amounts of sugarcane bagasse, wheat bran, and corn straw (w/w) results on a complex carbon source. The protein expression changes, as recorded for *R. emersonii*, with different culture media. This fact can be a mechanism directly or indirectly based on the accumulation in the medium of the products and substrates on which the enzymes are working and which will influence their induction<sup>30</sup>.

When analyzing the chemical composition of substrates used to induce xylanase production, it could be inferred that the combination of various substrates, such as sugarcane bagasse, corn straw, and wheat bran, is successful due to the heterogeneity of the composition to which the fungus was subjected. Corn straw has higher xylan values than the stalk of the plant, with 26.8% xylan in the straw versus 19.4% xylan in the stalk. In contrast, proteins constitute 1.2% in the fiber and 3.4% in the stem<sup>31</sup>. Sugarcane bagasse has a characteristic chemical composition that is high in cellulose, hemicellulose and lignin, while overall ash values are lower (1.0–5.5%)<sup>32</sup>, factors that make it attractive for the cultivation of microorganisms that produce lignocellulolytic enzymes. Studies use wheat bran as a substratum for the production of biomass because it is rich in starch; however, the oligosaccharides present in its composition are shown to be efficient in inducing cellulase and hemicellulase production<sup>33</sup>.

The optimum pH and temperature of xylanases on the crude enzymatic extract from *R. emersonii* was 5.5 (Fig. 1) and  $80 \text{ }^\circ\text{C}$  (Fig. 2), close to those described for *Talaromyces emersonii*, currently classified as *R. emersonii*, with solid-state wheat and beet pulp cultivation (1:1 w/w) at pH 4.5 and  $45 \text{ }^\circ\text{C}$ <sup>30</sup>. Another increase of activity occurred at pH 7.0 and suggests isoforms of the endoxylanases produced by *R. emersonii*, since the zymogram shown in Fig. 3 indicates four bands.

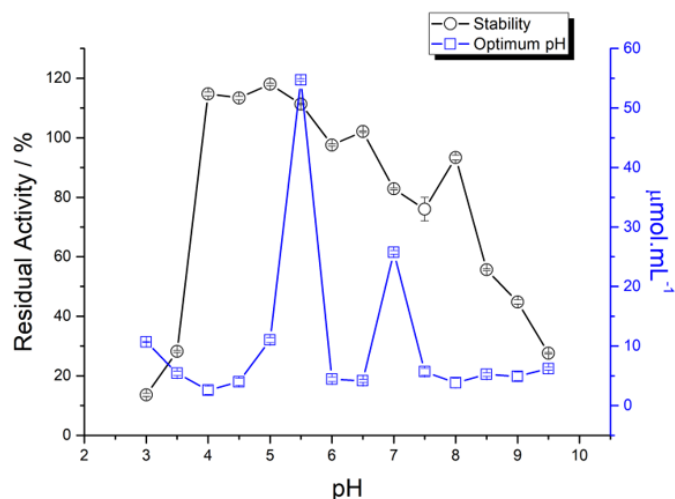


**Figure 1.** Effect of pH on xylanolytic activity in crude enzymatic extract produced by *R. emersonii*. Stability in relation to pH and optimum pH. The tests were performed at pH 5.5 with beechwood xylan. The symbol represents the average of three replicates.

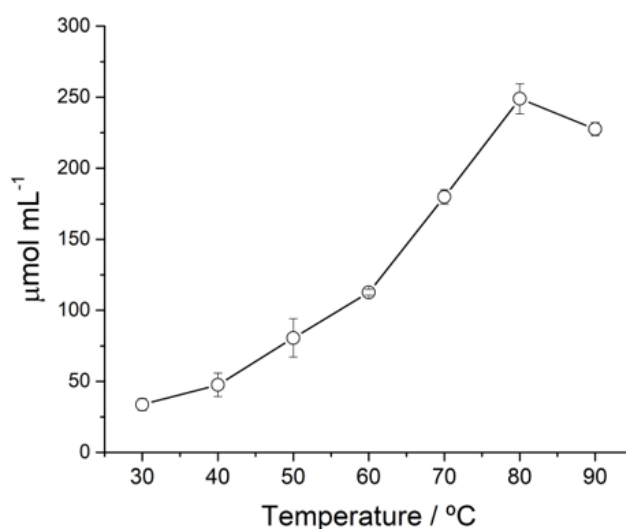


**Figure 2.** Effect of incubation temperature on xylanolytic activity from crude enzymatic extract produced by the thermophilic fungus *R. emersonii*. The tests were performed at pH 5.5 with beechwood xylan. The symbol represents the average of three replicates.

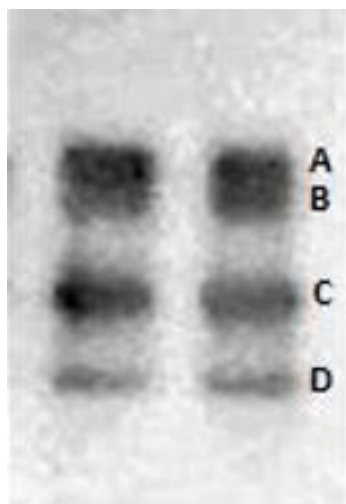


**Figure 3.** Zymogram of endoxylanases present from crude enzymatic extract produced by the fungus *R. emersonii*. The gel was stained with 0.1% congo red and detained with 1 mol L<sup>-1</sup> NaCl. The dark bands show the presence of xylanase and the letters (A, B, C and D) identify the possible isoforms of the enzyme (the image was transformed from color to shades of gray, then into its negative and the contrast became more evident using the free software GIMP version 2.8.10 for Linux).

Endoxylanolytic activity remained stable for pH ranging from 4 to 8, with relative activity above 70%, and from 4 to 5.5 with relative activity values above 100% (Fig. 1). The chemical species related to the pH can change the tridimensional structure of the enzyme, by protonation or deprotonation of the amino acid side chains on the enzyme surface or affecting the catalytic residues, becoming more favorable or unfavorable to interact with the substrate. Among these changes, electrostatic repulsions, destruction of salt bridges and formation of isolated buried charges stand out<sup>34</sup>.

Comparative analyses of structural changes in acid, neutral and alkaline xylanases from family 11 shows differences in the amino acid compositions and secondary structure. Neutral xylanases have a decrease on hydrophobic residues, while acidophilic xylanases have a decrease on positively charged residues. On the secondary structure, alkaline xylanases show an  $\alpha$  helix between  $\beta$  strands, and, in nonalkaline xylanases, this is substituted by a  $\beta$ -turn or a loop<sup>35</sup>.

In the absence and presence of glycerol, the two best storage conditions were obtained in liquid nitrogen at -196 °C with 99% relative activity in the absence and 170% in the presence of 50% glycerol, and in a -80 °C freezer, which kept 90.2% of activity in the absence and 163.8% in the presence of 50% glycerol (Fig. 4).

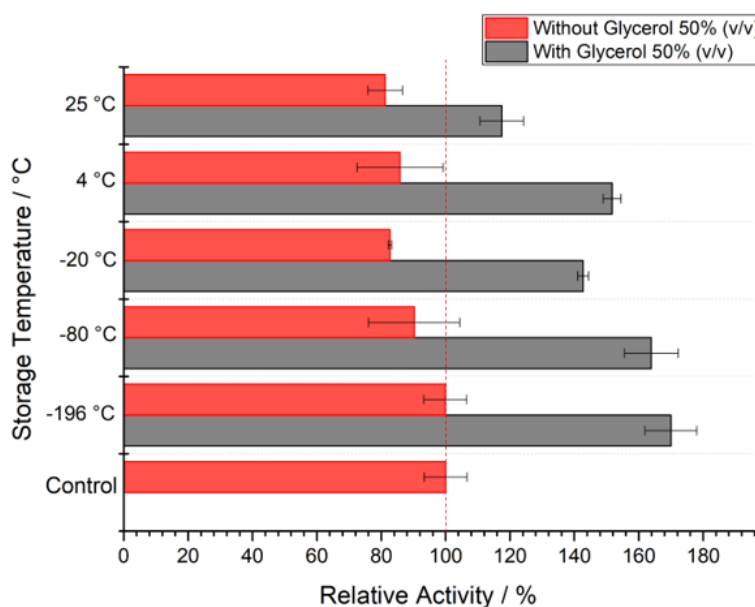


**Figure 4.** Effect of the storage temperature on the enzymatic activity of endoxylanases present in the crude enzymatic extract produced by *R. emersonii*. The tests were carried out after 24 h in the presence or in the absence of 50% glycerol (v/v). The results were compared with the enzymatic activity at the beginning of the experiment (control) and expressed in relative activity (%). The bar represents the value of the average of three replicates, the horizontal line represents the standard deviation.

The presence of glycerol during the storage process increased the endoxylanase activity on all the tested conditions. The effect of osmolytes on the conformational stability of proteins in adverse situations of cellular stress is known<sup>36</sup>. Similarly to sorbitol, it favors protein folding, making the polypeptide chain more compact and less flexible, since it acts by shifting the reaction balance to the less energetic state<sup>37</sup>.

The interaction of the enzyme with the osmolyte is not favorable for its function, so it is excluded from the surface of the protein, where a hydration layer is formed by several highly organized and less flexible water layers. Consequently, the unfolded state has a greater contact surface of the polypeptide chain with water molecules, resulting in a larger hydration layer, which will require more energy for stabilization. For this reason, glycerol acts by shifting the reaction

balance towards the native state, increasing levels of enzyme catalytic effect<sup>38</sup>.

### 3.2 Effect of phenolic compounds on the xylanolytic activity on the crude extract from *R. emersonii*

From all the tested phenolics (Fig. 5), the only one that decreased the xylanolytic activity was tannic acid, a large molecule with a molecular weight of 1,701.23 kDa, which is composed by 10 aromatic rings and 25 hydroxyls, characteristic that could explain the inactivation of the endoxylanolytic activity, according to observations previously cited<sup>39</sup>. Tannins can form a complex with the protein that results in precipitation, thus, the enzyme is removed from the solution, decreasing its catalytic capacity<sup>40,41</sup>.

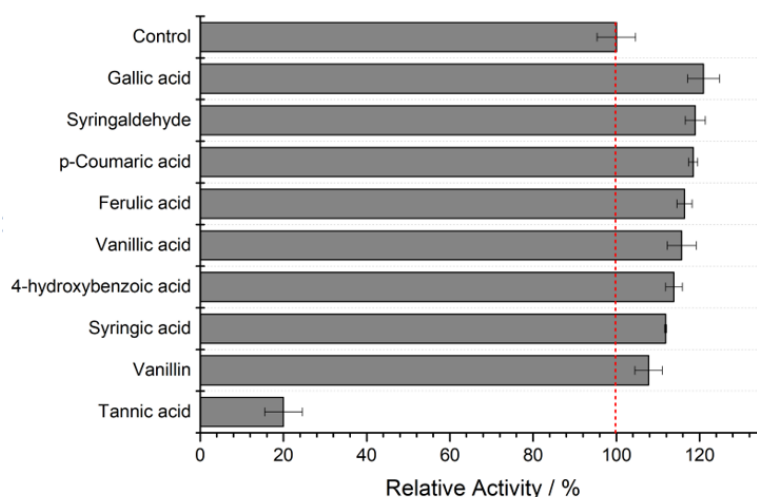


**Figure 5.** Effect of 48 h preincubation at 25 °C of phenolic compounds on the relative activity (%) of endoxylanases on crude extract produced by *R. emersonii*. The bar represents the value of the average of three replicates, the horizontal line represents the standard deviation.

The other compounds analyzed showed a modest or a significant increase of the relative activity compared to the control. The relative activity of the enzymes increased 12% for 4-hydroxybenzoic acid; 16% for vanillic acid; 26% for ferulic acid and 44% for syringic acid in a 30 mmol L<sup>-1</sup> final concentration<sup>42</sup>.

Phenolic compounds are generated from lignin degradation<sup>43</sup> during the pretreatment step of the biomass aiming second generation ethanol production and are reported as enzymatic inhibitors<sup>44,45</sup> including hemicellulase inhibition<sup>46</sup>. Some authors propose that phenolic acids at low concentrations can form a hydrophobic layer on the surface of the protein, ensuring more interaction with the substrate; however,

at high concentrations the increase in this hydrophobic layer causes protein precipitation due to increased interactions<sup>41,42,47</sup>. Boukari et al.<sup>39</sup> proposed the inhibition mechanism by phenolic compounds on family GH11 endo- $\beta$ -1,4-xylanase. The authors described a noncompetitive inhibition mechanism, and more than one aromatic molecule interacting with the enzyme molecule is necessary to induce complete inactivation. Effects on the enzyme activity by the phenolic compound interaction can be produced by forming soluble enzyme-inhibitor complex at low phenolic concentrations, while, at high concentrations, insoluble protein-phenolic complexes decrease the solubility of enzymes<sup>45</sup>.

The interaction of phenolic compounds with proteins involve amino acid residues present at the surface of the protein, and can occur in two ways: hydrophobic aromatic ring stacking with the tryptophan side chains, or hydrogen interacting with basic amino acid residues between their functional groups and phenolic hydroxyl<sup>39</sup>.

### 3.3 Enzymatic hydrolysis of pretreated sugarcane bagasse

The quantification of xylose was slightly higher in the washed sugarcane bagasse when compared to the nonwashed, in all evaluations, which difference increased with time. In hydrolysis for six hours, the xylose concentration was almost 1.5 times higher with washed sugarcane bagasse than with the unwashed one (Tab. 1). Glucose release presented a similar behavior.

Concentration of hemicellulose (14.1%) and cellulose (48.9%) on the insoluble fraction after the pretreatment process<sup>23</sup> was used to calculate the hydrolysis efficiency in terms of xylose and glucose. Under all analyzed conditions, the conversion of xylose

was greater than glucose (Tab. 1), presumably due to high xylanolytic activity in the *R. emersonii* crude enzymatic extract, and pretreated bagasse structural changes, that could affect cellulose and hemicellulose accessibility. The conversion of xylose was greater than glucose under all the analyzed conditions (Tab. 1), suggesting that the crude enzymatic extract from *R. emersonii* has many xylanolytic enzymes. However, auxiliary enzymes are necessary to have a greater effect on the breakdown of the xylan structure and make cellulose more accessible to hydrolysis<sup>48</sup>. Analysis of the secretome of *T. emersonii* shows 266 proteins, and 119 CAZymes identified with 40 different glycosyl hydrolase families, while the functional annotation of fungi genome shows represent 55 different glycosyl hydrolase families<sup>49</sup>. The secretion of protein by fungi relate directly to the carbon source used for fungi cultivation, so analyses of different complex carbon sources on the culture medium of *R. emersonii* can be performed to find how to improve the expression of enzymes for xylan hydrolysis.

**Table 1.** Sugars obtained by enzymatic hydrolysis of pretreated sugarcane bagasse with combined ozone and alkaline treatment, using crude enzymatic extract produced by *R. emersonii*.

| Xylose              |                                     |  |                                       |  |
|---------------------|-------------------------------------|--|---------------------------------------|--|
| Hydrolysis time / h | Washed bagasse / mg g <sup>-1</sup> | Yield washed bagasse / % g <sup>-1</sup> | Unwashed bagasse / mg g <sup>-1</sup> | Yield unwashed bagasse / % g <sup>-1</sup> |
| 2                   | 5.8 ± 0.3                           | 3.7 ± 0.2                                | 4.9 ± 0.3                             | 3.1 ± 0.5                                  |
| 4                   | 7.9 ± 0.3                           | 5.0 ± 1.2                                | 6.4 ± 0.6                             | 4.1 ± 0.4                                  |
| 6                   | 12.4 ± 1.0                          | 7.9 ± 0.6                                | 8.8 ± 0.2                             | 5.6 ± 0.5                                  |
| Glucose             |                                     |  |                                       |  |
| Hydrolysis time / h | Washed bagasse / mg g <sup>-1</sup> | Yield washed bagasse / % g <sup>-1</sup> | Unwashed bagasse / mg g <sup>-1</sup> | Yield unwashed bagasse / % g <sup>-1</sup> |
| 2                   | 6.4 ± 0.3                           | 2.1 ± 0.7                                | 5.3 ± 0.2                             | 1.3 ± 0.2                                  |
| 4                   | 10.0 ± 0.4                          | 1.7 ± 0.6                                | 7.3 ± 0.9                             | 1.3 ± 0.1                                  |
| 6                   | 13.7 ± 0.6                          | 1.7 ± 0.5                                | 7.4 ± 0.2                             | 1.1 ± 0.2                                  |

Average ± standard deviation (mean values of three independent measurements).

As noted earlier, the findings obtained could also be related to the effects of pretreatment on the lignocellulosic material structure. The pretreatment used in this study was proposed by Perrone et al.<sup>23</sup>, where the authors reported that the combined pretreatment of ozone and NaOH results in a greater amount of hemicellulose, when compared to the combined pretreatment of ozone with NaOH and ultrasound irradiation, and smaller amounts of hemicellulose than the pretreatment using only ozone. Still, according to the same authors, the insoluble fraction after the pretreatment has 6.7 mg of total phenolic compounds per gram of sugarcane bagasse.

Therefore, the phenolic compounds would be present in the pretreated unwashed sugarcane bagasse, which could negatively affect the enzymatic performance and result in a lower yield of released monosaccharides.

Although our results on the effect of phenolic compounds on endoxylanolytic activity are promising, with the only exception of tannic acid, there is a probability that negative results could be observed when several phenolic compounds are present in the same solution and submitted to higher temperatures.

The possible effect of pH resulting from the alkaline pretreatment was also considered, and, for that reason, it was performed an inhibition test with the soluble

fraction obtained after that procedure. In this inhibition test, the crude enzyme extract was diluted in the same volume with the insoluble fraction resulting from the sugar cane bagasse pretreatment process. The mixture remained in contact for 0, 2, 4 and 6 h, and, after each time, endoxylanase activity was evaluated and compared with the values obtained before the test. The maximum value of inhibition of relative activity was 10% for the time of 2 h, remaining essentially constant (9.8%) in 4 h and decreasing to 8.2% after 6 h. The pH was 6.1 after 2 h, 5.9 at 4 h and 5.7 after 6 h for the unwashed bagasse, while the pH was 5.5 for the washed bagasse. A reason for the lower activity may be the higher pH in the unwashed bagasse, above the optimum verified at 5.5.

Our hydrolysis results are similar to those presented by Marques et al.<sup>50</sup>. In their work, hydrothermally pretreated sugarcane bagasse was hydrolyzed using a mixture (1:1 v/v) of the enzymatic extracts produced by solid-state cultivation of fungi *Botryosphaeria* sp. AM01 and *Saccharicola* sp. EJC04. In this case, pretreated bagasse hydrolysis continued at 50 °C for 20 h with an enzymatic load of 150 U g<sup>-1</sup> of pretreated bagasse at 5% (m/v) concentration. The authors had 3.56 mg mL<sup>-1</sup> of glucose and 1.66 mg mL<sup>-1</sup> of xylose.

Our findings were 1.37 mg mL<sup>-1</sup> of glucose and 1.24 mg mL<sup>-1</sup> of xylose at 60 °C, using approximately one third of the incubation time and a lower enzymatic load (110 U g<sup>-1</sup>).

Our results are similar to those presented by Marques and coworkers. In their work, hydrothermally pretreated sugarcane bagasse was hydrolyzed using a mixture (1:1 v/v) of the enzymatic extracts produced by solid-state cultivation of fungi *Botryosphaeria* sp. AM01 and *Saccharicola* sp. EJC04. In this case, pretreated bagasse hydrolysis continued at 50 °C for 20 hours with an enzymatic load of 150 U/g of pretreated bagasse at 5 % (m/v) concentration. The authors had 3.56 mg/mL of glucose and 1.66 mg/mL of xylose<sup>50</sup>. Our findings were 1.37 mg/mL of glucose and 1.24 mg/mL of xylose at 60 °C using approximately one third of the incubation time and a lower enzymatic load (110 U/g). Table 2 shows more comparisons with the literature.

The lower sugar yields in the unwashed sugarcane bagasse could be the result of a sum of factors, such as the inhibitory effect of the residual alkaline pH of the pretreated bagasse that increased pH of the assay above the optimum value, and a potential inhibitory effect of a mixture of phenolic compounds.

**Table 2.** Comparative xylose and glucose conversion by enzymatic hydrolyze from sugarcane bagasse.

| Organism   | Hydrolysis time / h | Tempe. / °C | Sugarcane bagasse / % m/v | Xylose / mg mL <sup>-1</sup> | Glucose mg mL <sup>-1</sup> | Author             |
|--|---------------------|-------------|---------------------------|------------------------------|-----------------------------|--------------------|
| <i>Rasamsonia emersonii</i>                                      | 4                   | 60          | 5                         | 1.4                          | 1.24                        | This study         |
| <i>Thermomyces lanuginosus</i>                                   | 24                  | 40          | 3.5                       | 0.9                          | NA                          | Ref. <sup>51</sup> |
| <i>Trichoderma reesei</i>  | 24                  | 50          | 2                         | 1.0                          | 1.80                        | Ref. <sup>52</sup> |
| <i>Aspergillus awamori</i>                                       | 24                  | 50          | 2                         | 1.3                          | 3.80                        | Ref. <sup>53</sup> |
| <i>Botryosphaeria</i> sp. AM01 and <i>Saccharicola</i> sp. EJC04 | 20                  | 50          | 5                         | 1.7                          | 3.56                        | Ref. <sup>50</sup> |
| NS 50013 by Novozymes*   | 24                  | 50          | 5                         | 12.5                         | 20.0                        | Ref. <sup>53</sup> |

NA = not analyzed.

\*Commercial enzyme preparation.

### 3.4 Isolation and evaluation of specific endoxylanase catalysis substrate

The four isolated isoforms from polyacrylamide gel were evaluated by hydrolysis of synthetic substrates (pNPX and pNPG) and natural polymers (CMC, beechwood xylan and oat spelt xylan) (Tab. 3). None of the enzymes had activity against pNPG and CMC and only Xyl\_B had activity against synthetic substrates. The enzymes Xyl\_A, Xyl\_B and Xyl\_C showed high activity concerning natural polymers, whereas Xyl\_D showed lower activity.

Endoxylanases from *R. emersonii* are not able to recognize glucose to hydrolyze the glycosidic bond, which limits their action to xylan constituent carbohydrates. This is observed in the GH 11 family of glycosyl hydrolases, composed exclusively of endo β 1,4 xylanases, in which no other activity was observed. They are capable of cleaving internal β 1,4-xylosidic bonds, unlike GH10 xylanases, which are also capable of cleaving β 1,3-xylosidic and β 1,4 -glycosidic bonds<sup>54</sup>.

**Table 3.** Evaluation of activity of endoxylanases produced by *R. emersonii*.

|                             | Xyl_A              |    | Xyl_B              |     | Xyl_C              |    | Xyl_D              |    |
|-----------------------------|--------------------|----|--------------------|-----|--------------------|----|--------------------|----|
|                             | U mL <sup>-1</sup> | SD | U mL <sup>-1</sup> | SD  | U mL <sup>-1</sup> | SD | U mL <sup>-1</sup> | SD |
| 4 mmol L <sup>-1</sup> pNPG | ND                 | -  | ND                 | -   | ND                 | -  | ND                 | -  |
| 4 mmol L <sup>-1</sup> pNPX | ND                 | -  | 0.7                | 0.1 | ND                 | -  | ND                 | -  |
| 4% CMC                      | ND                 | -  | ND                 | -   | ND                 | -  | ND                 | -  |
| 1% beechwood xylan          | 35                 | 4  | 173                | 5   | 71                 | 3  | 5                  | 3  |
| 1% oat spelt xylan          | 35                 | 2  | 78                 | 3   | 56                 | 4  | 10                 | 3  |

Data ND: no detected activity. Average ± standard deviation (mean values of three independent measurements).

### 3.5 Thermodynamic analysis of the isolated Xyl\_C

Xylanase xyl\_C displayed the highest activity when tested against xylan: 70.87 U mL<sup>-1</sup> for beechwood xylan and 56.11 U mL<sup>-1</sup> for oat spelt xylan. Therefore, it was chosen for the thermodynamic analysis.

The Arrhenius plot (Fig. 6), allowed calculating the optimum temperature (80 °C) and the enzymatic activation energy (26.10 kJ mol<sup>-1</sup>). The first-order plot for the effect of temperature on enzyme activity (Fig. 7), was used to find the half-life and the first-order rate of thermal inactivation ( $k_d$ ). The  $k_d$  rates were used for the first-order Arrhenius plot (Fig. 8), allowing to determine the activation energy of denaturation ( $E_{a(d)}$ ), estimated as 99.58 kJ mol<sup>-1</sup>. The temperature coefficient decreases slightly with each increase of 10 °C (Tab. 4).

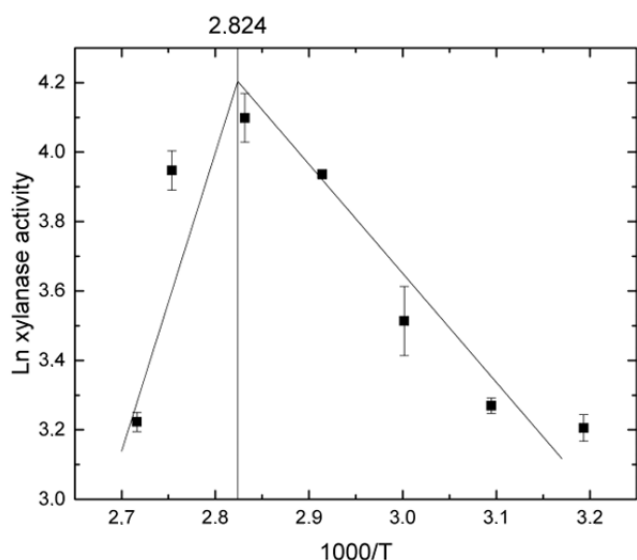


**Figure 6.** First-order Arrhenius plot showing the effect of temperature on activity of isolated Xyl\_C produced by *R. emersonii* using beechwood xylan as substrate.

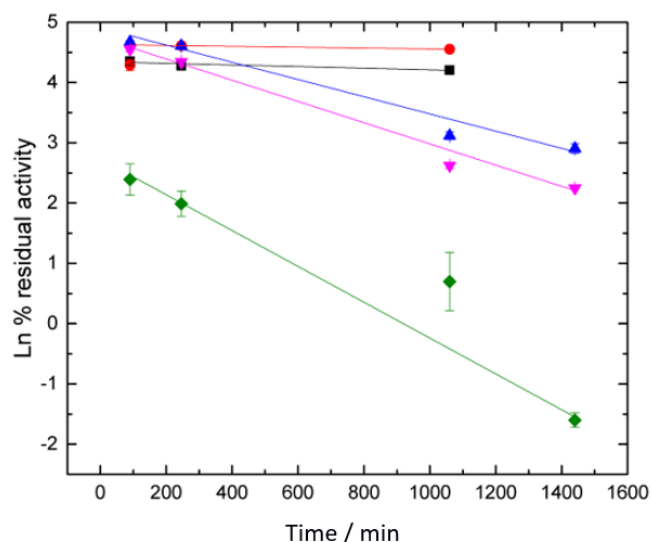


**Figure 7.** First-order plot for the effect of temperature on enzyme activity of isolated Xyl\_C produced by *R. emersonii* using Beechwood xylan as the substrate. Samples were incubated at 50 (•), 60 (■), 70 (▲), 80 (▼) and 90 °C (◆) for 90, 246, 1060 and 1440 min.

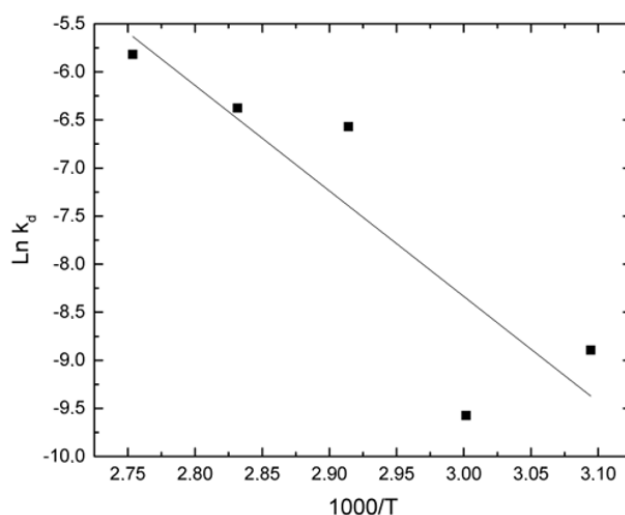


**Figure 8.** First-order Arrhenius plot for determination of activation energy of denaturation ( $E_{a(D)}$ ) of isolated Xyl\_C from *R. emersonii*. The values of  $k_d$  were taken from the slopes in Fig. 7.

**Table 4.** Temperature coefficient ( $Q_{10}$ ) from Xyl\_C produced by *R. emersonii*. Values estimated based on Arrhenius plot.

| Temp. / °C | Temp. / K | $Q_{10}$ |
|------------|-----------|----------|
| 50         | 313.15    | 1.35     |
| 60         | 323.15    | 1.33     |
| 70         | 333.15    | 1.31     |
| 80         | 343.15    | 1.29     |
| 90         | 353.15    | 1.27     |
| 95         | 363.15    | 1.26     |

**Table 5.** Kinetic and thermodynamic parameters of irreversible thermal inactivation.

| Temp. / °C | Temp. / K | $k_d / \text{min}^{-1}$ | $t^{1/2} / \text{min}$ | $\Delta H_d / \text{kJ mol}^{-1}$ | $\Delta G_d / \text{kJ mol}^{-1}$ | $\Delta S_d / \text{J mol}^{-1}$ |
|------------|-----------|-------------------------|------------------------|-----------------------------------|-----------------------------------|----------------------------------|
| 50         | 323.15    | 0.00012                 | 5056                   | 96.9                              | 114.3                             | -53.8                            |
| 60         | 333.15    | 0.00007                 | 1670                   | 96.8                              | 119.7                             | -68.9                            |
| 70         | 343.15    | 0.00143                 | 495                    | 96.7                              | 114.8                             | -52.7                            |
| 80         | 353.15    | 0.00176                 | 408                    | 96.6                              | 117.6                             | -59.4                            |
| 90         | 363.15    | 0.00297                 | 262                    | 96.6                              | 119.5                             | -63.0                            |

Some enzymes have an optimal catalytic performance at high temperatures and are useful in high temperatures processes and for brief times; however, when kept at high temperatures for a long time, many enzymes do not have stability to remain active throughout the process. The half-life of Xyl\_C was approximately 8 h at 50 °C, 27 h at 60 °C, 8 h at 70 °C, 6 h at 80 °C and 4 h at 90 °C. The half-life at 70 °C is larger than the value reported for a mutant xylanase from *Aspergillus fumigatus* produced by heterologous expression at *Escherichia coli* BL21, 42 min at 70 °C<sup>57</sup>. Site directed mutagenesis can improve the stability significantly. Alterations of N-terminal residues of a xylanase from *Penicillium janthinellum* MA21601 improved the half-life 107-fold higher than the wild-type strain, increasing from 30 s to 53.6 min at 60 °C<sup>58</sup>.

High half-life values at elevated temperatures can be directly related to high melting temperatures ( $T_m$ ). The  $T_m$  is described as the temperature at which the maximum activity drops by half. For Xyl\_C, the maximum activity occurred at 80 °C and decreased to 50% of that value at 93.3 °C (Fig. 9).

There was no significant variation in the enthalpy variation ( $\Delta H_d$ ) of thermal denaturation of Xyl\_C. The enthalpy values decrease slightly with increasing temperature (Tab. 4). This behavior, together with lower entropy values, is related to enzymatic thermostability<sup>59</sup>.

Gibbs free energy values found for Xyl\_C (114.3 kJ mol<sup>-1</sup>) at 50 °C are higher than those reported at 55 °C for wild and mutant enzymes from

*Thermomyces lanuginosus*: 108.5 and 112.4 kJ mol<sup>-1</sup>, respectively. The enzymes were produced by liquid cultivation with 2% of corn cobs at 45 °C<sup>59</sup>. These values suggest that Xyl\_C is more resistant to unfolding. Xyl\_C is also more resistant than *Melanocarpus albomyces* xylanase in the presence of glycerol and NaCl (96.6 kJ mol<sup>-1</sup>)<sup>60</sup>.

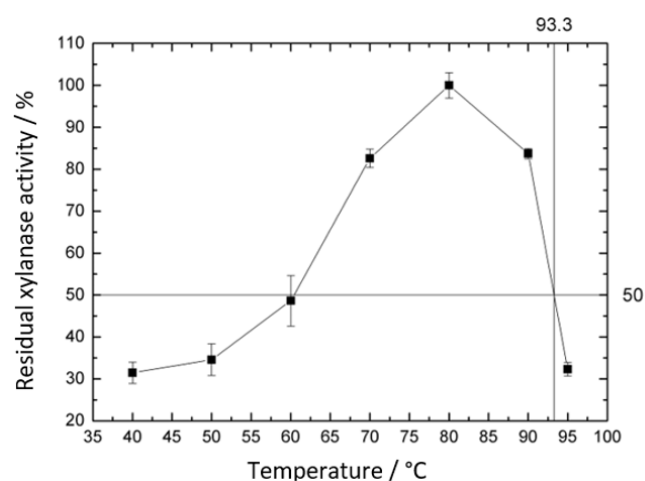


**Figure 9.** Determination of melting temperature ( $T_m$ ) for the isolated Xyl\_C produced by *R. emersonii*. The  $T_m$  corresponds to the temperature at which the enzyme activity drops to half of the initial activity.

Entropy is a measure of disorder in the system; the increase in disorder of the protein structure is a consequence of conformational changes in the protein. Conformational changes comprise changes in noncovalent interactions: ion-dipole, hydrogen and van

der Waals, and in the rotational positions controlled by the secondary bond structure<sup>61</sup>. A decrease in entropy values was observed with increasing temperature for Xyl\_C (Tab. 4).

Negative entropy ( $\Delta S_d$ ) and positive free energy ( $\Delta G_d$ ) values reveal the resistance for the denaturation reaction to occur. The increase in temperature promotes the weakening of polar interactions, and it strengthens hydrophobic interactions<sup>54</sup> ensuring resistance of the enzyme to thermal denaturation.

#### 4. Conclusions

The endoxylanases from solid state culture of *R. emersonii* present interesting properties, such as the tolerance to a wide pH range, as well as to the presence of diverse phenolic compounds. The enzymes also demonstrate higher activity and stability in the presence of glycerol and this is potentially relevant for industrial applications. The isolate Xyl\_C has good stability against thermal denaturation, properties which can be positive on the process requiring high temperature and long periods of xylan hydrolysis. On the breakdown of the sugarcane bagasse, *R. emersonii* crude extract has provided strong hemicellulose conversion values to xylose and can be used in the process of obtaining high-value products, such as xylooligosaccharides and, for the most part, biofuels from lignocellulose residues without any additional area of cultivation.

#### Acknowledgments

This work was supported by grants from FAPESP, CNPq, FINEP and CAPES (Brazil). JAZ received a CAPES fellowship and JOO received financial support from Universidad Santiago de Cali, Facultad de Ciencias Básicas, Cali, Colombia.

#### References

- [1] Abas, N., Kalair, A., Khan, N., Review of fossil fuels and future energy technologies, *Futures* 69 (2015) 31-49. <https://doi.org/10.1016/j.futures.2015.03.003>.
- [2] Uihlein, A., Schebek, L., Environmental impacts of a lignocellulose feedstock biorefinery system: An assessment, *Biomass and Bioenergy* 33 (5) (2009) 793-802. <https://doi.org/10.1016/j.biombioe.2008.12.001>.
- [3] Brenelli, L. B., Figueiredo, F. L., Damasio, A., Franco, T. T., Rabelo, S. C., An integrated approach to obtain xylooligosaccharides from sugarcane straw: From lab to pilot scale, *Bioresource Technology* 313 (2020) 123637. <https://doi.org/10.1016/j.biortech.2020.123637>.
- [4] Sarkar, N., Ghosh, S. K., Bannerjee, S., Aikat, K., Bioethanol production from agricultural wastes: An overview, *Renewable Energy* 37 (1) (2012) 19-27. <https://doi.org/10.1016/j.renene.2011.06.045>.
- [5] Jeffries, T. W., Biodegradation of lignin-carbohydrate complexes, In: *Physiology of Biodegradative Microorganisms*, Ratledge, C., ed., Springer: Dordrecht, Netherlands, 1991. [https://doi.org/10.1007/978-94-011-3452-1\\_7](https://doi.org/10.1007/978-94-011-3452-1_7).
- [6] Lin, S. Y., Accessibility of cellulose: a critical review, *Fibre Science and Technology* 5 (4) (1972) 303-314. [https://doi.org/10.1016/0015-0568\(72\)90022-X](https://doi.org/10.1016/0015-0568(72)90022-X).
- [7] Haltrich, D., Nidetzky, B., Kulbe, K. D., Steiner, W., Župančič, S., Production of fungal xylanases, *Bioresource Technology* 58 (2) (1996) 137-161. [https://doi.org/10.1016/S0960-8524\(96\)00094-6](https://doi.org/10.1016/S0960-8524(96)00094-6).
- [8] Bastawde, K. B., Xylan structure, microbial xylanases, and their mode of action, *World Journal of Microbiology and Biotechnology* 8 (1992) 353-368. <https://doi.org/10.1007/BF01198746>.
- [9] Kulkarni, N., Shendye, A., Rao, M., Molecular and biotechnological aspects of xylanases, *FEMS Microbiology Reviews* 23 (4) (1999) 411-456. <https://doi.org/10.1111/j.1574-6976.1999.tb00407.x>.
- [10] Andlar, M., Rezić, T., Marđetko, N., Kracher, D., Ludwig, R., Šantek, B., Lignocellulose degradation: An overview of fungi and fungal enzymes involved in lignocellulose degradation, *Engineering in Life Sciences* 18 (11) (2018) 768-778. <https://doi.org/10.1002/elsc.201800039>.
- [11] Niehaus, F., Bertoldo, C., Kähler, M., Antranikian, G., Extremophiles as a source of novel enzymes for industrial application, *Applied Microbiology and Biotechnology* 51 (1999) 711-729. <https://doi.org/10.1007/s002530051456>.
- [12] Subramanian, S., Prema, P., Biotechnology of Microbial Xylanases: Enzymology, Molecular Biology, and Application, *Critical Reviews in Biotechnology* 22 (1) (2002) 33-64. <https://doi.org/10.1080/07388550290789450>.
- [13] Lima, V. M. G., Krieger, N., Sarquis, M. I. M., Mitchell, D. A., Ramos, L. P., Fontana, J. D., Effect of nitrogen and carbon sources on lipase production by *Penicillium aurantiogriseum*, *Food Technology and Biotechnology* 41 (2003) 105-110.
- [14] Cui, Y. Q., Van der Lans, R. G. J. M., Luyben, K. C. A. M., Effects of dissolved oxygen tension and mechanical forces on fungal morphology in submerged fermentation,



- Biotechnology and Bioengineering 57 (4) (2000) 409-419. [https://doi.org/10.1002/\(SICI\)1097-0290\(19980220\)57:4%3C409::AID-BIT4%3E3.0.CO;2-Q](https://doi.org/10.1002/(SICI)1097-0290(19980220)57:4%3C409::AID-BIT4%3E3.0.CO;2-Q).
- [15] Raimbault, M., Alazard, D., Culture method to study fungal growth in solid fermentation, *European journal of applied microbiology and biotechnology* 9 (1980) 199-209. <https://doi.org/10.1007/BF00504486>.
- [16] Hölker, U., Höfer, M., Lenz, J., Biotechnological advantages of laboratory-scale solid-state fermentation with fungi, *Applied Microbiology and Biotechnology* volume 64 (2004) 175-186. <https://doi.org/10.1007/s00253-003-1504-3>.
- [17] Bhat, M. K., Hazlewood, G. P., Enzymology and other characteristics of cellulases and xylanases, In: *Enzym Farm Animal Nutrition*, Bedford, M. R., Partridge, G. G., CABI Publishing: Oxfordshire, England, 2001, Ch. 11.
- [18] Sun Y, Cheng J., Hydrolysis of Lignocellulosic Materials for Ethanol Production: A Review, *ChemInform* 34 (1) (2003). <https://doi.org/10.1002/chin.200301272>.
- [19] Mosier, N., Wyman, C., Dale, B., Elander, R., Lee, Y. Y., Holtzapple, M., Ladisch, M., Features of promising technologies for pretreatment of lignocellulosic biomass, *Bioresource Technology* 96 (6) (2005) 673-686.
- [20] Rosa, I. Z., Isolamento e seleção de fungos filamentosos termofílicos produtores de celulasas, xilanases e celobiose desidrogenase com potencial para sacarificação do bagaço de cana-de-açúcar, master thesis, São José do Rio Preto, Universidade Estadual Paulista "Julho de Mesquita Filho" - Unesp, 2014.
- [21] Bailey, M. J., Biely, P., Poutanen, K., Interlaboratory testing of methods for assay of xylanase activity, *Journal of Biotechnology* 23 (3) (1992) 257-270. [https://doi.org/10.1016/0168-1656\(92\)90074-J](https://doi.org/10.1016/0168-1656(92)90074-J).
- [22] Miller, G. L., Use of Dinitrosalicylic Acid Reagent for Determination of Reducing Sugar, *Analytical Chemistry* 31 (3) (1959) 426-428. <https://doi.org/10.1021/ac60147a030>.
- [23] Perrone, O. M., Colombari, F. M., Rossi, J. S., Moretti, M. M. S., Bordignon, S. E., Nunes, C. da C. C., Gomes, E., Boscolo, M., da Silva, R., Ozonolysis combined with ultrasound as a pretreatment of sugarcane bagasse: Effect on the enzymatic saccharification and the physical and chemical characteristics of the substrate, *Bioresource Technology* 218 (2016) 69-76. <https://doi.org/10.1016/j.biortech.2016.06.072>.
- [24] Liao, H., Xu, C., Tan, S., Wei, Z., Ling, N., Yu, G., Raza, W., Zhang, R., Shen, Q., Xu, Y., Production and characterization of acidophilic xylanolytic enzymes from *Penicillium oxalicum* GZ-2, *Bioresource Technology* 123 (123) 117-124. <https://doi.org/10.1016/j.biortech.2012.07.051>.
- [25] Polizelli, P. P., Facchini, F. D. A., Cabral, H., Bonilla-Rodriguez, G. O., A New Lipase Isolated from Oleaginous Seeds from *Pachira aquatica* (Bombacaceae), *Applied Biochemistry and Biotechnology* 150 (2008) 233-242. <https://doi.org/10.1007/s12010-008-8145-z>.
- [26] Saqib, A. A. N., Farooq, A., Iqbal, M., Hassan, J. U., Hayat, U., Baig, S., A Thermostable Crude Endoglucanase Produced by *Aspergillus fumigatus* in a Novel Solid State Fermentation Process Using Isolated Free Water, *Enzyme Research* 2012 (2012) 196853. <https://doi.org/10.1155/2012/196853>.
- [27] Saqib, A. A. N., Hassan, M., Khan, N. F., Baig, S., Thermostability of crude endoglucanase from *Aspergillus fumigatus* grown under solid state fermentation (SSF) and submerged fermentation (SmF), *Process Biochemistry* 45 (5) (2010) 641-646. <https://doi.org/10.1016/j.procbio.2009.12.011>.
- [28] Bonfá, E. C., Moretti, M. M. de S., Gomes, E., Bonilla-Rodriguez, G. O., Biochemical characterization of an isolated 50 kDa beta-glucosidase from the thermophilic fungus *Myceliophthora thermophila* M.7.7, *Biocatalysis and Agricultural Biotechnology* 13 (2018) 311-318. <https://doi.org/10.1016/j.bcab.2018.01.008>.
- [29] Trindade, L.V., Desagiacomo, C., Polizeli, M. de L. T. de M., Damasio, A. R. de L., Lima, A. M. F., Gomes, E., Bonilla-Rodriguez, O. G., Biochemical Characterization, Thermal Stability, and Partial Sequence of a Novel Exo-Polygalacturonase from the Thermophilic Fungus *Rhizomucor pusillus* A13.36 Obtained by Submerged Cultivation, *BioMed Research International* 2016 (2016) 8653583. <https://doi.org/10.1155/2016/8653583>.
- [30] Tuohy, M. G., Coughlan, M. P., Production of thermostable xylan-degrading enzymes by *Talaromyces emersonii*, *Bioresource Technology* 39 (2) (1992) 131-137. [https://doi.org/10.1016/0960-8524\(92\)90131-G](https://doi.org/10.1016/0960-8524(92)90131-G).
- [31] Pordesimo, L. O., Hames, B. R., Sokhansanj, S., Edens, W. C., Variation in corn stover composition and energy content with crop maturity, *Biomass and Bioenergy* 28 (4) (2005) 366-374. <https://doi.org/10.1016/j.biombioe.2004.09.003>.
- [32] Canilha, L., Rodrigues, R. C. L. B., Antunes, F. A. F., Chandel, A. K., Milessi, T. S. S., Felipe, M. G. A., da Silva, S. S., Bioconversion of Hemicellulose, In: *Sustainable Products Sustainable Products, Sustainable Degradation of Lignocellulosic Biomass - Techniques, Applications and Commercialization*, Chandel, A. K., da Silva S. S., Eds., IntechOpen: London, England, 2013. <https://doi.org/10.5772/53832>.
- [33] Sun, X., Liu, Z., Qu, Y., Li, X., The Effects of Wheat Bran Composition on the Production of Biomass-Hydrolyzing Enzymes by *Penicillium decumbens*, *Appl*

Applied Biochemistry and Biotechnology 146 (2008) 119-128. <https://doi.org/10.1007/s12010-007-8049-3>.

[34] Nath, D., Rao, M., pH dependent conformational and structural changes of xylanase from an alkalophilic thermophilic *Bacillus* sp (NCIM 59), *Enzyme and Microbial Technology* 28 (4-5) (2001) 397-403. [https://doi.org/10.1016/S0141-0229\(00\)00359-8](https://doi.org/10.1016/S0141-0229(00)00359-8).

[35] Bai, W., Zhou, C., Zhao, Y., Wang, Q., Ma, Y., Structural Insight into and Mutational Analysis of Family 11 Xylanases: Implications for Mechanisms of Higher pH Catalytic Adaptation, *PLoS One* 10 (7) (2015) e0132834. <https://doi.org/10.1371/journal.pone.0132834>.

[36] Viana, Y. A., Garrote Filho, M. da S., Penha-Silva, N., Estabilização de proteínas por osmólitos, *Bioscience Journal* 21 (2) (2005) 83-88.

[37] Bhatnagar, B. S., Bogner, R. H., Pikal, M. J., Protein Stability During Freezing: Separation of Stresses and Mechanisms of Protein Stabilization, *Pharmaceutical Development and Technology* 12 (5) (2007) 505-523. <https://doi.org/10.1080/10837450701481157>.

[38] Qu, Y., Bolen, C. L., Bolen, D. W., Osmolyte-driven contraction of a random coil protein, *Proceedings of the National Academy of Sciences USA* 95 (1998) 9268-9273. <https://doi.org/10.1073/pnas.95.16.9268>.

[39] Boukari, I., O'Donohue, M., Rémond, C., Chabbert, B., Probing a family GH11 endo- $\beta$ -1,4-xylanase inhibition mechanism by phenolic compounds: Role of functional phenolic groups, *Journal of Molecular Catalysis B: Enzymatic* 72 (3-4) (2011) 130-138. <https://doi.org/10.1016/j.molcatb.2011.05.010>.

[40] Haslam, E., Polyphenol-protein interactions, *Biochemical Journal* 139 (1) (1974) 285-288. <https://doi.org/10.1042/bj1390285>.

[41] Kim, Y., Ximenes, E., Mosier, N. S., Ladisch, M. R., Soluble inhibitors/deactivators of cellulase enzymes from lignocellulosic biomass, *Enzyme and Microbial Technology* 48 (4-5) (2011) 408-415. <https://doi.org/10.1016/j.enzmictec.2011.01.007>.

[42] Oliveira, D. M., Hoshino, É. P., Mota, T. R., Marchiosi, R., Ferrarese-Filho, O., dos Santos, W. D., Modulation of cellulase activity by lignin-related compounds, *Bioresource Technology Reports* 10 (2020) 100390. <https://doi.org/10.1016/j.biteb.2020.100390>.

[43] Freudenberg, K., Lignin: Its Constitution and Formation from p-Hydroxycinnamyl Alcohols, *Science* 148 (3670) (1965) 595-600. <https://doi.org/10.1126/science.148.3670.595>.

[44] Mes-Hartree, M., Saddler, J. N., The nature of inhibitory materials present in pretreated lignocellulosic substrates which inhibit the enzymatic hydrolysis of cellulose, *Biotechnology Letters* 5 (1983) 531-536. <https://doi.org/10.1007/BF01184944>.

[45] Ximenes, E., Kim, Y., Mosier, N., Dien, B., Ladisch, M. Inhibition of cellulases by phenols, *Enzyme and Microbial Technology* 46 (3-4) (2010) 170-176.

[46] Sharma, A., Milstein, O., Vered, Y., Gressel, J., Flowers, H. M., Effects of aromatic compounds on hemicellulose-degrading enzymes in *Aspergillus japonicus*, *Biotechnology and Bioengineering* 1985;27 (8) (1985) 1095-1101. <https://doi.org/10.1002/bit.260270802>.

[47] Zhao, J., Chen, H., Stimulation of Cellulases by Small Phenolic Compounds in Pretreated Stover, *Journal of Agricultural and Food Chemistry* 62 (2014) 3223-3229. <https://doi.org/10.1021/jf405046m>.

[48] Li, H., Wu, H., Xiong, L., Chen, X., Wang, C., Qi, G., Huang, C., Guo, H., Luo, M., Liu, J., Long, M., Chen, X., The hydrolytic efficiency and synergistic action of recombinant xylan-degrading enzymes on xylan isolated from sugarcane bagasse, *Carbohydrate Polymers* 175 (2017) 199-206. <https://doi.org/10.1016/j.carbpol.2017.07.075>.

[49] Raheja, Y., Kaur, B., Falco, M., Tsang, A., Chadha, B. S., Secretome analysis of *Talaromyces emersonii* reveals distinct CAZymes profile and enhanced cellulase production through response surface methodology, *Industrial Crops and Products* 152 (2020) 112554. <https://doi.org/10.1016/j.indcrop.2020.112554>.

[50] Marques, N. P., Pereira, J. de C., Gomes E, da Silva, R., Araújo, A. R., Ferreira, H., Rodrigues, A., Dussán, K. J., Bocchini, D. A., Cellulases and xylanases production by endophytic fungi by solid state fermentation using lignocellulosic substrates and enzymatic saccharification of pretreated sugarcane bagasse, *Industrial Crops and Products* 122 (2018) 66-75. <https://doi.org/10.1016/j.indcrop.2018.05.022>.

[51] Damaso, M. C. T., Almeida, M. S., Kurtenbach, E., Martins, O. B., Pereira Junior, N., Andrade, C. M. M. C., Albano, R. M., Optimized expression of a thermostable xylanase from *Thermomyces lanuginosus* in *Pichia pastoris*, *Applied and Environmental Microbiology* 69 (10) (2003) 6064-6072. <https://doi.org/10.1128/AEM.69.10.6064-6072.2003>.

[52] Gottschalk, L. M. F., Oliveira, R. A., Bon, E. P. da S. Cellulases, xylanases,  $\beta$ -glucosidase and ferulic acid esterase produced by *Trichoderma* and *Aspergillus* act synergistically in the hydrolysis of sugarcane bagasse. *Biochemical Engineering Journal* 51 (1-2) (2010) 72-78. <https://doi.org/10.1016/j.bej.2010.05.003>.

[53] Zhao, X., Song, Y., Liu, D., Enzymatic hydrolysis and simultaneous saccharification and fermentation of alkali/peracetic acid-pretreated sugarcane bagasse for ethanol and 2,3-butanediol production, *Enzyme and Microbial Technology* 49 (4) (2011) 413-419. <https://doi.org/10.1016/j.enzmictec.2011.07.003>.

[54] Pollet, A., Delcour, J. A., Courtin, C. M., Structural determinants of the substrate specificities of xylanases from different glycoside hydrolase families, *Critical Reviews in Biotechnology* 30 (3) (2010) 176-191. <https://doi.org/10.3109/07388551003645599>.

[55] Montes, F. J., Battaner, E., Catalán, J., Galán M., Kinetics and Heat-inactivation mechanisms of d-amino acid oxidase, *Process Biochemistry* 30 (3) (1995) 217-224. [https://doi.org/10.1016/0032-9592\(95\)85002-3](https://doi.org/10.1016/0032-9592(95)85002-3).

[56] Rashid, M. H., Siddiqui, K. S., Thermodynamic and kinetic study of stability of the native and chemically modified  $\beta$ -glucosidases from *Aspergillus niger*, *Process Biochemistry* 33 (2) (1998) 109-115. [https://doi.org/10.1016/S0032-9592\(97\)00036-8](https://doi.org/10.1016/S0032-9592(97)00036-8).

[57] Wahab M. K. H. A., Jonet M. A., Illias R. M., Thermostability enhancement of xylanase *Aspergillus fumigatus* RT-1, *Journal of Molecular Catalysis B: Enzymatic* 2016 134 (Part A) (2016) 154-163. <https://doi.org/10.1016/j.molcatb.2016.09.020>.

[58] Xiong, K., Hou, J., Jiang, Y., Li, X., Teng, C., Li, Q., Fan, G., Yang, R., Zhang, C., Mutagenesis of N-terminal residues confer thermostability on a *Penicillium janthinellum* MA21601 xylanase, *BMC Biotechnology* 19 (2019) 51. <https://doi.org/10.1186/s12896-019-0541-7>.

[59] Bokhari, S. A. I., Latif, F., Rajoka, M. I., Purification and characterization of xylanases from *Thermomyces lanuginosus* and its mutant derivative possessing novel kinetic and thermodynamic properties, *World Journal of Microbiology and Biotechnology* 25 (2009) 493-502. <https://doi.org/10.1007/s11274-008-9915-z>.

[60] Gupta, G., Sahai, V., Gupta, R. K., Thermal stability and thermodynamics of xylanase from *Melanocarpus albomyces* in presence of polyols and salts, *BioResources* 9 (4) (2014) 5801-5816. <https://doi.org/10.15376/biores.9.4.5801-5816>.

[61] Lumry, R., Eyring, H., Conformation Changes of Proteins, *The Journal of Physical Chemistry* 58 (2) (1954) 110-120. <https://doi.org/10.1021/j150512a005>.

# Antioxidative activity of gold and platinum nanoparticles assessed through electron spin resonance

Angela Kinoshita<sup>1</sup>, Iara Lima<sup>2</sup>, Éder José Guidelli<sup>2</sup>, Oswaldo Baffa Filho<sup>2+</sup>

1. Universidade do Oeste Paulista, Pró-Reitoria de Pesquisa e Pós- Graduação, Presidente Prudente, Brazil.  
2. Universidade de São Paulo, Faculdade de Filosofia, Ciências e Letras de Ribeirão Preto, Ribeirão Preto, Brazil.

**+Corresponding author:** Oswaldo Baffa Filho, **Phone:** +55 16 3315-3642, **Email address:** [baffa@usp.br](mailto:baffa@usp.br)

## ARTICLE INFO

*Article history:*

**Received:** September 13, 2020

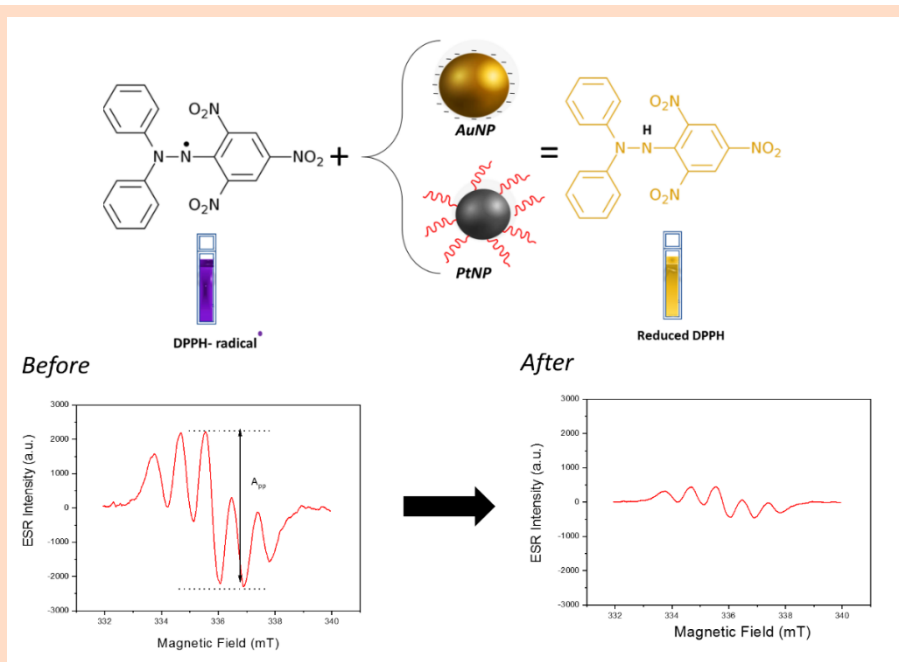
**Accepted:** November 17, 2020

**Published:** April xx, 2021

## Keywords

1. gold nanoparticle
2. platinum nanoparticle
3. antioxidative
4. DPPH

**ABSTRACT:** Gold nanoparticle (AuNP) is a well-known biocompatible structure with several biomedical applications for labeling, heating, and sensing, besides delivery of drugs to cells. Similarly, platinum nanoparticles (PtNPs) have important applications in medicine. Traditional applications of these nanoparticles in medicine/biomedicine depend on their physical-chemical properties. In this work, a preliminary study of the antioxidative properties of AuNP and PtNP was performed using electron spin resonance (ESR) spectroscopy. Antioxidant activity against DPPH (1,1-diphenyl-2-picrylhydrazyl) radical was found for both nanoparticles, but the PtNP was more reactive than the AuNP to reduce the DPPH ESR signal. The decay time for the signal intensity was  $T = 3.1 \pm 0.1 \text{ min}^{-1}$  for AuNP and  $T = 1.80 \pm 0.07 \text{ min}^{-1}$  for PtNP.



## 1. Introduction

Metal nanoparticles have been known for a long time and have always called the attention due to their optical features. The photophysical properties of the particles or of nearby molecules (such as absorption, scattering, fluorescence, and Raman scattering) are enhanced due to the interaction of light with the free electrons on the metal nanoparticle surface. The electromagnetic field of light causes a coherent collective oscillation of the conduction band electrons giving rise to the surface plasmon resonance<sup>1</sup>.

These nanoparticles can be synthesized by several methods. For instance, the most traditional protocol for gold nanoparticles (AuNPs) synthesis was proposed by Turkevich, consisting of the reduction of tetrachloroauric acid (HAuCl<sub>4</sub>) with sodium citrate at 90–100 °C. Sodium citrate acts both as reducing and stabilizing agent, but other agents have been used, such as borohydrides, aminoboranes, hydrazine, formaldehyde, etc.<sup>2</sup>. Deraedt et al.<sup>3</sup> observed that the ratio between salt and Borohydride during reaction alters the particle dimensions and, consequently, its optical and catalytic properties. For each proportion, a different color of colloidal suspension was obtained; the ratio 1Au:10 NaBH<sub>4</sub> produced AuNPs with size of about 3 nm and high stability.

Polymers can stabilize AuNPs; they are versatile and enable to control the size, solubility, amphiphilicity, compatibility among other characteristics with the use of specific ones<sup>2</sup>. Chitosan is a commonly used polymer employed to produce AuNP, it is a natural product and can be used as stabilizing and reducing agent, making a green synthesis of nanoparticles possible. Offering good biocompatibility and other features enabling applications in biomedicine and several others areas<sup>4</sup>. Similarly, alanine is an amino acid that can be used to stabilize AuNP. One of the important applications of alanine is as an ionizing radiation sensor and dosimeter<sup>5</sup>. When associated with AuNPs, this dosimeter becomes more sensitive, allowing the detection of smaller doses of radiation, which expands the field of applications in ionizing radiation dosimetry<sup>6</sup>.

The fact that polymers and other molecules can bind to AuNP greatly expands its application. In the field of biological applications, Sperling<sup>7</sup> explains in details several uses in which highlights labeling, delivering, heating, and sensing. For labeling, usually a molecule with a functional group that associates with specific sites in cells is linked to the nanoparticle. This bond can be directly on the surface of the nanoparticle or by

partial replacement of the stabilizer. Thus, this molecule will direct AuNP to regions of interest in the material, concentrating AuNP, providing contrast at these specific sites. Subsequently, the visualization can be optical by the interaction of AuNP with light or by transmission electron microscopy (TEM), since Au is a metal with a high atomic weight, causing high contrast. It is also possible to obtain contrasted images with X-rays. Gold nanoparticles are conjugated with specific antibodies or ligands, the solution is applied (in animals) and it is specifically uptake by the organ of interest. Thus, in X-ray tomography it is possible to visualize the region of interest with high contrast and resolution by the presence of AuNP.

Nie et al.<sup>8</sup> functionalized AuNP with Trolox, an antioxidant substance. Their results showed an improvement of chemical reactivity, enhancing the antioxidant activity, suggesting that the assembling of organic molecules on AuNP can endow these molecules with reactivity higher than the sum of the monomers. Other studies such as Rajan et al.<sup>9</sup> used phytochemicals present in *Areca catechu* to synthesize AuNP and obtained a compound with antioxidant, antibacterial, and anticancer potential.

Gold nanoparticles are also used as delivery vehicles for substances. These are attached to the nanoparticle surface, that are introduced into the cells. Inside the cells, the substances detach themselves. Similarly, in hyperthermia, nanoparticles are introduced in cells. They can be targeted, for example, to cancer cells through ligands that are specific to the receptors of these cells. Through absorption of light, AuNPs are heated, raising the temperature of the neighborhood, which can lead to the death of cancer cells. The heating triggered by light also allows AuNP to control the delivery of substances. In this case, AuNPs are associated with polymers that form small capsules, containing the substance. Thus, through interaction with the light, this capsule heats up, breaks, and then the substance is released.

The use of AuNP as sensors in the colorimetric method is based on altering the wavelength peak of plasmonic absorption in the presence of the substance to be detected. Gold nanoparticles can be functionalized by molecules that specifically bind to a particular substance. In this case, the substance leads to the agglomeration of AuNP, shifting the plasmonic peak and consequently changing its color, from red to white or blue. In other techniques, fluorescent substances are used. When in close contact with AuNP, the fluorescence is annihilated and, when the fluorophores are far away, with the presence/absence

of analyte, the light emitted is detected and related to the concentration.

In the last decades, platinum nanoparticles (PtNPs) have also been employed extensively in the field of chemistry and medicine, as glucose and gas sensors<sup>10</sup>, catalysts in fuel cells<sup>11,12</sup> and in cancer treatment<sup>13</sup>. Also, PtNPs are a promising alternative as an agent that enhance the dose of ionizing radiation in cancer treatment<sup>13</sup>. In radiotherapy, the insertion of PtNPs could increase the probability of interaction with ionizing radiation due to its high atomic number and consequently increasing the local dose and the radiosensitization of the tumor tissue<sup>14–16</sup>.

The anticancer drugs known as cisplatin and oxaliplatin have been employed in chemotherapy for quite some time with good results<sup>17,18</sup>. Platinum nanoparticles present low toxicity in human cells and are therefore used commercially in chemotherapy<sup>19</sup>. Studies about the toxicity of 5–8 nm PtNPs in human cells concluded that the toxicity can be passivated by coating their surfaces with polyvinyl alcohol (PVA). It is also shown, in cell culture, that the toxicity depends on the concentration of PtNPs (higher concentration, higher toxicity); and are independent of time and cell lineages. In addition, the functionalization of the PtNPs surface can reduce the damage in renal tissues caused by cisplatin; as demonstrated in the literature, the combination of an antihypertensive and antioxidant carvedilol (CV) with chemotherapy drug was able to reduce kidney damage without interfering in the biodistribution or genotoxicity of cisplatin<sup>20</sup>.

The properties of PtNPs depend strongly on the size, shape and structure that can be controlled in the synthesis process. The most common routes for synthesis of PtNPs in colloidal suspension is through chemical reduction<sup>21</sup>, microemulsions<sup>22</sup>, green synthesis<sup>23</sup> and gamma irradiation<sup>24</sup> by the reduction of precursors, such as  $Pt^{4+}$  or  $Pt^{2+}$  ions in the presence of coating agent. In order to control size and morphology, polyacrylate and polyvinylpyrrolidone were used<sup>25</sup>; however, the use of  $NaBH_4$  is related as a faster reducing agent employed for the synthesis and control of size<sup>26</sup>.

Moreover, PtNPs have been shown to have potential antioxidant activity<sup>27</sup>. Platinum nanoparticles reduced the effect of reactive oxygen species (ROS)<sup>28,29</sup>. Due to this strong antioxidant activity, PtNPs have been effectively used in the pharmaceutical area, as antiaging formulations in the cosmetic sector. This antioxidant potential was used to prevent the effects of ROS lung diseases attributed to oxidative stress<sup>30</sup>.

Electron spin resonance (ESR) is a powerful spectroscopic technique to detect and quantify free radicals in different mediums. In solid state free radicals created by ionizing radiation can be used for dosimetry<sup>5,31–33</sup> and archeological dating<sup>34,35</sup> for instance. In solutions, the nature of radicals created by different processes can also be studied<sup>36</sup>. The antioxidant effect of different substances can also be studied in a straightforward way<sup>37,38</sup>. Because it is not a colorimetric method, it can be useful for substances that are not colorless. Thus, antioxidant extracts of plants were studied allowing a fast selection of those with potential for pharmaceutical use<sup>39</sup>. In this work, AuNP and PtNP were prepared by reducing gold salt  $HAuCl_4$  and platinum salt ( $H_2PtCl_6 \cdot 6H_2O$ ) by sodium borohydride  $NaBH_4$ . The antioxidant activity of AuNP was studied by ESR, through the observation of DPPH (1,1-diphenyl-2-picrylhydrazyl) radical annihilation. These properties are important in the biomedical area, since free radicals are associated with several pathologies, including delay of the healing processes.

## 2. Experimental

### 2.1 Synthesis AuNP

All chemicals and solvents used for the syntheses were of commercially available reagent grade and applied without further purification.

Gold nanoparticles were obtained by chemical reduction of the gold salt,  $HAuCl_4$  (4 mmol  $L^{-1}$ ) by sodium borohydride  $NaBH_4$  (8 mmol  $L^{-1}$ ), under vigorous stirring. The system is kept under agitation of 400 rpm, for 12 h in order to guarantee the total reduction of gold. The formation of AuNP can be confirmed by changing the color of the solution from yellow to red, indicating the formation of colloidal gold and the presence of the plasmonic peak in the UV-Vis spectrum around 515 nm<sup>6</sup>.

### 2.2 Synthesis PtNP

Platinum nanoparticles were synthesized by the chemical reduction of the platinum salt  $H_2PtCl_6 \cdot 6H_2O$  (2 mmol  $L^{-1}$ ) in the presence of sodium borohydride  $NaBH_4$  (4 mmol  $L^{-1}$ ) using polyvinyl alcohol (PVA) as capping agent. The system was kept under vigorous stirring for 18 h for all reduction. The color of the system became immediately bright yellow, indicating the formation of a colloidal dispersion. The characteristic absorption peak of the PtNPs in the UV-Vis spectrum is 260 nm<sup>40</sup>.

### 2.3 Anti-oxidative activity against DPPH

The anti-free radical activity of the synthesized AuNP and PtNP was studied by ESR spectroscopy. For these tests, 200  $\mu\text{L}$  of the nanoparticle solution and 200  $\mu\text{L}$  of the ethanol solution 200  $\mu\text{mol L}^{-1}$  DPPH free radical (1,1-diphenyl-2-picrylhydrazyl radical) were used. After the reaction, the resulting solution was transferred to a glass capillary tube (hematocrit tube), inserted in a quartz tube, and placed in the ESR resonant cavity to take the spectra.

The ESR spectra were acquired sequentially every 1 min on the ESR Jeol FA-200-Band X spectrometer, at room temperature, to study the kinetics of the reaction between the nanoparticles and the DPPH radical.

The parameters of the spectrometer for spectra acquisition were: central field 345 mT, scan 10 mT, scan time 1 min, modulation amplitude 0.1 mT, power 1 mW, modulation frequency 100 kHz and microwave frequency 9.5 GHz.

## 3. Results and Discussion

### 3.1 Anti-oxidative activity against DPPH

In this work, ESR and DPPH were employed to determine the antioxidant activity of AuNP. The DPPH is widely used as a radical molecule to evaluate the antioxidative properties of various compounds, using ESR. The DPPH radical is able to accept an electron or hydrogen atom (proton) to become a stable diamagnetic molecule<sup>41</sup>. Nie et al.<sup>8</sup> studied AuNP functionalized with antioxidant molecules through ESR DPPH radical scavenging tests. They observed an enhancement of antioxidative ability after functionalization. Esumi et al.<sup>4</sup> showed the antioxidative ability of AuNP prepared in the presence of chitosan. The authors used the spin trapping method with DMPO (5,5-dimethyl-1-pyrroline-N-oxide) to monitor the elimination of hydroxyl radicals generated by Fenton reaction. They observed a decrease of ESR DMPO-OH signal when increasing the concentration of gold-chitosan.

In this sense, by monitoring the signal intensity of the ESR spectrum, the radical scavenging activity of substances can be studied. The antioxidant activity of substances can also be assessed with DPPH and the optical method, since the DPPH solution has its color changed from violet to yellowish as the reaction occurs. So, the natural coloring of the substances can interfere in the procedure, which does not occur when

using the ESR, since the radical is detected directly without color interference. Figure 1a shows DPPH ESR spectrum reacted with methanol and the  $A_{pp}$ , Amplitude considered to monitor the reaction. After reaction with AuNP, the amplitude  $A_{pp}$  decays, showing the free radical scavenging capacity (Fig. 1b).

Experimental data points were adjusted with a single exponential curve decay (Eq. 1):

$$I = I_0 \cdot e^{-t/T} + c \quad (1)$$

Resulting in  $I_0 = 3791 \pm 65$ ,  $T = 3.1 \pm 0.1 \text{ min}^{-1}$ ,  $c = 552 \pm 14$ , and adjusted R-square 0.993 for AuNP; and  $I_0 = 3701 \pm 51$ ,  $T = 1.80 \pm 0.07 \text{ min}^{-1}$ ,  $c = 604 \pm 10$ , and R-square 0.995 for PtNP, revealing superior antioxidative properties of PtNPs compared to AuNPs.

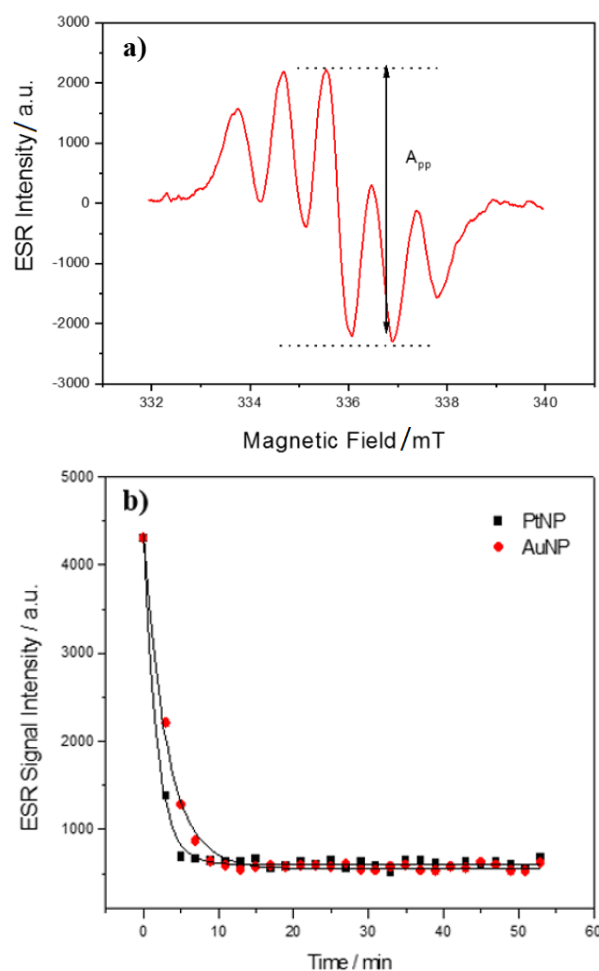


**Figure 1.** (a) Electron spin resonance spectrum of DPPH 200  $\mu\text{mol L}^{-1}$  and (b) decay of DPPH ESR signal amplitude after reaction with AuNP (circle) and with PtNP (square).

## 4. Conclusions

Gold and platinum nanoparticles can be easily produced by reducing the salt with sodium borohydride. Both nanoparticles presented antioxidative properties, but the results suggest that superior antioxidative properties of PtNPs. These results can be of great importance for biological environments, evidencing that their antioxidative effect should be considered in biomedical applications.

## Acknowledgments

This research was partially funded by the Brazilian agencies Fundação de Amparo à Pesquisa do Estado de São Paulo (FAPESP CEPID-NEUROMAT 13/07699-0), Coordenação de Aperfeiçoamento de Pessoal de Nível Superior (CAPES, finance code 001) and Conselho Nacional de Desenvolvimento Científico e Tecnológico (CNPq grant 304107/2019-0). The technical support of Eldereis de Paula, Lourenço Rocha and Carlos R. da Silva is also appreciated.

## References

- [1] Huang, X., Jain, P. K., El-Sayed, I. H., El-Sayed, M. A., Gold nanoparticles: interesting optical properties and recent applications in cancer diagnostics and therapy, *Nanomedicine* 2 (5) (2007) 681-693. <https://doi.org/10.2217/17435889.2.5.681>.
- [2] Zhao, P., Li, N., Astruc, D., State of the art in gold nanoparticle synthesis, *Coordination Chemistry Reviews* 257 (3-4) (2013) 638-665. <https://doi.org/10.1016/j.ccr.2012.09.002>.
- [3] Deraedt, C., Salmon, L., Gatard, S., Ciganda, R., Hernandez, R., Ruiz, J., Astruc, D., Sodium borohydride stabilizes very active gold nanoparticle catalysts, *Chemical Communications* 50 (91) (2014) 14194-14196. <https://doi.org/10.1039/C4CC05946H>.
- [4] Esumi, K., Takei, N., Yoshimura, T., Antioxidant-potentiality of gold-chitosan nanocomposites, *Colloids and Surfaces B: Biointerfaces* 32 (2) (2003) 117-123. [https://doi.org/10.1016/S0927-7765\(03\)00151-6](https://doi.org/10.1016/S0927-7765(03)00151-6).
- [5] Baffa, O., Kinoshita, A., Clinical applications of alanine/electron spin resonance dosimetry, *Radiation and Environmental Biophysics* 53 (2014) 233-240. <https://doi.org/10.1007/s00411-013-0509-2>.
- [6] Guidelli, E. J., Ramos, A. P., Zaniquelli, M. E. D., Nicolucci, P., Baffa, O., Synthesis and Characterization of Gold/Alanine Nanocomposites with Potential Properties for Medical Application as Radiation Sensors, *Applied Materials & Interfaces* 4 (11) (2012) 5844-5851. <https://doi.org/10.1021/am3014899>.
- [7] Sperling, R. A., Gil, P. R., Zangh, F., Zanella, M., Parak, W. J., Biological applications of gold nanoparticles, *Chemical Society Reviews* 37 (9) (2008) 1896-1908. <https://doi.org/10.1039/b712170a>.
- [8] Nie, Z., Liu, K. J., Chong, C.-J., Wang, L.-F., Yang, Y., Tian, Q., Liu, Y., Enhanced radical scavenging activity by antioxidant-functionalized gold nanoparticles: A novel inspiration for development of new artificial antioxidants, *Free Radical Biology and Medicine* 43 (9) (2007) 1243-1254. <https://doi.org/10.1016/j.freeradbiomed.2007.06.011>.
- [9] Rajan, A., Vilas, V., Philip, D., Studies on catalytic, antioxidant, antibacterial and anticancer activities of biogenic gold nanoparticles, *Journal of Molecular Liquids* 212 (2015) 331-339. <https://doi.org/10.1016/j.molliq.2015.09.013>.
- [10] Kang, W. P., Kim, C. K., Novel platinum-tin oxide-silicon nitride-silicon dioxide-silicon gas sensing component for oxygen and carbon monoxide gases at low temperature, *Applied Physics Letters* 63 (1993) 421-423. <https://doi.org/10.1063/1.110012>.
- [11] Xie, J., Wang, S., Aryasomayajula, L., Varadan, V. K., Platinum decorated carbon nanotubes for highly sensitive amperometric glucose sensing, *Nanotechnology* 18 (6) (2007) 065503. <https://doi.org/10.1088/0957-4484/18/6/065503>.
- [12] Chen, A., Holt-Hindle, P., Platinum-Based Nanostructured Materials: Synthesis, Properties, and Applications, *Chemical Reviews* 110 (6) (2010) 3767-3804. <https://doi.org/10.1021/cr9003902>.
- [13] Porcel, E., Liehn, S., Remita, H., Usami, N., Kibayashi, K., Furusawa, Y., Le Sech, C., Lacombe, S., Platinum nanoparticles: a promising material for future cancer therapy? *Nanotechnology* 21 (8) (2010) 085103. <https://doi.org/10.1088/0957-4484/21/8/085103>.
- [14] Butterworth, K. T., Wyer, J. A., Brennan-Fournet, M., Shah, M. B., Currel, E. J., Hirst, D. G., Variation of Strand Break Yield for Plasmid DNA Irradiated with High-Z Metal Nanoparticles, *Radiation Research* 170 (3) (2008) 381-387. <https://doi.org/10.1667/RR1320.1>.
- [15] Herold, D. M., Das, C. C., Iyer, R. V., Chapman, J. D., Gold microspheres: a selective technique for producing biologically effective dose enhancement, *International Journal of Radiation Biology* 76 (10) (2000) 1357-1364. <https://doi.org/10.1080/09553000050151637>.
- [16] Jain, S., Coulter, J. A., Hounsell, A. R., Butterworth, K. T., McMahon, S. J., Hyland, W. B., Hons, B. S., Muir, M. F., Dickson, G. R., Prise, K. M., Currell, F. J., O'Sullivan, J.



- M., Hirst, D. G., Cell-Specific Radiosensitization by Gold Nanoparticles at Megavoltage Radiation Energies, *International Journal of Radiation Oncology Biology Physics* 79 (2) (2011) 531-539. <https://doi.org/10.1016/j.ijrobp.2010.08.044>.
- [17] Dhar, S., Daniel, W. L., Giljohann, D. A., Mirkin, C. A., Lippard, S. J., Polyvalent Oligonucleotide Gold Nanoparticle Conjugates as Delivery Vehicles for Platinum(IV) Warheads, *Journal of the American Chemical Society* 131 (41) (2009) 14652-14653. <https://doi.org/10.1021/ja9071282>.
- [18] Brown, S. D., Nativo, P., Smith, J.-A., Stirling, D., Edwards, P. R., Venugopal, B., Flint, D., J., Plumb, J. A., Graham, D., Wheate, N. J., Gold Nanoparticles for the Improved Anticancer Drug Delivery of the Active Component of Oxaliplatin, *Journal of the American Chemical Society* 132 (13) (2010) 4678-4684. <https://doi.org/10.1021/ja908117a>.
- [19] Boulikas, T., Pantos, A., Bellis, E., Christofis, P., Designing platinum compounds in cancer: structures and mechanisms, *Cancer Therapy* 5 (2007) 537-583.
- [20] Rodrigues, M. A. C., dos Santos, N. A. G., Faria, M. C. da, S., Rodrigues, J. L., Kinoshita, A., Baffa, O., Antunes, L. M. G., Barbosa Junior, F., Gobe, G. C., dos Santos, A. C., Carvedilol protects the kidneys of tumor-bearing mice without impairing the biodistribution or the genotoxicity of cisplatin, *Chemico-Biological Interactions* 245 (2016) 59-65. <https://doi.org/10.1016/j.cbi.2015.12.020>.
- [21] Li, F., Li, F., Song, J., Song, J., Han, D., Li, N., Green synthesis of highly stable platinum nanoparticles stabilized by amino-terminated ionic liquid and its electrocatalysts for dioxygen reduction and methanol oxidation, *Electrochemistry Communications* 11 (2) (2009) 351-354. <https://doi.org/10.1016/j.elecom.2008.11.042>.
- [22] Ingelsten, H. H., Bagwe, R., Palmqvist, A., Skoglundh, M., Svanberg, C., Holmberg, K., Shah, D. O., Kinetics of the Formation of Nano-Sized Platinum Particles in Water-in-Oil Microemulsions, *Journal of Colloid and Interface Science* 241 (1) (2011) 104-111. <https://doi.org/10.1006/jcis.2001.7747>.
- [23] Coccia, F., Tonucci, L., Bosco, D., Bressan, M., d'Alessandro, N., One-pot synthesis of lignin-stabilised platinum and palladium nanoparticles and their catalytic behaviour in oxidation and reduction reactions, *Green Chemistry* 14 (4) (2012) 1073-1078. <https://doi.org/10.1039/c2gc16524d>.
- [24] Gharibshahi, E., Saion, E., Influence of Dose on Particle Size and Optical Properties of Colloidal Platinum Nanoparticles, *International Journal of Molecular Sciences* 13 (11) (2012) 14723-14741. <https://doi.org/10.3390/ijms131114723>.
- [25] Ahmadi, T. S., Wang, Z. L., Green, T. C., Henglein, A., El-Sayed, M. A., Shape-Controlled Synthesis of Colloidal Platinum Nanoparticles, *Science* 272 (5270) (1996) 1924-1925. <https://doi.org/10.1126/science.272.5270.1924>.
- [26] Nagao, H., Ichiji, M., Hirasawa, I., Synthesis of Platinum Nanoparticles by Reductive Crystallization Using Polyethyleneimine, *Chemical Engineering & Technology* 40 (7) (2017) 1242-1246. <https://doi.org/10.1002/ceat.201600656>.
- [27] Yusof, F., Ismail, N. A. S., Antioxidants effects of Platinum Nanoparticles: A Potential Alternative Treatment to Lung Diseases, *Journal of Applied Pharmaceutical Science* 5 (7) (2015) 140-145. <https://doi.org/10.7324/JAPS.2015.50722>.
- [28] Asharani, P. V., Lianwu, Y., Gong, Z., Valiyaveetil, S., Comparison of the toxicity of silver, gold and platinum nanoparticles in developing zebrafish embryos, *Nanotoxicology* 5 (1) (2011) 43-54. <https://doi.org/10.3109/17435390.2010.489207>.
- [29] Nomura, M., Yoshimura, Y., Kikuri, T., Hasegawa, T., Taniguchi, Y., Deyama, Y., Koshiro, K.-I., Sano, H., Suzuki, K., Inoue, N., Platinum Nanoparticles Suppress Osteoclastogenesis Through Scavenging of Reactive Oxygen Species Produced in RAW264.7 Cells, *Journal of Pharmacological Sciences* 117 (4) (2011) 243-252. <https://doi.org/10.1254/jphs.11099FP>.
- [30] Cheng, H., Xi, C., Meng, X., Hao, Y., Yu, Y., Zhao, F., Polyethylene glycol-stabilized platinum nanoparticles: The efficient and recyclable catalysts for selective hydrogenation of o-chloronitrobenzene to o-chloroaniline, *Journal of Colloid and Interface Science* 336 (2) (2009) 675-678. <https://doi.org/10.1016/j.jcis.2009.04.076>.
- [31] Kinoshita, A., Calcina, C. S. G., Sakamoto-Hojo, E. T., Camparato, M. L., Baffa, O., Evaluation of a High Dose to a Finger from a <sup>60</sup>Co Accident, *Health Physics* 84 (4) (2003) 477-482. <https://doi.org/10.1097/00004032-200304000-00007>.
- [32] Kinoshita, A., Braga, F. J. H. N., Graeff, C. F. O., Baffa, O., ESR dosimetry of <sup>89</sup>Sr- and <sup>153</sup>Sm-in bone, *Applied Radiation and Isotopes* 54 (2) (2001) 269-274. [https://doi.org/10.1016/S0969-8043\(00\)00159-7](https://doi.org/10.1016/S0969-8043(00)00159-7).
- [33] Kinoshita, A., Baffa, O., Mascarenhas, S., Electron spin resonance (ESR) dose measurement in bone of Hiroshima A-bomb victim, *PLoS One* 13 (2) (2018) e0192444. <https://doi.org/10.1371/journal.pone.0192444>.
- [34] Kinoshita, A., Skinner, A. R., Guidon, N., Ignacio, E., Felice, G. D., Buco, C. de A., Tatum, S., Yee, M., Figueiredo, A. M. G., Baffa, O., Dating human occupation at Toca do Serrote das Moendas, São Raimundo Nonato, Piauí-Brasil by electron spin resonance and optically stimulated

luminescence, *Journal of Human Evolution* 77 (2014) 187-195. <https://doi.org/10.1016/j.jhevol.2014.09.006>.

[35] Lopes, R. P., Pereira, J. C., Dillenburg, S. R., Tatumi, S. H., Yee, M., Figueiredo, A. M. G., Kinoshita, A., Baffa, O., Late Pleistocene-Holocene fossils from Mirim Lake, Southern Brazil, and their paleoenvironmental significance: I – Vertebrates, *Journal of South American Earth Sciences* 100 (2020) 102566. <https://doi.org/10.1016/j.jsames.2020.102566>.

[36] Swartz, H. M., Bolton, J. R., Borg, D. C., *Biological Applications of Electron Spin Resonance*, Wiley-Interscience, New York, 1972.

[37] Barbosa, J. H. O., Luna, J. A. G., Kinoshita, A. M. O., Baffa Filho, O., Correlation Between Antioxidant Activity and Coffee Beverage Quality by Electron Spin Resonance Spectroscopic, *Ciência e Agrotecnologia* 37 (6) (2013) 495-501. <https://doi.org/10.1590/S1413-70542013000600002>.

[38] Barros Silva, R., Santos, N. A. G., Martins, N., M., Ferreira, D. A. S., Barbosa Junior, F., Souza, V. C. O., Baffa, O., Del-Bel, E., Santos, A. C., Caffeic acid phenethyl ester protects against the dopaminergic neuronal loss induced by 6-hydroxydopamine in rats, *Neuroscience* 233 (2013) 86-94. <https://doi.org/10.1016/j.neuroscience.2012.12.041>.

[39] Miyahara, M. R. M., Imamura, P. M., de Freitas, J. C., Leonor, S. J., Baffa, O., Kinoshita, A., de Paula-Zurron, A. C. B., Anti-oxidative and anti-ulcerogenic activity of *Ipomoea imperati*, *Revista Brasileira de Farmacognosia* 21 (6) (2011) 978-985.

[40] Chen, S., Kimura, K., Synthesis of Thiolate-Stabilized Platinum Nanoparticles in Protolytic Solvents as Isolable Colloids, *The Journal of Physical Chemistry B* 105 (23) (2001) 5397-5403. <https://doi.org/10.1021/jp0037798>.

[41] Morales, N. P., Sirijaroonwong, S., Yamanont, P., Phisalaphong, C., Electron Paramagnetic Resonance Study of the Free Radical Scavenging Capacity of Curcumin and Its Demethoxy and Hydrogenated Derivatives, *Biological and Pharmaceutical Bulletin* 38 (10) (2015) 1478-1483. <https://doi.org/10.1248/bpb.b15-00209>.

# Metallo-stannosilicates as inorganic supports to immobilization of lipase from *Thermomyces lanuginosus* for biodiesel production

Danilo Antonio da Silva<sup>1</sup>, Adriano de Vasconcellos<sup>1</sup>, José Geraldo Nery<sup>1+</sup>

1. São Paulo State University, Institute of Biosciences, Letters and Exact Sciences, São José Rio Preto, Brazil.

**+Corresponding author:** José Geraldo Nery, **Phone:** +55 17 3221-2490, **Email address:** geraldo.nery@unesp.br

## ARTICLE INFO

### Article history:

**Received:** September 08, 2020

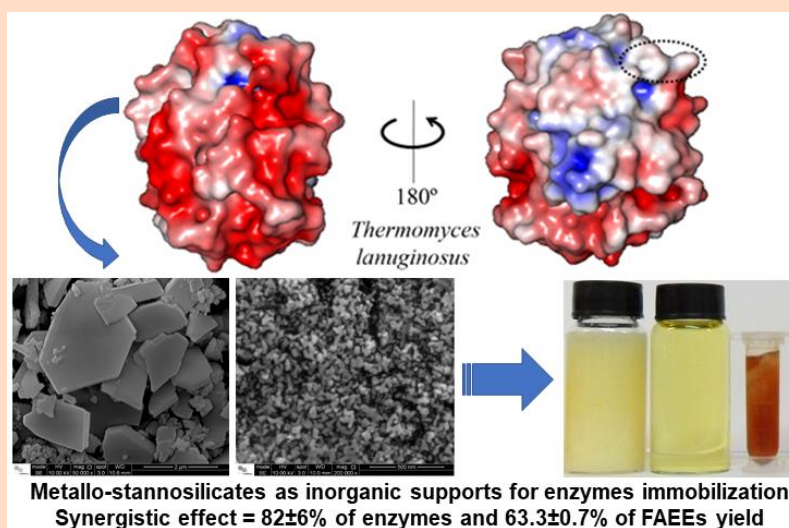
**Accepted:** February 10, 2021

**Published:** April xx, 2021

## Keywords

1. Stannosilicates
2. biofuels
3. heterogeneous catalysts
4. enzymes immobilization
5. enzymatic catalysis

**ABSTRACT:** This study reports the application of metallo-stannosilicates as potential inorganic solid matrixes for enzymes immobilization and their use as a heterogenous catalysts in enzymatic transesterification reactions for the conversion of triacylglycerides into fatty acid ethyl esters (FAEEs). Several stannosilicates were synthesized and physicochemical characterized by X-ray powder diffraction (XRD), scanning electron microscopy with energy dispersive X-ray spectrometry (SEM-EDS), Brunauer–Emmett–Teller (BET)-N<sub>2</sub> surface area analysis and solid-state magic-angle spinning nuclear magnetic resonance (MAS NMR <sup>29</sup>Si and <sup>119</sup>Sn nuclei) techniques. The experimental results for enzymes immobilization were promising, especially for a nickel ion-exchanged metallo-stannosilicate, which were able to immobilize 82 ± 6% of *Thermomyces lanuginosus* lipase and also kept a high enzymatic activity (42 ± 3 U mg<sup>-1</sup>). Systematic catalytic reactions for conversion of refined palm oil (*Elaeis guineensis*) using some of these stannosilicates enzymes complexes yielded 63.3 ± 0.7% of FAEEs. It is worth noticing that, when the transesterification reaction was performed with (a) the as-made stannosilicate without enzymes and (b) the equivalent amount of immobilized *Thermomyces lanuginosus* lipase in its free form, the FAEEs yield sharply decreased to < 5.0% and 6.3 ± 0.3%, respectively. This result is a clear evidence of a synergistic effect among the metallo-stannosilicates and the immobilized enzymes.



## 1. Introduction

The development of alternative biofuels as viable ways to replace or reduce the use of fossil fuels has stimulated the efforts of the scientific community. The energy demand arises from numerous factors, including environmental concerns and the depletion of fossil fuel resources that have stimulated the development of new alternative sources of more sustainable fuels. Among the various options, biodiesel is attractive because it is a sustainable and renewable form of energy<sup>1</sup>. Chemically, biodiesel consists of a mixture of fatty acid alkyl esters (FAEs) and is predominantly produced, in industrial scale, by means of transesterification reactions using refined vegetable oils as triacylglycerides sources, together with short chain alcohols (methanol or ethanol) and homogeneous catalysts. The appropriate choice of triacylglycerides feedstocks and catalysts are the main challenges and have precluded a faster development of this industry.

Concerning the available triacylglycerides sources, the use of edible oils has raised ethical and economic questions, one of the reasons to search alternative lipid feedstocks that do not compete with food production<sup>2,3</sup>. There are several lipids feedstocks for biodiesel production, such as: palm, castor, soybean, cotton, peanuts, jatropha, sunflower (vegetable oils), besides the utilization of animal fats, nonedible and waste oils. Considering oils from vegetable origin, the palm tree (*Elaeis guineensis*) is an excellent option due of its low price, relatively high oil content (palm fruit contains approximately 40% of oil) and high productivity (2500–4000 kg hectare<sup>-1</sup> year<sup>-1</sup>). Furthermore, palm oil is more saturated and has greater oxidation stability when compared to other vegetable oils, in addition to being an important alternative for the sustainable development of some Brazilian regions, mainly in the Amazon<sup>4,5</sup>. Another important component in the biodiesel production process is the short chain alcohol source. In Brazil, the use of ethanol is a viable option, since the country is the world's second largest producer of ethanol. However, most industrial biodiesel plants do not have the technology to synthesize biodiesel by applying ethanol as a solvent, since that the production of biodiesel via the ethylic route presents some obstacles, such as high alcohol consumption and difficulty in separating the final products (glycerol and biodiesel), which generates greater energy costs for this process.

In terms of catalyst technology, sodium hydroxide (NaOH), potassium hydroxide (KOH) and sodium methoxide (NaOCH<sub>3</sub>) are currently the main homogeneous catalysts employed in the biodiesel

industry. Their disadvantages are associated with the impossibility of use low-quality feedstocks, with high contents of water and free fatty acids (FFAs)<sup>6</sup>. Although not currently applied in industrial scale for biodiesel production, heterogeneous acid catalysts could be an interesting alternative to solve this problem due the fact of being less sensitive to FFAs content and perform simultaneously the esterification and transesterification reactions. Moreover, the heterogeneous catalyst can be recycled (reused), there is none or very little amount of wastewater produced during the catalytic process and the separation of the catalysts from biodiesel and glycerol is relatively easy. Nevertheless, its application in the biodiesel industry is precluded due the necessity of employing longer reaction times, higher reaction temperatures and large alcohol to oil molar ratios<sup>7–10</sup>. The combination of all these factors has a negative impact in the final price of the biodiesel, therefore the search for new heterogeneous catalysts able to overcome these drawbacks is a technical and scientific challenge.

Zeolites and Mixed Octahedral-Pentahedral-Tetrahedral Silicates (OPT) materials are inorganic microporous framework oxides and can be an interesting option to overcome these challenges. Mixed framework OPT materials containing coordinated tetrahedra or octahedra, namely stannosilicates, is one of these materials subject of research. Stannosilicates and tin-zeotypes materials have been reported as ion exchangers, sorbents and catalysts for several types of reaction, as purification of natural gas with sulfur compounds, like hydrogen sulfides or oxysulfides<sup>11</sup>, and catalytic reactions for decomposition of propan-2-ol and oxidation of cyclohexene<sup>12</sup>, Baeyer–Villiger oxidation reactions<sup>13</sup>, monosaccharide isomerization reactions<sup>14,15</sup> and application as heterogeneous catalysts for biofuels production<sup>16</sup>. Tin-based homogeneous and heterogeneous catalysts have been used in transesterification reactions, mainly using refined edible oils as feedstocks and methanol, typically providing high yields of fatty acid methyl esters (FAMEs)<sup>17–24</sup>.

The use of lipases (triacylglycerol acylhydrolases, E.C.3.1.1.3) as catalysts in the biodiesel production is also an attractive option due to their high specificity for the transesterification of triacylglycerides to FAMEs or FAEs in comparison with the other conventional chemical catalysts employed in industrial biodiesel production. In comparison to the basic homogeneous catalysts, enzymes exhibit high selectivity and catalytic activity under mild operative conditions. In addition, lipases can also catalyze the transesterification of waste feedstocks that contain a high content of free fatty

acids (FFAs) and water, therefore decreasing the probability of forming soap and emulsion<sup>25</sup>. Some examples of biodiesel production by enzymatic catalysis are the transesterification of soybean oil (*Glycine max*) by applying different lipases and experimental parameters (quantity of biocatalyst, reaction time, amount of water added and turnover of lipases)<sup>26–28</sup>, esterification reactions of oleic acid<sup>29</sup> and FAEEs production by enzymatic transesterification of triolein<sup>30</sup>. Besides all the advantages of the enzymatic process in comparison to the other ones, there are important drawbacks that preclude their large use in industrial scale process for biodiesel production. Between them are the enzymes expensive costs, the difficulty of its separation (recover of the enzymes and reuse in its free form), besides the possible deactivation of enzymes active sites by glycerol, a subproduct of triacylglycerides transesterification. In this context, the enzymes immobilization is a viable alternative for overcoming these obstacles<sup>31–36</sup>.

The use of supports for enzymatic immobilization is an effective way to combine the advantages of both heterogeneous and enzymatic catalysts. Enzymatic immobilization consists of locating or confining an enzyme on a solid support or matrix. The methods are basically classified as chemical or physical processes, and the choice of the appropriate support depends of physical-chemical characteristics, such as mechanical, chemical and microbial resistance, thermal stability, high loading capacity, adequate pore diameter and hydrophilic/hydrophobic behavior that allows the immobilization of the enzymes<sup>37</sup>. Several solid materials, such as ceramics, kaolinites, silica, cellulose, polymers and zeolites, have been used as supports for enzymes immobilization. Specifically, in the case of zeolites and mixed framework oxides, the aim of the immobilization is to create a zeolite-enzyme complex that can be applied as biocatalysts. It is clear from these studies<sup>38–40</sup> that both the zeolites and the enzymes can themselves alone catalyze the transesterification reaction: each one of them have their own particularity that determines the rate and yield of the final product.

This study is a sequence of previous work reported by the authors research group<sup>16</sup> concerning the application of a metallo-stannosilicate for biodiesel production using edible, nonedible and waste oils as feedstocks. In this paper, several stannosilicates were synthesized using different sol-gel chemical compositions. The stannosilicates were physicochemical characterized and, afterwards, used as heterogeneous catalysts in the transesterification of refined palm oil (*Elaeis guineensis*) by ethanolysis reactions. Furthermore, these materials were also

studied as potential inorganic solid matrixes for immobilization of *Thermomyces lanuginosus* lipase and tested in enzymatic transesterification reactions with the following aims: are metallo-stannosilicates feasible for use as inorganic supports for enzymes immobilization? What can be learned from catalytic results about the appropriated application of different catalysts in specific reactions for biodiesel production?

To the best our knowledge, metallo-stannosilicates were not previously explored as inorganic supports for enzymes immobilization and as heterogeneous catalysts in enzymatic transesterification reactions for biodiesel production by applying the feedstocks (refined palm oil and ethanol) used in this work.

## 2. Experimental

### 2.1 Materials

The syntheses of the metallo-stannosilicates, the nickel ion-exchange experiments, the catalytic reactions for biodiesel production and the enzymes immobilization reactions employed the following chemicals: Ludox HS-40 colloidal silica (40 wt.% SiO<sub>2</sub> in water), tin chloride pentahydrate (SnCl<sub>4</sub>•5H<sub>2</sub>O, 98%), sodium hydroxide (NaOH), potassium hydroxide (KOH), nickel(II) sulfate hexahydrate (NiSO<sub>4</sub>•6H<sub>2</sub>O, 98%), Bradford reagent (1-1,400 µg mL<sup>-1</sup> protein) and enzyme lipolase 100 L (from *Thermomyces lanuginosus* lipase, molecular weight 30 kDa, pI 4.4, solution ≥ 100,000 U g<sup>-1</sup>) were purchased from Sigma-Aldrich (Steinheim, Germany) and used as received, without further purification.

The *Thermomyces lanuginosus* is a purified enzyme 1,3-specific lipases (EC 3.1.1.3) and industrially produced through the submerged fermentation of a genetically modified *Aspergillus oryzae* fungus<sup>41</sup>. This lipase was used based on satisfactory results reported by our research group<sup>35,36</sup> among other examples of application of this enzyme to biodiesel production<sup>42–44</sup>. Anhydrous ethyl alcohol (99.8%) was purchased from Dinâmica Chemistry (Diadema, Brazil). The refined palm oil (*Elaeis guineensis*) predominantly composed by palmitic acid (C16), stearic acid (C18), oleic acid (C18:1) and linoleic acid (C18:2) were obtained from Agropalma Company (Belém, Brazil). The gas chromatogram (GC-FID), which illustrates these major components in the oil composition, is illustrated and discussed in the supplementary material.

## 2.2 Hydrothermal syntheses of stannosilicates

The stannosilicates were synthesized according to experimental procedures adapted from the literature<sup>45,46</sup> by hydrothermal crystallization in the Na<sub>2</sub>O-SnO<sub>2</sub>-SiO<sub>2</sub> oxides system. Detailed experimental conditions of all the stannosilicates synthesized are summarized in Tab. 1. A typical synthesis for the material named stannosilicate I, using Sn<sup>4+</sup> (SnCl<sub>4</sub>•5H<sub>2</sub>O as the tin source) and gel composition of 1Na<sub>2</sub>O:SnO<sub>2</sub>:4SiO<sub>2</sub>:80H<sub>2</sub>O was performed at the following manner: 14.9 g of sodium hydroxide (NaOH) was dissolved in 20 g of water (solution A). A second solution (solution B) was prepared by dissolving 20 g

of SnCl<sub>4</sub>•5H<sub>2</sub>O in 30 g of distilled water. This solution B was added to the solution A and homogenized under 500 rpm of stirring during 60 min at 25 °C of temperature (solution C). Finally, solution C was added to 27.4 g of Ludox HS-40 colloidal silica (40 wt.% SiO<sub>2</sub> in water) and this final gel was also kept stirring for 30 min at 500 rpm. The sol-gel solution was transferred to a 125 mL teflon-lined stainless-steel autoclave (Parr Instruments Co., Illinois, USA) and kept at 200 °C for 7 days. Afterwards, the reactor was cooled down, the product collected by filtration, washed with distilled water and dried at 100 °C for 12 h.

**Table 1.** Summary of the experimental procedures for the metallo-stannosilicates syntheses.

| Gel composition   | Nomenclature | Step 1 (solution A) |                      | Step 2 (solution B)                      |                      | Step 3 (solution C)***                               | Step 4 Ludox HS-40 / g | Step 5 (final gel)***         | Surface area / m <sup>2</sup> g <sup>-1</sup> |
|---|--------------|---------------------|----------------------|--|----------------------|--|------------------------|-------------------------------|---|
|   |              | NaOH / g            | H <sub>2</sub> O / g | SnCl <sub>4</sub> •5H <sub>2</sub> O / g | H <sub>2</sub> O / g |  |                        |                               |   |
| 1Na <sub>2</sub> O:SnO <sub>2</sub> :4SiO <sub>2</sub> :80H <sub>2</sub> O  | I*           | 14.9                | 20.0                 | 20.0                                     | 30.0                 | Add solution B to solution A                         | 27.4                   | Add solution C to Ludox HS-40 | 18.73   |
| 2Na <sub>2</sub> O:SnO <sub>2</sub> :4SiO <sub>2</sub> :80H <sub>2</sub> O  | II*          | 29.8                | 20.0                 | 20.0                                     | 30.0                 |  | 27.4                   |                               | 22.40   |
| 1Na <sub>2</sub> O:SnO <sub>2</sub> :10SiO <sub>2</sub> :80H <sub>2</sub> O | III**        | 4.2                 | 10.0                 | 16.0                                     | 22.0                 |  | 54.8                   |                               | 86.95   |
| 2Na <sub>2</sub> O:SnO <sub>2</sub> :10SiO <sub>2</sub> :80H <sub>2</sub> O | IV**         | 8.4                 | 10.0                 | 16.0                                     | 22.0                 |  | 54.8                   |                               | 50.45   |
| 5Na <sub>2</sub> O:SnO <sub>2</sub> :10SiO <sub>2</sub> :80H <sub>2</sub> O | V**          | 21.1                | 20.0                 | 16.0                                     | ---                  | Add SnCl <sub>4</sub> •5H <sub>2</sub> O in solution | 54.9                   |                               | 8.16  |

\*Time of hydrothermal synthesis = 7 days; \*\*Time of hydrothermal synthesis = 21 days; \*\*\*The gel was homogenized at 500 rpm for 60 min at ambient temperature of 25 °C.

## 2.3 Nickel ion-exchange experiments

Prior to the enzyme immobilization, all stannosilicates synthesized were subjected to nickel ion-exchange experiments. The experiments were made as follows: 30 mL of 0.5 mol L<sup>-1</sup> NiSO<sub>4</sub> solution (3.94 g of NiSO<sub>4</sub>•6H<sub>2</sub>O was dissolved in 30 mL of distilled water) was added into a teflon bottle. Afterwards, 1 g of the stannosilicates was added to this solution and kept stirring at 500 rpm for 60 min and 25 °C of temperature. Afterwards, the solution was heated at 80 °C for 24 h. After this period, the nickel-stannosilicates were cooled down, collected by filtration, washed with distilled water and dried at 100 °C for 12 h.

## 2.4 Physicochemical characterization of the solid materials

### 2.4.1 X-ray diffraction, BET-N<sub>2</sub> surface area and SEM-EDS

All the stannosilicates synthesized were characterized by XRD using a Rigaku Miniflex

(Rigaku, Tokyo, Japan) operated at 40 kV, 15 mA and using a Ni-filtered Cu-K $\alpha$  radiation ( $\lambda = 1.5418 \text{ \AA}$ ) in the range of  $2\theta$  from 3 to 80° with goniometer rate of 2° ( $2\theta$ ) min<sup>-1</sup>. Surface area measurements at 77 K were performed on a Micromeritics ASAP 2020 (Micromeritics Instrument Corporation, Norcross, USA) using the facilities of the BAM Federal Institute for Materials Research and Testing (Division 1.3. Structural Analysis, Berlin, Germany). Prior to the measurement, all samples were degassed at temperature of 300 °C and pressure of  $5 \times 10^{-5}$  mbar for 3 h, and isotherms were processed by the BET (Brunauer–Emmett–Teller) method<sup>47</sup>. Scanning electron microscopy (SEM) and energy-dispersive X-ray spectrometry (EDS) results were recorded on a FEI Inspect F50 (FEI Instruments, Oregon, USA) using the facilities of the Brazilian National Laboratory of Nanotechnology (LNNano, Electron Microscopy Laboratory, Campinas, Brazil). The electronic microscope is equipped with a Schottky field emission source, probe current at 200 nA and an electron beam with accelerating voltages between 0.2 and 30 kV.

### 2.4.2 Solid-state MAS NMR

Solid-state magic angle spinning NMR (MAS NMR) experiments were performed using the facilities of the BAM Federal Institute for Materials Research and Testing (Division 1.3. Structural Analysis, Berlin, Germany). The fully hydrated metallo-stannosilicates samples were characterized by  $^{29}\text{Si}$  and  $^{119}\text{Sn}$  Single-Pulse MAS NMR using a Bruker Avance 400 spectrometer (9.4 T). The data were analyzed and processed in the software TopSpin 3.6.2 version. All the experiments were carried out at room temperature and the samples were filled into zirconia rotors equipped with Kel-F caps (Bruker, Wissembourg, France) of 7 and 4 mm for  $^{29}\text{Si}$  and  $^{119}\text{Sn}$  nuclei, respectively. The  $^{29}\text{Si}$  single-pulse MAS NMR spectra were obtained using radiofrequency pulses at the Larmor frequency of 79.5 MHz, MAS frequency of 6.5 kHz,  $90^\circ$  pulse length of 6.0  $\mu\text{s}$  and recycle delay of 300 s.  $^1\text{H}\{^{29}\text{Si}\}$  cross-polarization (CPMAS) experiments were also made by applying  $90^\circ$  pulse of 3.0  $\mu\text{s}$ , cross-polarization time of 6.0 ms and repetition time of 3.0 s were used in order to maximize  $^{29}\text{Si}$  signal intensities. A 50% amplitude CP ramp and TPPM15 (decoupling power level is the same as for the  $90^\circ$   $^1\text{H}$  pulse of 3.0  $\mu\text{s}$ ) was also applied. The  $^{29}\text{Si}$  chemical shifts were reported relative to kaolinite as secondary reference ( $\delta = -91.5$  ppm). The  $^{119}\text{Sn}$  single-pulse MAS NMR spectra were obtained using radiofrequency pulses at the Larmor frequency of 149.1 MHz, MAS frequency of 12.5 kHz,  $90^\circ$  pulse length of 2.5  $\mu\text{s}$  and recycle delay of 600 s. The  $^{119}\text{Sn}$  chemical shifts were reported relative to  $\text{SnO}_2$  ( $\delta = -604$  ppm)<sup>48</sup>.

### 2.4.3 Zeta potential of the stannosilicates and stannosilicates-lipases complexes

The zeta potential of the stannosilicates and stannosilicates-enzymes complexes were measured in a Nano Zetasizer ZS90 equipment (Malvern Instruments, Worcester Shire, UK). Prior to the measurements, 1 mg of the materials and 1 mL of deionized water were placed in Eppendorf tubes and stabilized during 30 min at 25 °C, and then transferred to a DTS1060 cell, equipped with golden electrodes. A wide angle ( $90^\circ$ ) laser Doppler velocimetry was used to measure the electrophoretic mobility and the  $\zeta$  potential (zeta

potential), expressed in mV, was calculated by Smoluchowski equation<sup>49</sup>.

### 2.5 Enzymes immobilization on the stannosilicates

The enzymes immobilization experiments were made in triplicate, according to adapted procedures from the literature<sup>35,50</sup>. The initial concentration of 2 mg mL<sup>-1</sup> of the commercial lipases (enzyme Lipolase 100 L, from *Thermomyces lanuginosus* lipase) was added in a phosphate buffer solution, 20 mmol L<sup>-1</sup> and pH 7, according to a proportion of 1:40 (25  $\mu\text{L}$  of commercial lipase:1 mL phosphate buffer:50 mg of stannosilicates) and stirred at 300 rpm for 16 h at room temperature of 25 °C, followed by the separation of stannosilicates-lipases complexes via centrifugation at 12,000 rpm for 1 min. The products were washed twice with deionized water, dried at 25 °C overnight and stored at 4 °C. The amount of the enzymes immobilized was determined according to proposed by Bradford<sup>51</sup> and based on procedures adapted from the literature<sup>52</sup>.

### 2.6 Determination of percentual of enzymes immobilized on the stannosilicates

The percentual of *Thermomyces lanuginosus* lipase immobilized on the stannosilicates supports were determined by the method described Bradford<sup>46</sup>, which uses bovine serum albumin as standard and its absorption in the ultraviolet wavelength ( $\lambda = 595$  nm). For these measurements, three different solutions were prepared, previously the measurements: (a) supernatant solution that remain after the enzymes immobilization reactions, (b) a solution with the same quantity of enzymes prepared for the immobilization reaction, diluted in the phosphate buffer solution (20 mM and pH 7) and (c) only the same amount of the phosphate buffer solution, which has its absorbance subtracted of the other solutions. Afterwards, a mixture of Bradford reagent (1–1,400  $\mu\text{g mL}^{-1}$  protein, Sigma Aldrich, Germany) and the samples described above were mixed in the proportion of 1:20 (50  $\mu\text{L}$  of solution:950  $\mu\text{L}$  of Bradford reagent) and kept out of the luminosity for 20 min. The percentage of enzymes immobilized was calculated from the relationship<sup>52</sup> shown in Eq. 1:

$$\% \text{ enzymes immobilized} = \frac{\text{initial amount of enzymes (solution b)} - \text{amount of enzymes after immobilization (solution a)}}{\text{initial amount of enzymes (solution b)}} \times 100 \quad (1)$$

## 2.7 Enzymatic hydrolytic activity of stannosilicates-enzymes complexes

The enzymatic hydrolytic activity of stannosilicate-enzymes complexes was determined by titrimetric method<sup>35,53</sup> and following ACS specifications in the sigma standard enzymatic assays for lipases (triacylglycerol acylhydrolases, E.C.3.1.1.3). Since that, the enzymatic activity is obtained by a hydrolysis reaction, one unit of lipase activity was defined as the amount stannosilicate-enzymes complexes releasing one mole of FFAs from a triacylglyceride source in 1 h of reaction at  $40 \pm 2$  °C, expressed by the unity of  $\text{U mg}^{-1}$  (unit of lipase activity/mg of stannosilicate-enzymes complexes). In a typical measurement, 10 mL of a mixture containing  $20 \text{ mmol L}^{-1}$  at pH 7 of phosphate buffer and a triacylglyceride substrate (refined soybean oil, *Glycine max*) was prepared in the volume proportion of 1:1.

This solution was thoroughly mixed and equilibrated at 37 °C. Afterwards, 30 mg of the stannosilicates-enzymes complexes was added and the reaction maintained at 37 °C for 30 min. Finally, the reaction was quenched by adding 3 mL of ethanol (95 %, Sigma Aldrich, Steinheim, Germany) and then cooled to the temperature of - 4 °C by using a mixture of ice and ethanol for 10 min. The solution was centrifuged at 12,000 rpm for 1 min and the FFAs obtained as a result of the enzymatic hydrolysis reaction were neutralized by a titration with a solution of  $50 \text{ mmol L}^{-1}$  NaOH in the presence of thymolphthalein as indicator. One unit of stannosilicate-enzymes activity was expressed as micro equivalents of FFAs released from the triacylglyceride substrate in 1 h at 37 °C, calculated according to Eq. 2:

$$\frac{\text{Units}}{\text{mg}} \text{solid} = \frac{(\text{NaOH})(\text{Molarity of NaOH})(1000)(2)}{\text{mass of the solid}} \quad (2)$$

NaOH = volume (mL)

1000 = conversion factor from  $10^{-3}$  equivalents to  $10^{-6}$  equivalents

2 = time conversion factor from 30 min to 1 h (unit definition)

Mass of the solid = mass (mg) of stannosilicate-lipase complexes used in the hydrolysis reaction

## 2.8 Enzymatic transesterification of refined palm oil (*Elaeis guineensis*) for FAEEs production

Enzymatic transesterification of refined palm oil (*Elaeis guineensis*) by ethanolysis reaction catalyzed by free enzymes and stannosilicate-enzymes

complexes were performed in 10 mL flasks, with an oil:ethanol ratio of 1:4, 3% of stannosilicates-enzymes complexes referred to the oil mass and temperature of  $40 \pm 2$  °C for 48 h. In order to avoid the inactivation of the enzymes, the total amount of ethanol was equally divided and added stepwise over four different time intervals (0, 3, 6 and 12 h after the start of the reaction). Afterwards, FAEEs and glycerol were separated by centrifugation at 12,000 rpm for 1 min.

## 2.9 Heterogeneous transesterification of refined palm oil (*Elaeis guineensis*) for FAEEs production

Syntheses of FAEEs through the heterogeneous transesterification reactions were performed in triplicate (as performed for the enzymatic transesterification reactions) using refined palm oil (*Elaeis guineensis*) as triacylglycerides feedstock. In a typical transesterification reaction, 20.0 g of refined palm oil (FFAs content = 0.3 wt.%, acid value of  $0.6 \text{ mg KOH g}^{-1}$ ) was added in a 100 mL open glass reactor (catalytic reaction made at atmosphere pressure) with a reflux condenser, in a thermostatic bath equipped with a magnetic stirrer. Anhydrous ethyl alcohol was added according to alcohol:oil molar ratio of 1:30. The appropriate amount of catalyst (3% of heterogeneous catalyst referred to oil mass) was added and the mixture heated at 100 °C for 12 h, magnetic stirrer was set at 900 rpm and the reflux temperature adjusted of  $10 \pm 2$  °C. After the reaction time, the mixture was filtered, the excess of alcohol was removed using a rotary evaporator (Büchi Rotavapor R-210, Flawil, Switzerland) and glycerol were separated by centrifugation at 12,000 rpm for 1 min.

## 2.10 Quantification of FAEEs yields by gas chromatography (GC-FID)

The measurements of FAEEs yields were made under the following experimental conditions: the measurements were made in a gas chromatograph (PerkinElmer, Massachusetts, USA) using a sample injection volume of 1 mL, helium as gas carrier at a flow rate of  $2 \text{ mL min}^{-1}$  and pressure of 83 kPa, injector and detector temperatures of 250 °C. The oven temperature started at 50 °C for 1 min, increased up to 250 °C at a rate of  $5 \text{ °C min}^{-1}$ . In a typical measurement, solutions of  $20 \text{ mg mL}^{-1}$  of the ethyl myristate (C14:0) and ethyl nervonate (C24:1) standards were prepared. Additionally, an ethylic nonadecanoate standard solution was prepared in a



concentration of 10 mg mL<sup>-1</sup>. The range of peaks integration were identified using the ethyl ester standards C14:0, C24:1 and an ethylic ester (C19:0) as the internal standard (IS). The FAEs contents were obtained by integrating the peak areas from C14:0 to C24:1 and subtracting the nonadecanoate area, according to Eq. 3:

$$C = \frac{\sum A - A_{IS}}{A_{IS}} \times \frac{C_{IS} - V_{IS}}{m} \times 100\% \quad (3)$$

$\sum A$  = sum of the areas of all peaks ranging from C14:0 and C24:0

$A_{IS}$  = C19:0 internal standard area

$C_{IS}$  = concentration (mg mL<sup>-1</sup>) of the C19:0 solution

$V_{IS}$  = volume of the C19:0 solution added to sample

$m$  = mass of the FAEs sample (mg)

### 3. Results and Discussion

#### 3.1 Physicochemical characterization of the stannosilicates

The XRD patterns of the stannosilicates synthesized according to sol-gel chemical compositions detailed in

Tab. 1 are shown in Fig. 1a. The stannosilicate I presented a XRD pattern characteristic of a crystalline material and has structural similarity with the stannosilicate AV-10<sup>54</sup>. The stannosilicate AV-10 has an orthorhombic unit cell ( $a = 7.945 \text{ \AA}$ ,  $b = 10.344 \text{ \AA}$  and  $c = 11.625 \text{ \AA}$ ) and its gel composition (8.5Na<sub>2</sub>O:5.4SiO<sub>2</sub>:1.0SnO<sub>2</sub>:115H<sub>2</sub>O) contained lowest SiO<sub>2</sub>:Na<sub>2</sub>O ratio ( $\approx 0.6$ ) in comparison with stannosilicate I ( $\approx 4.0$ ). X-ray diffraction patterns of stannosilicate II (gel composition of 2Na<sub>2</sub>O:Sn<sub>2</sub>O:4SiO<sub>2</sub>:80H<sub>2</sub>O) indicate the formation of a new microporous material (XRD pattern not reported previously), while the stannosilicate V (gel composition of 5Na<sub>2</sub>O:Sn<sub>2</sub>O:10SiO<sub>2</sub>:80H<sub>2</sub>O) is similar to phase L<sup>46</sup>. The effects of the sol-gel composition were observed in the crystallization of these materials. The experimental evidences indicated that SiO<sub>2</sub>:Na<sub>2</sub>O ratio in the range of 5–10, as the ones used for the syntheses of stannosilicates III (2Na<sub>2</sub>O:Sn<sub>2</sub>O:10SiO<sub>2</sub>:80H<sub>2</sub>O) and stannosilicates IV (1Na<sub>2</sub>O:Sn<sub>2</sub>O:10SiO<sub>2</sub>:80H<sub>2</sub>O), induce the formation of tin oxide, clearly noticed in the XRD pattern of the stannosilicate III (Fig. 1a), as most of diffraction peaks were assigned to the SnO<sub>2</sub> phase (JCPDS 41-1445).

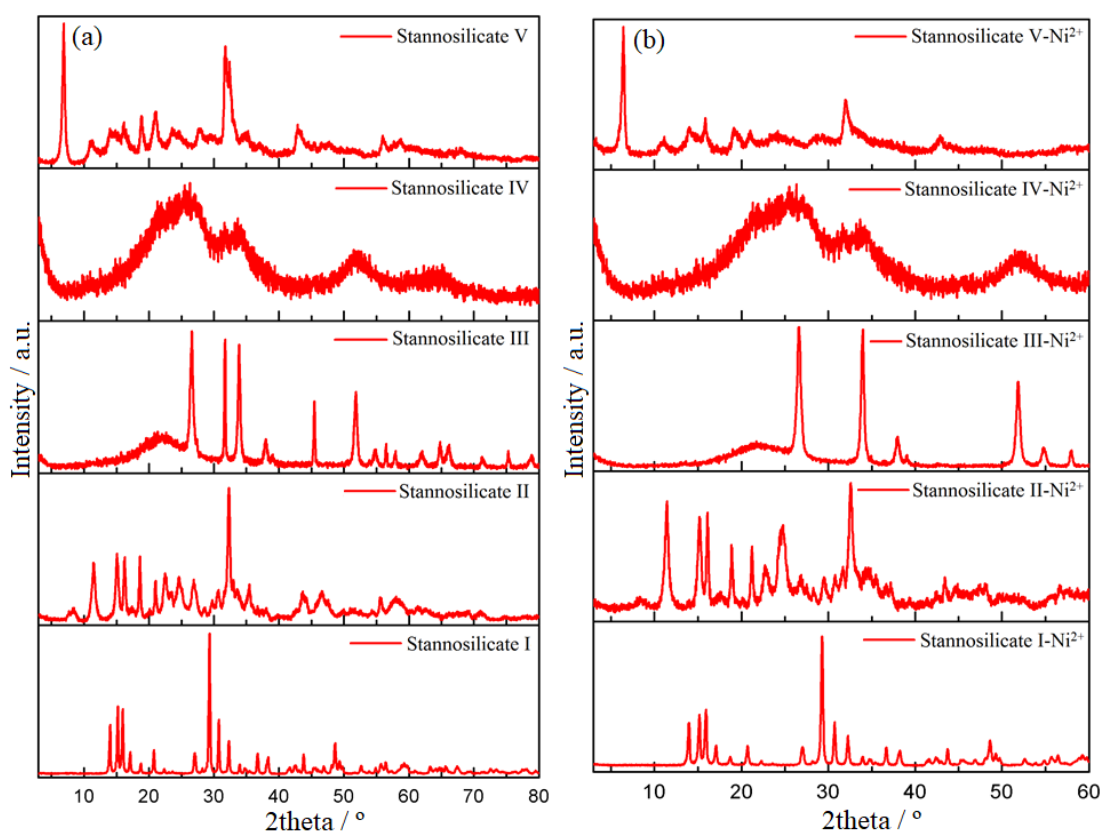


**Figure 1.** X-ray powder diffraction patterns of metallo-stannosilicates (a) before and (b) after the nickel ion-exchange experiments (a.u. = arbitrary units).

The  $^{29}\text{Si}$  Single-Pulse MAS NMR results are shown in Fig. 2. The result for stannosilicate I (spectrum not shown) is similar to reported for stannosilicate AV-10<sup>54</sup>. The spectrum presents two resonance lines with chemical shift positions at  $\delta_1 = -87.0$  ppm and  $\delta_2 = -88.7$  ppm with relative intensities of 1:2 and are associated with the Si(2Si, 2Sn) environment. This similarity between both materials was proved recently by our research group<sup>55</sup> in a solid-state NMR study, where the stannosilicate I was used as a model compound for developing a solid-state NMR strategy to verify the connectivity of  $\text{SiO}_4$  and  $\text{SnO}_6$  polyhedral,

despite the very low natural abundances of 4.68% for  $^{29}\text{Si}$  and 8.59% for  $^{29}\text{Si}$  and  $^{119}\text{Sn}$  nuclei, respectively. The  $^{29}\text{Si}\{^{119}\text{Sn}\}$  and  $^{119}\text{Sn}\{^{29}\text{Si}\}$  REDOR (rotational-echo double-resonance) NMR,  $^{29}\text{Si}\{^{119}\text{Sn}\}$  and  $^{119}\text{Sn}\{^{29}\text{Si}\}$  REPT-HMQC (recoupled polarization transfer-heteronuclear multiple-quantum correlation) NMR and 2D  $^{29}\text{Si}$  INADEQUATE NMR experiments using the crystallographic data of the sodium stannosilicate AV-10 (chemical composition  $\text{Na}_2\text{SnSi}_3\text{O}_9 \cdot 2\text{H}_2\text{O}$ ) proved that both stannosilicates consist of the same materials.

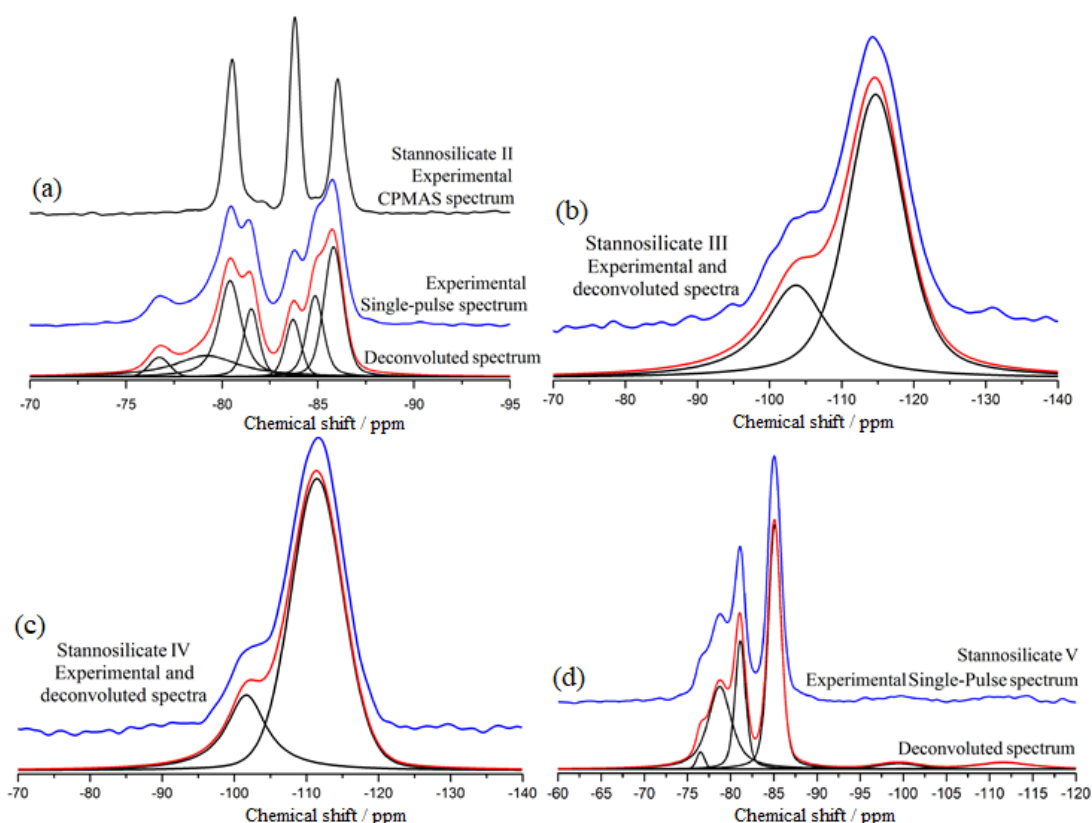


**Figure 2.**  $^{29}\text{Si}$  single-pulse MAS NMR spectra of stannosilicates II, III, IV and V.

The  $^{29}\text{Si}$  single-pulse MAS NMR spectra for the stannosilicates II, III, IV and V can be analyzed based in the seminal researches for  $^{29}\text{Si}$  solid-state MAS NMR of aluminosilicates structures<sup>56,57</sup>. Deconvolution of the spectrum for the stannosilicate II have resulted in seven resonance lines with the following chemical shifts values:  $\delta_1 = -76.7$  ppm,  $\delta_2 = -79.1$  ppm,  $\delta_3 = -80.4$  ppm,  $\delta_4 = -81.5$  ppm,  $\delta_5 = -83.7$  ppm,  $\delta_6 = -84.8$  ppm and  $\delta_7 = -85.8$  ppm. The  $^{29}\text{Si}$  single-pulse MAS NMR spectrum for the stannosilicate III showed two resonances lines with chemical shifts at  $\delta_1 = -102.2$  ppm and  $\delta_2 = -111.4$  ppm, which are associated to the Si(3Si, 1Sn) and Si(4Si) environments, respectively.

The stannosilicate IV showed a spectrum with two resonance lines at  $\delta_1 = -101.9$  ppm and  $\delta_2 = -111.4$  ppm positions. The  $^{29}\text{Si}$  single-pulse MAS NMR spectrum for the stannosilicate V shows six resonance lines with the following chemical shift values:  $\delta_1 = -76.4$  ppm,  $\delta_2 = -78.7$  ppm,  $\delta_3 = -81.0$  ppm,  $\delta_4 = -85.0$  ppm,  $\delta_5 = -99.4$  ppm and  $\delta_6 = -111.6$  ppm. The results in the chemical shift range from  $\delta = -97.1$  ppm to  $\delta = -111.6$  ppm are associated to the Si(3Si, 1Sn) and Si(4Si) environments.

The  $^{119}\text{Sn}$  single-pulse MAS NMR spectra are shown in Fig. 3. The stannosilicate III presents a chemical shift at the position of  $\delta = -604$  ppm,

therefore confirming the formation of a pure  $\text{SnO}_2$  phase<sup>14</sup>. The stannosilicates IV presented weak  $^{119}\text{Sn}$  MAS NMR signals (spectra not shown). The  $^{119}\text{Sn}$  single-pulse MAS NMR spectra of the stannosilicates

I, II and V have shown chemical shifts in the range from  $\delta = -660$  ppm to  $\delta = -720$  ppm, which are assigned to the tin species in the  $\text{Sn}^{4+}$  oxidation state<sup>58,59</sup>.

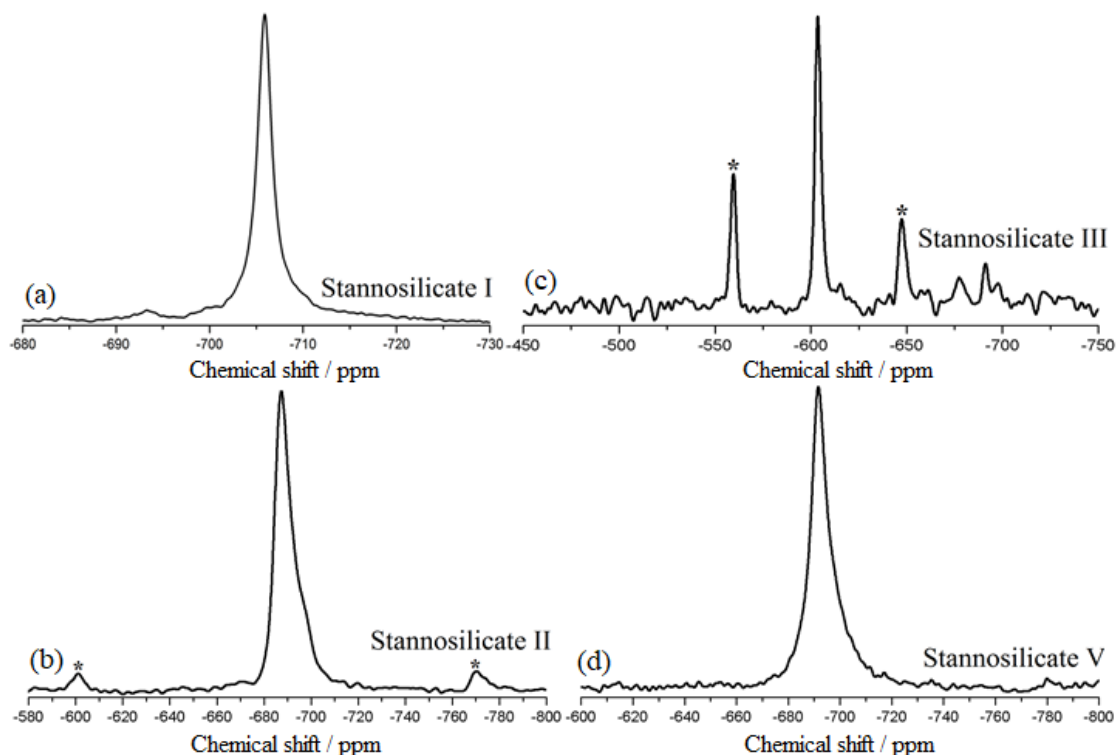


**Figure 3.**  $^{119}\text{Sn}$  single-pulse MAS NMR spectra of stannosilicates I, II, III and V (\*spinning sidebands, MAS frequency of 12.5 kHz).

Surface area results obtained by BET- $\text{N}_2$  isotherms are shown in **Tab. 1**. The materials have low surface areas and maximum values were observed for the stannosilicates III and IV (86.95–and 50.45  $\text{m}^2 \text{g}^{-1}$ , respectively), which are similar to the values reported in the literature for the  $\text{SnO}_2$  nanoparticles synthesized by different methods<sup>60–62</sup>. The morphology of the stannosilicates is shown in **Figs. 4** and **5**. The

crystalline stannosilicate I (**Fig. 4a**) consist of micrometric plates with dimensions of  $2 \times 1 \times 0.2 \mu\text{m}$ . The stannosilicates II and V (**Fig. 4b** and **4c**, respectively) are built up by micrometric plates, while an aggregate of spherical particles with particles size smaller than 100 nm were observed for stannosilicates III and IV (**Fig. 5a** and **5b**, respectively).

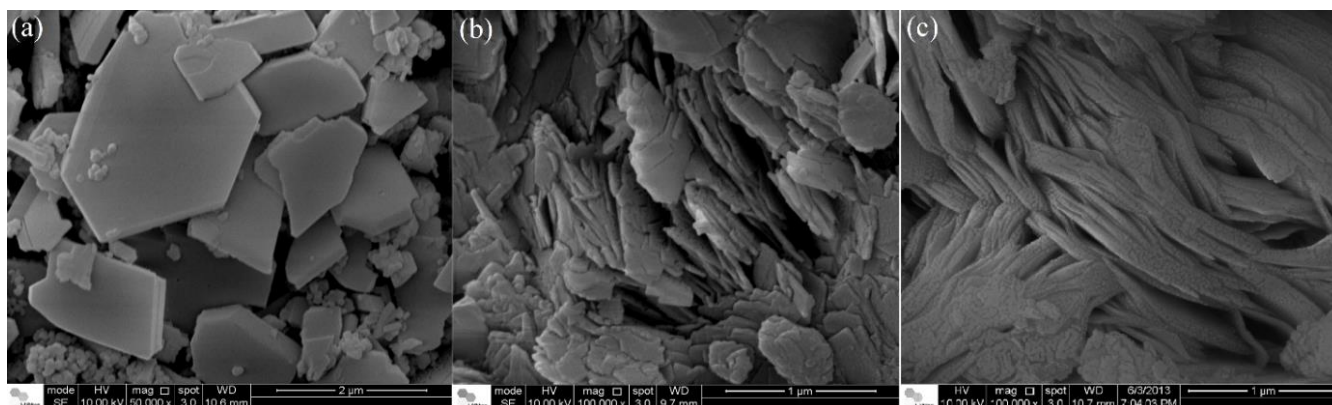


**Figure 4.** Scanning electron microscope-images of stannosilicates (a) I, (b) II and (c) V.

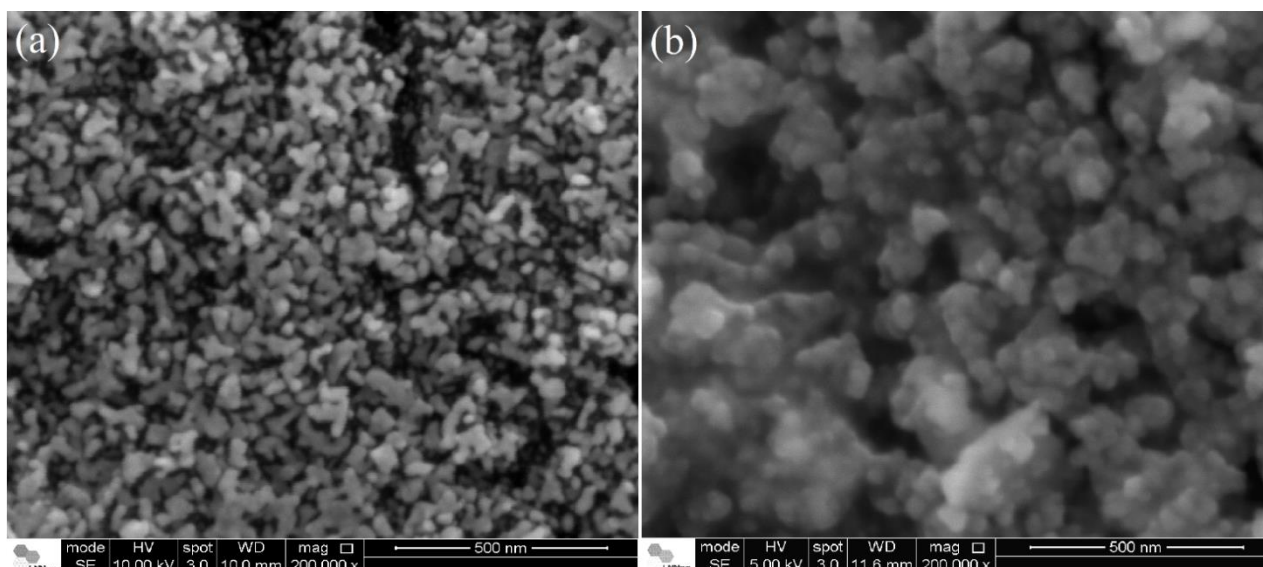


**Figure 5.** Scanning electron microscope images of stannosilicates (a) III and (b) IV.

### 3.2 Enzymes immobilization and enzymatic activity of the stannosilicate-enzymes complexes

Prior to the enzyme immobilization, the stannosilicates were submitted to nickel ion-exchange reactions. The important role played by nickel in enzymes immobilization and enzymatic activity has been reported previously<sup>34,35</sup> and was also observed here for the stannosilicates supports nickel-exchanged. The amount of Ni<sup>2+</sup> incorporated on the stannosilicates were determined by EDS analyses and the results are shown in Tab. 2. The nickel ion-exchange reactions have not caused significative changes in the

stannosilicates structures (Fig. 1b). The zeta potential measurements of the as-made stannosilicates and the nickel-stannosilicates are also presented in Tab. 2 and the results showed an increase in the surface charge after the nickel-exchange reactions (except for the stannosilicate III, which presented the lowest amount of nickel), as well as the percentual of immobilized enzymes (Tab. 3). The enzymatic activity of stannosilicates-enzymes complexes is also presented in Tab. 3: the as-made stannosilicate III enzymes and stannosilicate IV-Ni<sup>2+</sup>-enzymes presented the highest enzymatic activities of  $52.3 \pm 3.8$  and  $58.0 \pm 3.2$  U mg<sup>-1</sup>, respectively.

**Table 2.** Zeta potential (before and after nickel ion-exchange experiments) for the metallo-stannosilicates synthesized and nickel composition determined by energy dispersive X-ray spectroscopy (EDS).

| Stannosilicate | Zeta potencial / mV | Stannosilicate       | Zeta potencial / mV | Nickel / % |
|----------------|---------------------|----------------------|---------------------|------------|
| I              | - 34 ± 5            | I-Ni <sup>2+</sup>   | - 12 ± 4            | 0.5 ± 0.1  |
| II             | - 44 ± 6            | II-Ni <sup>2+</sup>  | - 7 ± 2             | 4.5 ± 0.1  |
| III            | 7 ± 4               | III-Ni <sup>2+</sup> | - 18 ± 4            | < 0.2      |
| IV             | - 40 ± 6            | IV-Ni <sup>2+</sup>  | - 19 ± 3            | 0.4 ± 0.1  |
| V              | - 58 ± 6            | V-Ni <sup>2+</sup>   | - 17 ± 3            | 6.3 ± 0.1  |

**Table 3.** Percentage of *Thermomyces lanuginosus* lipase immobilized on the as-made stannosilicates and stannosilicates-nickel materials. In the table also are presented the enzymatic activity results for the as-made stannosilicates-enzymes and stannosilicates-Ni<sup>2+</sup>-enzymes complexes.

| Stannosilicate | Enzymes immobilized / % | Enzymatic activity / U mg <sup>-1</sup> | Stannosilicate       | Enzymes immobilized / % | Enzymatic activity / U mg <sup>-1</sup> |
|----------------|-------------------------|---|----------------------|-------------------------|---|
| I              | 28 ± 10                 | 2.4 ± 0.6                               | I-Ni <sup>2+</sup>   | 29 ± 9                  | 32 ± 9                                  |
| II             | 7.1 ± 0.9               | 1.0 ± 0.4                               | II-Ni <sup>2+</sup>  | 33 ± 4                  | 21 ± 3                                  |
| III            | 63 ± 10                 | 52 ± 4                                  | III-Ni <sup>2+</sup> | 82 ± 6                  | 42 ± 3                                  |
| IV             | 39 ± 16                 | 43 ± 8                                  | IV-Ni <sup>2+</sup>  | 36 ± 2                  | 58 ± 3                                  |
| V              | 5 ± 2                   | 1.6 ± 0.1                               | V-Ni <sup>2+</sup>   | 42 ± 7                  | 28 ± 3                                  |

### 3.3 Fatty acid ethyl esters production by transesterification of refined palm oil (*Elaeis guineensis*) using stannosilicates and stannosilicates-enzymes complexes as heterogeneous catalysts

Fatty acid ethyl esters yields obtained in the heterogeneous transesterification of refined palm oil (*Elaeis guineensis*) are shown in the Tab. 4. The as-made stannosilicates I, III and IV have shown no catalytic activity (FAEEs yields below 5%), while the catalytic conversion of triacylglycerides using the stannosilicates II (Na:Sn =  $2.0 \pm 0.2$ ) and V (Na:Sn =  $4.1 \pm 0.7$ ) have yielded  $28.3 \pm 0.2\%$  and  $60.8 \pm 0.5\%$ , respectively. The FAEEs yields using the stannosilicates-Ni<sup>2+</sup>-enzymes complexes as enzymatic catalysts are also presented in Tab. 4. The triacylglycerides conversion into FAEEs using the stannosilicates-Ni<sup>2+</sup>-enzymes complexes I, III and IV have yielded the following amounts of FAEEs: stannosilicate I Ni<sup>2+</sup> enzyme  $63.3 \pm 0.7\%$ , stannosilicate III Ni<sup>2+</sup> enzyme  $39.9 \pm 0.3\%$  and stannosilicate IV-Ni<sup>2+</sup>-enzyme  $38.5 \pm 0.7\%$ . An

example of gas chromatogram (GC-FID) for the highest FAEEs conversion (stannosilicate I Ni<sup>2+</sup> enzyme as biocatalyst) is illustrated in the supplementary material. It should be noticed that these metallo-stannosilicates in their as-made forms have shown no catalytic activity, nevertheless these positive catalytic results indicate their possible application as solid matrixes for enzymes immobilization.

The results indicated that the highest yield of FAEEs was obtained for the stannosilicate I Ni<sup>2+</sup> enzyme complex, which has  $29 \pm 9\%$  of enzymes immobilized. In order to verify the possible occurrence of a synergistic effect as reported by other authors<sup>34,35</sup>, the equivalent amount of enzyme immobilized on this catalyst was used in its free form in the transesterification of refined palm oil (*Elaeis guineensis*) under the same experimental condition. The FAEEs yield of  $6.3 \pm 0.3\%$  obtained in this reaction is a clear evidence of a synergistic effect among the nickel-stannosilicates used as inorganic supports and the *Thermomyces lanuginosus* lipase applied in transesterification reactions for biodiesel production.

**Table 4.** Results for the FAEEs yields by the transesterification of refined palm oil (*Elaeis guineensis*) using the as-made stannosilicates and stannosilicate-Ni<sup>2+</sup>-enzymes complexes as heterogeneous catalysts.

| As-made stannosilicates* | FAEEs yield / % | Stannosilicate-enzymes complexes** | FAEEs yield / %      |
|--------------------------|-----------------|------------------------------------|----------------------|
| I                        | < 5.0           | I-Ni <sup>2+</sup> -enzymes        | $63.3 \pm 0.7^{***}$ |
| II                       | $28.3 \pm 0.2$  | II-Ni <sup>2+</sup> -enzymes       | $44.6 \pm 0.5$       |
| III                      | < 5.0           | III-Ni <sup>2+</sup> -enzymes      | $39.9 \pm 0.3$       |
| IV                       | < 5.0           | IV-Ni <sup>2+</sup> -enzymes       | $38.5 \pm 0.7$       |
| V                        | $60.8 \pm 0.5$  | V-Ni <sup>2+</sup> -enzymes        | $42.5 \pm 0.6$       |

\*Experimental conditions: reactions were made in an open glass reactor (reflux condenser), temperature = 100 °C, oil:alcohol molar ratio = 1:30, time of reaction = 12 h and amount of catalyst = 3% of catalyst referred to oil mass;

\*\*Experimental conditions: reactions were made in 10 mL flasks, temperature =  $40 \pm 2$  °C, time of reaction = 48 h, oil:alcohol molar ratio = 1:4 and amount of catalyst = 5% referred to oil mass;

\*\*\*FAEEs yield for the amount of free enzyme immobilized on this support ( $29 \pm 9\%$ ) applied in catalytic reaction =  $6.3 \pm 0.3\%$ .

## 4. Conclusions

Several metallo-stannosilicates were synthesized and characterized by XRD, SEM, BET-N<sub>2</sub> surface area and solid-state MAS NMR (<sup>29</sup>Si and <sup>119</sup>Sn nuclei) techniques. These materials were studied as potential inorganic solid matrixes for immobilization of *Thermomyces lanuginosus* lipase and also as heterogeneous catalysts in the transesterification of refined palm oil (*Elaeis guineensis*) by ethanolysis reactions. The results were promising, since that as-made and nickel-exchanged stannosilicates were able to immobilize from  $5 \pm 2\%$  to  $82 \pm 6\%$  of enzymes and presented enzymatic activity varying

from  $1.0 \pm 0.4 \text{ U mg}^{-1}$  to  $58 \pm 3 \text{ U mg}^{-1}$ . Some of these as-made materials, when applied as heterogeneous catalysts, presented no catalytic activity. However, when applied as biocatalysts in enzymatic transesterification reactions, stannosilicate-Ni<sup>2+</sup>-enzymes produced FAEEs yields varying from  $38.5 \pm 0.7\%$  to  $63.3 \pm 0.7\%$ . These results are an evidence of a synergistic effect among the stannosilicates and enzymes, contributing to the advancement of research in the field of biodiesel production since these results were not reported previously for this class of mixed framework oxides.

## Acknowledgments

We thank the State of São Paulo Research Foundation (FAPESP) and National Council for Scientific and Technological Development (CNPq) for the grant awards No. #11/51851-5 and No. #406761/2013-2, respectively. D.A.S. thanks CAPES (Proc. No. BEX 2428/15-6) and CNPq (Proc. No.142029/2012-2) for his fellowships. We acknowledge Mr. Carsten Prinz and Ms. Annett Zimathies (BAM Federal Institute for Materials Research and Testing, Division 1.3. Structure Analyses) for the BET-N<sub>2</sub> measurements. We appreciate the assistance of Dr. Carlos A. O. Ramirez and Dr Jefferson Bettini (Brazilian National Laboratory of Nanotechnology, LNNano) for the analysis of SEM-EDS. We also thank Prof. Dr. Christian Jäger (BAM Federal Institute for Materials Research and Testing, Division 1.3. Structure Analyses) for the Solid-State MAS NMR experiments and Prof. Dra. Marcia P. dos Santos Cabrera (São Paulo State University, IBILCE) for the Zeta Potential Measurements.

## References

- [1] Singh, S. P., Singh, D., Biodiesel production through the use of different sources and characterization of oils and their esters as the substitute of diesel: A review, *Renewable and Sustainable Energy Reviews* 14 (1) (2010) 200-216. <https://doi.org/10.1016/j.rser.2009.07.017>.
- [2] Balat, M., Potential alternatives to edible oils for biodiesel production – A review of current work, *Energy Conversion and Management* 52 (2) (2011) 1479-1492. <https://doi.org/10.1016/j.enconman.2010.10.011>.
- [3] Gui, M. M., Lee, K. T., Bhatia, S., Feasibility of edible oil vs. non-edible oil vs. waste edible oil as biodiesel feedstock, *Energy* 33 (11) (2008) 1646-1653. <https://doi.org/10.1016/j.energy.2008.06.002>.
- [4] Mekhilef, S., Siga, S., Saidur, R., A review on palm oil biodiesel as a source of renewable fuel, *Renewable and Sustainable Energy Reviews* 33 (4) (2011) 1937-1949. <https://doi.org/10.1016/j.rser.2010.12.012>.
- [5] Issariyakul, T., Dalai, A. K., Biodiesel from vegetable oils, *Renewable and Sustainable Energy Reviews* 31 (2014) 446-471. <https://doi.org/10.1016/j.rser.2013.11.001>.
- [6] Semwal, S., Arora, A. K., Badoni, R. P., Tuli, D. K., Biodiesel production using heterogeneous catalysts, *Bioresource Technology* 102 (3) (2011) 2151-2161. <https://doi.org/10.1016/j.biortech.2010.10.080>.
- [7] Chouhan, A. P. S., Sarma, A. K., Modern heterogeneous catalysts for biodiesel production: A comprehensive review, *Renewable and Sustainable Energy Reviews* 15 (9) (2011) 4378-4399. <https://doi.org/10.1016/j.rser.2011.07.112>.
- [8] Sakai, T., Kawashima, A., Koshikawa, T., Economic assessment of batch biodiesel production processes using homogeneous and heterogeneous alkali catalysts, *Bioresource Technology* 100 (13) (2009) 3268-3276. <https://doi.org/10.1016/j.biortech.2009.02.010>.
- [9] Lam, M. K., Lee, K. T., Mohamed, A. R., Homogeneous, heterogeneous and enzymatic catalysis for transesterification of high free fatty acid oil (waste cooking oil) to biodiesel: A review, *Biotechnology Advances* 28 (4) (2010) 500-518. <https://doi.org/10.1016/j.biotechadv.2010.03.002>.
- [10] Dossin, T. F., Reyniers, M.-F., Berger, R. J., Marin, G. B., Simulation of heterogeneously MgO-catalyzed transesterification for fine-chemical and biodiesel industrial production, *Applied Catalysis B: Environmental* 67 (1-2) (2006) 136-148. <https://doi.org/10.1016/j.apcatb.2006.04.008>.
- [11] Corcoran, E. W., Vaughan, D. E. W., Eberly Junior, P. E., Efirid, K. D., Substituted stannosilicates, their preparation and use as natural gas purification agents (C-2668), US 5 264 193 A, 1993. <https://patents.google.com/patent/US5264193A/en>.
- [12] Janiszewska, E., Kowalak, S., Supronowicz, W., Roessner, F., Synthesis and properties of stannosilicates, Microporous and Mesoporous Materials 117 (1-2) (2009) 423-430. <https://doi.org/10.1016/j.micromeso.2008.07.032>.
- [13] Li, P., Liu, G., Wu, H., Liu, Y., Jiang, J.-G., Wu, P., Postsynthesis and Selective Oxidation Properties of Nanosized Sn-Beta Zeolite, *The Journal Physical Chemistry C* 115 (9) (2011) 3663-3670. <https://doi.org/10.1021/jp1076966>.
- [14] Moliner, M., Román-Leshkov, Y., Davis, M. E., Tin-containing zeolites are highly active catalysts for the isomerization of glucose in water, *Proceedings of the National Academy of Sciences of the United States of America* 107 (14) (2010) 6164-6168. <https://doi.org/10.1073/pnas.1002358107>.
- [15] Román-Leshkov, Y., Moliner, M., Labinger, J. A., Davis, M. E., Mechanism of Glucose Isomerization Using a Solid Lewis Acid Catalyst in Water, *Angewandte Chemie International Edition* 49 (47) (2010) 8954-8957. <https://doi.org/10.1002/anie.201004689>.
- [16] da Silva, D. A., Santisteban, O. A. N., de Vasconcellos, A., Paula, A. S., Aranda, D. A. G., Giotto, M. V., Jaeger, C., Nery, J. G., Metallo-stannosilicate heterogeneous catalyst for biodiesel production using edible, non-edible and waste oils as feedstock, *Journal of Environmental Chemical Engineering* 6 (2018) 5488-5497. <https://doi.org/10.1016/j.jece.2018.08.047>.

- [17] Abreu, F. R., Lima, D. G., Hamú, E. H., Einloft, S., Rubim, J. C., Suarez, P. A. Z., New metal catalysts for soybean oil transesterification, *Journal of the American Oil Chemists' Society* 80 (6) (2003) 601-604. <https://doi.org/10.1007/s11746-003-0745-6>.
- [18] Ferreira, D. A. C., Meneghetti, M. R., Meneghetti, S. M. P., Wolf, C. R., Methanolysis of soybean oil in the presence of tin(IV) complexes, *Applied Catalysis A: General* 317 (1) (2007) 58-61. <https://doi.org/10.1016/j.apcata.2006.10.002>.
- [19] Serra, T. M., de Mendonça, D. R., da Silva, J. P. V., Meneghetti, M. R., Plentz Meneghetti, S. M. P., Comparison of soybean oil and castor oil methanolysis in the presence of tin(IV) complexes, *Fuel* 90 (6) (2011) 2203-2206. <https://doi.org/10.1016/j.fuel.2011.02.027>.
- [20] Xie, W., Wang, H., Li, H., Silica-Supported Tin Oxides as Heterogeneous Acid Catalysts for Transesterification of Soybean Oil with Methanol, *Industrial & Engineering Chemistry Research* 51 (1) (2012) 225-231. <https://doi.org/10.1021/ie202262t>.
- [21] Abreu, F. R., Lima, D. G., Hamú, E. H., Wolf, C., Suarez, P. A., Utilization of metal complexes as catalysts in the transesterification of Brazilian vegetable oils with different alcohols, *Journal of Molecular Catalysis A: Chemical* 209 (1-2) (2004) 29-33. <https://doi.org/10.1016/j.molcata.2003.08.003>.
- [22] Casas, A., Ramos, M. J., Rodríguez, J. F., Pérez, Á., Tin compounds as Lewis acid catalysts for esterification and transesterification of acid vegetable oils, *Fuel Processing Technology* 106 (2013) 321-325. <https://doi.org/10.1016/j.fuproc.2012.08.015>.
- [23] Lam, M. K., Lee, K. T., Mixed methanol-ethanol technology to produce greener biodiesel from waste cooking oil: A breakthrough for  $\text{SO}_4^{2-}/\text{SnO}_2\text{-SiO}_2$  catalyst, *Fuel Processing Technology* 92 (8) (2011) 1639-1645. <https://doi.org/10.1016/j.fuproc.2011.04.012>.
- [24] Lam, M. K., Lee, K. T., Accelerating transesterification reaction with biodiesel as co-solvent: A case study for solid acid sulfated tin oxide catalyst, *Fuel* 89 (12) (2010) 3866-3870. <https://doi.org/10.1016/j.fuel.2010.07.005>.
- [25] Bajaj, A., Lohan, P., Jha, P. N., Mehrotra, R., Biodiesel production through lipase catalyzed transesterification: An overview, *Journal of Molecular Catalysis B: Enzymatic* 62 (1) (2010) 9-14. <https://doi.org/10.1016/j.molcatb.2009.09.018>.
- [26] Rosset, I. G., Tavares, M. C. H., Assaf, E. M., Porto, A. L. M., Catalytic ethanolysis of soybean oil with immobilized lipase from *Candida antarctica* and  $^1\text{H}$  NMR and GC quantification of the ethyl esters (biodiesel) produced, *Applied Catalysis A: General* 392 (1-2) (2011) 136-142. <https://doi.org/10.1016/j.apcata.2010.10.035>.
- [27] Ferreira, I. M., Ganzeli, L. de S., Rosset, I. G., Yoshioka, S. A., Porto, A. L. M., Ethylic Biodiesel Production Using Lipase Immobilized in Silk Fibroin-Alginate Spheres by Encapsulation, *Catalysis Letters* 147 (2017) 269-280. <https://doi.org/10.1007/s10562-016-1917-0>.
- [28] Rosset, I. G., Porto, A. L. M., *Catálise Enzimática: Transesterificação do Óleo de Soja e Esterificação do Ácido Oleico via Lipases*, *Revista Brasileira de Energias Renováveis* 4 (2) (2015) 64-78. <https://doi.org/10.5380/rber.v4i2.42288>.
- [29] Rosset, I. G., Cavalheiro, M. C. H. T., Assaf, E. M., Porto, A. L. M., Enzymatic Esterification of Oleic Acid with Aliphatic Alcohols for the Biodiesel Production by *Candida antarctica* Lipase, *Catalysis Letters* 143 (2013) 863-872. <https://doi.org/10.1007/s10562-013-1044-0>.
- [30] Rosset, I. G., Assaf, E. M., Porto, A. L. M., Biocatalytic Production of Ethyl Esters (Biodiesel) by Enzymatic Transesterification from Synthetic Triolein, *Current Catalysis* 2 (1) (2013) 53-61. <https://doi.org/10.2174/2211544711302010009>.
- [31] Antczak, M. S., Kubiak, A., Antczak, T., Bielecki, S., Enzymatic biodiesel synthesis – Key factors affecting efficiency of the process, *Renewable Energy* 34 (5) (2009) 1185-1194. <https://doi.org/10.1016/j.renene.2008.11.013>.
- [32] Jegannathan, K. R., Abang, S., Poncelet, D., Chan, E. S., Ravindra, P., Production of Biodiesel Using Immobilized Lipase—A Critical Review, *Critical Reviews in Biotechnology* 28 (4) (2008) 253-264. <https://doi.org/10.1080/07388550802428392>.
- [33] Bergamasco, J., de Araujo, M. V., de Vasconcellos, A., Luizon Filho, R. A., Hatanaka, R. R., Giotto, M. V., Aranda, D. A. G., Nery, J. G., Enzymatic transesterification of soybean oil with ethanol using lipases immobilized on highly crystalline PVA microspheres, *Biomass and Bioenergy* 59 (2013) 218-233. <https://doi.org/10.1016/j.biombioe.2013.09.006>.
- [34] de Vasconcellos, A., Paula, A. S., Luizon Filho, R. A., Farias, L. A., Gomes, E., Aranda, D. A. G., Nery, J. G., Synergistic effect in the catalytic activity of lipase *Rhizomucor miehei* immobilized on zeolites for the production of biodiesel, *Microporous and Mesoporous Materials* 163 (2012) 343-355. <https://doi.org/10.1016/j.micromeso.2012.07.043>.
- [35] de Vasconcellos, A., Laurenti, J. B., Miller, A. H., da Silva, D. A., de Moraes, F. R., Aranda, D. A. G., Nery, J. G., Potential new biocatalysts for biofuel production: The fungal lipases of *Thermomyces lanuginosus* and *Rhizomucor miehei* immobilized on zeolitic supports ion exchanged with

- transition metals, *Microporous and Mesoporous Materials* 214 (2015) 166-180. <https://doi.org/10.1016/j.micromeso.2015.05.007>.
- [36] de Vasconcellos, A., Miller, A. H., Aranda, D. A. G., Nery, J. G., Biocatalysts based on nanozeolite-enzyme complexes: Effects of alkoxysilane surface functionalization and biofuel production using microalgae lipids feedstock, *Colloids and Surfaces B: Biointerfaces* 165 (2018) 150-157. <https://doi.org/10.1016/j.colsurfb.2018.02.029>.
- [37] MacArio, A., Giordano, G., Setti, L., Parise, A., Campelo, J. M., Marinas, J. M., Luna, D., Study of lipase immobilization on zeolitic support and transesterification reaction in a solvent free-system, *Biocatalysis and Biotransformation* 25 (2-4) (2007) 328-335. <https://doi.org/10.1080/10242420701444256>.
- [38] Macario, A., Molimer, M., Diaz, U., Jorda, J. L., Corma, A., Giordano, G., Biodiesel production by immobilized lipase on zeolites and related materials, *Studies in Surface Science and Catalysis* 174 (Part B) (2008) 1011-1016. [https://doi.org/10.1016/S0167-2991\(08\)80061-4](https://doi.org/10.1016/S0167-2991(08)80061-4).
- [39] Brito, A., Borges, M. E., Otero, N., Zeolite Y as a Heterogeneous Catalyst in Biodiesel Fuel Production from Used Vegetable Oil, *Energy & Fuels* 21 (6) (2007) 3280-3283. <https://doi.org/10.1021/ef700455r>.
- [40] Costa, L., Brissos, V., Lemos, F., Ribeiro, F. R., Cabral, J. M. S., Enhancing the thermal stability of lipases through mutagenesis and immobilization on zeolites, *Bioprocess and Biosystems Engineering* 32 (2009) 53-61. <https://doi.org/10.1007/s00449-008-0220-x>.
- [41] Hölker, U., Höfer, M., Lenz, J., Biotechnological advantages of laboratory-scale solid-state fermentation with fungi, *Applied Microbiology and Biotechnology* 64 (2004) 175-186. <https://doi.org/10.1007/s00253-003-1504-3>.
- [42] Verdugo, C., Luna, D., Posadillo, A., Sancho, E. D., Rodrigues, S., Bautista, F., Luque, R., Marinas, J. M., Romero, A. A., Production of a new second generation biodiesel with a low cost lipase derived from *Thermomyces lanuginosus*: Optimization by response surface methodology, *Catalysis Today* 167 (1) (2011) 107-112. <https://doi.org/10.1016/j.cattod.2010.12.028>.
- [43] Du, W., Xu, Y.-Y., Liu, D.-H., Li, Z.-B., Study on acyl migration in immobilized lipozyme TL-catalyzed transesterification of soybean oil for biodiesel production, *Journal of Molecular Catalysis B: Enzymatic* 37 (1-6) (2005) 68-71. <https://doi.org/10.1016/j.molcatb.2005.09.008>.
- [44] Zhang, W.-W., Yang, X.-L., Jia, J.-Q., Wang, N., Hu, C.-L., Yu, X.-Q., Surfactant-activated magnetic cross-linked enzyme aggregates (magnetic CLEAs) of *Thermomyces lanuginosus* lipase for biodiesel production, *Journal of Molecular Catalysis B: Enzymatic* 115 (2015) 83-89. <https://doi.org/10.1016/j.molcatb.2015.02.003>.
- [45] Corcoran Junior, E. W., Vaughan, D. E. W., Hydrothermal synthesis of mixed octahedral-tetrahedral oxides: Synthesis and characterization of sodium stannosilicates, *Solid State Ionics* 32-33 (Part 1) (1989) 423-429. [https://doi.org/10.1016/0167-2738\(89\)90250-6](https://doi.org/10.1016/0167-2738(89)90250-6).
- [46] Corcoran Junior, E. W., Vaughan, D. E. W., Eberly, P. E., Stannosilicates and preparation thereof (C-2417), US 5 110 571A, 1992. <https://patents.google.com/patent/US5110571A/en>.
- [47] Brunauer, S., Emmett, P. H., Teller, E., Adsorption of Gases in Multimolecular Layers, *Journal of the American Chemical Society* 60 (2) (1938) 309-319. <https://doi.org/10.1021/ja01269a023>.
- [48] Cossement, C., Darville, J., Gilles, J.-M., Nagy, J. B., Fernandez, C., Amoureux, J.-P., Chemical shift anisotropy and indirect coupling in SnO<sub>2</sub> and SnO, *Magnetic Resonance in Chemistry* 30 (3) (1992) 263-270. <https://doi.org/10.1002/mrc.1260300313>.
- [49] Alkan, M., Demirbaş, Ö., Doğan, M., Electrokinetic properties of sepiolite suspensions in different electrolyte media, *Journal of Colloid and Interface Science* 281 (1) (2005) 240-248. <https://doi.org/10.1016/j.jcis.2004.08.036>.
- [50] Hu, Y.-Y., Zhang, Y.-H., Ren, N., Tang, Y., Crystal Plane- and Size-Dependent Protein Adsorption on Nanozeolite, *The Journal of Physical Chemistry C* 113 (42) (2009) 18040-18046. <https://doi.org/10.1021/jp903989p>.
- [51] Bradford, M. M., A rapid and sensitive method for the quantitation of microgram quantities of protein utilizing the principle of protein-dye binding, *Analytical Biochemistry* 72 (1-2) (1976) 248-254. [https://doi.org/10.1016/0003-2697\(76\)90527-3](https://doi.org/10.1016/0003-2697(76)90527-3).
- [52] Ghiaci, M., Aghaei, H., Soleimani, S., Sedaghat, M. E., Enzyme immobilization: Part 1. Modified bentonite as a new and efficient support for immobilization of *Candida rugosa* lipase, *Applied Clay Science* 43 (3-4) (2009) 289-295. <https://doi.org/10.1016/j.clay.2008.09.008>.
- [53] Gupta, P., Upadhyay, L. S. B., Shrivastava, R., Lipase Catalyzed-transesterification of Vegetable Oils by Lipolytic Bacteria, *Research Journal of Microbiology* 6 (3) (2011) 281-288. <https://doi.org/10.3923/jm.2011.281.288>.
- [54] Ferreira, A., Lin, Z., Rocha, J., Morais, C. M., Lopes, M., Fernandez, C., Ab Initio Structure Determination of a Small-Pore Framework Sodium Stannosilicate, *Inorganic Chemistry* 40 (14) (2001) 3330-3335. <https://doi.org/10.1021/ic0012571>.



[55] da Silva, D. A., Greiser, S., Contro, J., Medeiros, V. L., Nery, J. G., Jaeger, C.,  $^1\text{H}$ ,  $^{29}\text{Si}$  and  $^{119}\text{Sn}$  double and triple resonance NMR spectroscopy of the small-pore framework sodium stannosilicate  $\text{Na}_2\text{SnSi}_3\text{O}_9 \cdot 2\text{H}_2\text{O}$ , *Solid State Nuclear Magnetic Resonance* 107 (2020) 101661. <https://doi.org/10.1016/j.ssnmr.2020.101661>.

[56] Klinowski, J., Recent Advances in Solid-State NMR of Zeolites, *Annual Review of Materials Science* 18 (1988) 189-218. <https://doi.org/10.1146/annurev.ms.18.080188.001201>.

[57] Fyfe, C. A., Feng, Y., Gondey, H., Kokotailo, G. T., Gies, H., One- and two-dimensional high-resolution solid-state NMR studies of zeolite lattice structures, *Chemical Reviews* 91 (7) (1991) 1525-1543. <https://doi.org/10.1021/cr00007a013>.

[58] Mal, N. K., Bhaumik, A., Kumar, R., Ramaswamy, A. V., Sn-ZSM-12, a new, large pore MTW type tin-silicate molecular sieve: synthesis, characterization and catalytic properties in oxidation reactions, *Catalysis Letters* 33 (1995) 387-394. <https://doi.org/10.1007/BF00814240>.

[59] Cruz, M., Morales, J., Espinos, J. P., Sanz, J., XRD, XPS and  $^{119}\text{Sn}$  NMR study of tin sulfides obtained by using chemical vapor transport methods, *Journal of Solid State Chemistry* 175 (2) (2003) 359-365. [https://doi.org/10.1016/S0022-4596\(03\)00329-3](https://doi.org/10.1016/S0022-4596(03)00329-3).

[60] Song, K. C., Kang, Y., Preparation of high surface area tin oxide powders by a homogeneous precipitation method, *Materials Letters* 42 (5) (2000) 283-289. [https://doi.org/10.1016/S0167-577X\(99\)00199-8](https://doi.org/10.1016/S0167-577X(99)00199-8).

[61] Leite, E. R., Weber, I. T., Longo, E., Varela, J. A., A New Method to Control Particle Size and Particle Size Distribution of  $\text{SnO}_2$  Nanoparticles for Gas Sensor Applications, *Advanced Materials* 12 (13) (2000) 965-968. [https://doi.org/10.1002/1521-4095\(200006\)12:13%3C965:AID-ADMA965%3E3.0.CO;2-7](https://doi.org/10.1002/1521-4095(200006)12:13%3C965:AID-ADMA965%3E3.0.CO;2-7).

[62] Song, K. C., Kim, J. H., Synthesis of high surface area tin oxide powders via water-in-oil microemulsions, *Powder Technology* 107 (3) (2000) 268-272. [https://doi.org/10.1016/S0032-5910\(99\)00255-7](https://doi.org/10.1016/S0032-5910(99)00255-7).